# The calculation, scattering and stability of topographic Rossby waves

PhD Thesis

Gavin Anthony Schmidt

Department of Mathematics

University College London

UNIVERSITY OF LONDON

October 1993

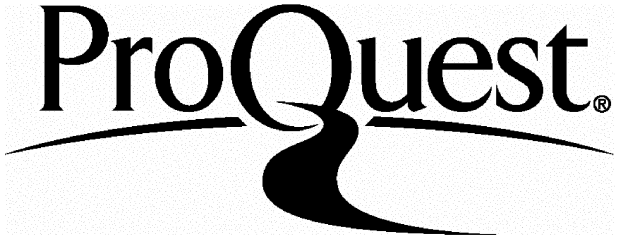

## Abstract

This thesis discusses the calculation and properties of topographic Rossby waves in homogeneous and continuously stratified rotating flow. These waves exist due to variations in the background potential vorticity arising from changes in topography or rotation.

The first part considers the calculation of the frequency and wavenumber of trapped topographic Rossby waves over various types of topography - along a coastal shelf (giving coastally trapped waves), over a submerged ridge and around an axisymmetric sea mount. A new direct method of calculation in the low frequency continuously stratified case is introduced. This uses a Green's function to reduce the problem to a one dimensional integral across the shelf. Asymptotic expansions in the stratification parameter $B = ND/fL$, where $N$ is the buoyancy frequency, $D$ a typical depth, $L$ a typical length and $f$ the Coriolis parameter are presented. Both strong stratification ($B \gg 1$) and weak stratification ($B \ll 1$) are treated in this fashion and approximations that are accurate for all $B$ are constructed for certain simple topographies.

The circumstances that can lead to singularities appearing in the solution are investigated and the consequences for general circulation models discussed.

The numerical method is applied to the solution of scattering problems as the topography changes and to determining the wind-forced response. An isobath tracing result is used to calculate the distribution of energy among the transmitted waves. Examples are given using various geometries including straits and ridges abutting a coastal shelf.

The stability of horizontal shear flow to small disturbances is considered. These disturbances have the form of topographic Rossby waves. Unstable modes can occur over ridges. Detailed examples are worked out in the barotropic case and in the continuously stratified long-wave case. In both cases the instabilities are centred at points where the shear flow brings two opposing waves relatively to rest.

# Table of contents

## Acknowledgements

This thesis would not have been possible without the help and support of many friends and colleagues. Among those most deserving of thanks are first and foremost my supervisor Prof. E.R. Johnson, without whom I literally would not have had a clue, my grandmother, who has put up with me for three years, and Donald Knuth, without whom this would have been a far more difficult undertaking.

Gavin Schmidt, October 1993.

This work was supported by funds awarded under the F.R.A.M. special topic award from the Natural and Environmental Research Council.

# Chapter 1

# Introduction

The study of the weather and of the movement of the oceans has long fascinated scientists but it has only been in the last hundred years or so that much mathematical headway has been made. The full processes involved in shaping the flow are, in the main, still poorly understood but a great deal of the global circulation can be well approximated by relatively simple models. The two effects which distinguish the study of these complex phenomena from other related disciplines are the rotation of the earth and the stratification of the atmosphere and oceans by temperature and salinity.

The recognition of the part temperature and density play in the circulation of the atmosphere was recognised by Halley (1686). He hypothesised that the lower density of hot air at the tropics compared with cold air at the poles would induce a circulation of hot air rising at the tropics, moving polewards, descending and cooling and returning to the tropics to be reheated. This model did not however adequately account for the easterly component of the trade winds. The explanation for this was given by Hadley (1735). Because of the rotation of the earth, air moving towards the equator from the poles has less angular momentum than that required for a rigid rotation at the equator. Hence air travelling south gains a westward velocity relative to an observer rotating with the earth. This model for the circulation is now called a "Hadley cell". This however, is not seen in practice for reasons discussed later.

The analytical starting point for the whole subject of fluid dynamics was the writing down of the equations of motion for an inviscid fluid by Euler (1755). The appropriate equations for flow in a rotating frame were used by Laplace (1778,1779) in his work on tides. The implications of the extra terms in the equations were also discussed by Coriolis (1835) after whom they are now named.

Proudman (1916) and Taylor (1917) were the first to discuss the importance of topography in rotating flow. They proved that in an inviscid, homogeneous, rapidly rotating flow the streamlines are independent of depth. Hence if flow has to move around an obstacle at one depth then the streamlines will follow the same pattern at all depths! This phenomena is known as a "Taylor column" or "cap" and was demonstrated in some very simple experiments done by Taylor

(1923) where he towed an object slowly through fluid in a rotating tank and observed a stagnant column of water above the object and moving with it.

The modern study of geophysical fluid dynamics though, really started with the work of Rossby in the 1930's. In a non-rotating flow a disturbance in the free surface quickly adjusts to the equilibrium of zero flow and a flat surface. However Rossby (1937,1938) showed that the analogous process in a rotating flow leads not to a static position but to a dynamic balance between the terms representing the Coriolis force and the pressure gradient. This is now called the "geostrophic equilibrium" and it is found to approximate the actual situation in the atmosphere and oceans over a remarkable percentage of the globe.

He also found that simply knowing that a fluid is in geostrophic equilibrium is not enough to determine the flow. Due to a degeneracy in the equations of motion some account must be taken of small departures from geostrophy. This led Rossby to discover the principle of the conservation of "potential vorticity". For the simplest case of homogeneous inviscid incompressible rotating flow this principle can be expressed very simply. If $\zeta$ is the relative vorticity of the flow, $f$ the Coriolis frequency and $h$ the depth of fluid then

$$\frac{D}{Dt}\left(\frac{\zeta + f}{h}\right) = 0, \tag{1.1}$$

where $D/Dt$ is the material derivative or "rate of change following the fluid". The quantity in brackets is called the potential vorticity(PV) and this equation shows that it is conserved for every fluid element. Hence a knowledge of the initial PV field of a fluid in geostrophic equilibrium is sufficient to determine the subsequent flow.

There are some other important consequences of this conservation law. On the earth, both the Coriolis frequency and the depth of the ocean or atmosphere vary from place to place. Hence so does the background PV $(f/h)$. If a column of fluid moves from an area of high background PV to one of low background PV then the conservation law requires that the relative vorticity must increase. But this anti-clockwise rotation in turn forces adjacent fluid columns to move in such a way as to restore the column to its original level but slightly to one side. It will tend to overshoot due to inertia and an oscillation will develop which will always propagate with low background PV to the left. These waves are called topo-

graphic or planetary Rossby waves depending on whether change in topography or variation of the Coriolis frequency is the main restoring mechanism.

Lord Kelvin (Thompson, 1879) also investigated the properties of waves in rotating fluids. In particular, he found that wave motions were possible in the presence of a side boundary and a flat bottom. These "Kelvin" waves arise as a balance between the Coriolis acceleration and gravity on the surface and satisfy the same dispersion relation as external gravity waves, i.e.

$$\omega = k\sqrt{gD}, \tag{1.2}$$

where $D$ is the depth of fluid, $\omega$ is the frequency and $k$ the wavenumber. The distance that the Kelvin wave extends out to sea is $O(r_e) = O(\sqrt{gD}/f)$. This length is called the Rossby radius of deformation and it is an indication of distance over which the tendency of gravity to flatten the surface is balanced by the tendency of rotation to deform it. These waves, in common with Rossby waves, are unidirectional and always travel with the boundary to the right.

Stratification, whether due to temperature differences or salinity, adds an important dimension to the range of possible wave motions. One way of characterising the strength of the stratification in a fluid is to consider the frequency of oscillation of a fluid element displaced vertically from its equilibrium position. Brunt (1927) and Väisälä (1925) introduced the idea of this buoyancy frequency, sometimes known as the Brunt-Väisälä frequency, $N^2$ which is a function of depth and can be written

$$N^2(z) = -\frac{g}{\rho}\frac{d\rho}{dz}, \tag{1.3}$$

where $\rho(z)$ is the equilibrium density distribution. The larger $N^2$ is, the more stable the fluid. A negative $N^2$ implies that the fluid is unstable i.e. lighter fluid lying under heavier fluid.

The concept of potential vorticity, which is only really an expression of angular momentum divided by the volume, can be extended to stratified flow. It is straightforward in the linear cases and the general form was given by Ertel (1942). The quantity that is conserved is then called Ertel's potential vorticity. It has many of the same qualities as the potential vorticity mentioned above and reduces to it in the limit of barotropic flow.

In non-rotating flow stratification allows for the propagation of internal gravity waves and in rotating flow it allows "internal" Kelvin waves to propagate along a side boundary. These are similar in structure to the "external" Kelvin wave discussed above but have a sinusoidal structure in the vertical. Unlike the external Kelvin wave though, these do not require a displacement in the free surface to exist. If the buoyancy frequency, $N$, is constant they satisfy the dispersion relation

$$\omega = \frac{kND}{\alpha_n}, n = 0, 1, 2 \ldots, \tag{1.4}$$

where $\alpha_n$ are the solutions of $\alpha \tan \alpha = N^2 D/g$. These waves have a length scale out to sea of $O(ND/f)$ which is usually much smaller than the Rossby radius, $r_e$. In general, stratification reduces vertical movement and inhibits the vertical transmission of information. It also increases the horizontal speed of the waves.

In the vicinity of a coastal or continental shelf there are very large variations of depth. Because of the changes in the background potential vorticity, topographic Rossby waves would be expected to propagate along such a shelf. But, due to the stratification of the ocean at such a sharp change of depth, Kelvin waves would also be expected. Both types of wave are unidirectional and travel with the shelf to their right. Robinson (1964) considered the homogeneous problem and christened these waves "continental shelf waves" or "coastal trapped waves". They are "trapped" in the sense that, if the variation of the Coriolis frequency with longitude is negligible, there is no mechanism capable of transmitting energy away from the coastal wall and out to the open ocean. More grammatically perhaps, they are described as "coastally trapped waves" in later papers and in the remainder of this thesis.

Stratification can be added to this model in a number of ways. Allen (1975) and Mysak (1967) used various two-layer models while Wang and Mooers (1976) and subsequent authors used continuous stratification based on the concept of the buoyancy frequency $N^2(z)$. These continental shelf waves combine aspects of both Kelvin waves and topographic Rossby waves, and it is only in extreme cases that there is a clear distinction between the two limiting forms. The parameters determining the structure of the waves are simply the ratio of the topographic length scale $L$ (the width of the shelf) and the two important Kelvin wave length

scales. These are the "Burger" number $B = ND/fL$ and the ratio $a = r_e/L$ and will appear throughout this thesis. For depth profiles where $L \ll ND/f$ the shelf topography is unimportant and all waves are essentially baroclinic Kelvin modes.

The lack of analytical results has led to attention being focused mainly on numerical schemes to determine the frequency and structure. Huthnance (1978) and Brink and Chapman (1986) both developed two-dimensional grid methods to find these modes as functions of wavenumber, stratification and topography. A different approach (Middleton and Wright,1990, Johnson,1991) is to use asymptotic expansions in $B$ to find analytic results in certain extreme parameter regimes and for simple topographies. The work in Chapter 2 extends the use of asymptotic expansions to both extremes of $B$ and provides approximations that are valid for $B$ of order one.

A new numerical method is also introduced in the long-wave continuously stratified case. This uses a Green's function to reduce the two-dimensional partial differentiation problem to a one dimensional integral on the shelf. This greatly increases the accuracy and efficiency of the numerics over previous methods. The correlation between the numerics and the asymptotics is very good.

In a two-layer model, where there is a forced separation between the modes, Allen found that the different modes can "kiss" as the stratification changes. This occurs as the speed of the Kelvin wave approaches that of the first topographic mode. Instead of crossing they kiss and exchange characteristics. This is confirmed by the new numerical method but is found to occur only in some rather special cases.

Of course, these types of wave relying on both topography and stratification are not unique to coastal shelves. The same analysis can be applied to submerged ridges such as a mid-ocean scarp or to isolated features such as seamounts. Longuet-Higgins (1968) called the modes over a scarp "double Kelvin waves" and Rhines (1969a,b) considered the extension to isolated seamounts and other topography. In Chapter 3 similar analysis for the stratified case is performed and the numerical method extended for the infinite ridge case.

A complication arises as the stratification increases due to a singularity appearing in the solution at corners with an internal angle greater than $\pi$. Analysis

in §3.2 shows that the relevant governing equation in the immediate vicinity of a corner is the two-dimensional Laplace equation. If there is no influence from the other boundaries then the classical singular solution at a corner is valid. The boundaries will not influence the solution there if the vertical scale of the motion ($fL/N$) is much less than the depth i.e. $B \gg 1$. Some methods of solution however are not affected by the singularities. An example in §3.3 uses matched Fourier expansions for a ridge with a top-hat stepped profile. The sharp peak in the pressure gradients predicted arises even for quite moderate values of $B$.

This has implications for General Circulation Models (GCMs) that use simplified step topography. In §3.4 an example (Sherwin and Dale, 1992) of the inaccuracy of these models is shown. The frequency of a TRW around a sea mount is found semi-analytically using the same methods as in §3.3 and the results are analysed and compared to the output from a GCM. The model introduces large errors at the corners which lead to significant inaccuracies in the calculation of the frequencies of the waves.

There are two main problems to which this method has been profitably applied, the scattering of low-frequency energy as the topography changes (Johnson, 1989a) and the response of coastal waters to applied wind stress (Clarke and van Gorder, 1986). These theories rely mainly upon the orthogonality of the wave modes and only use the values of the pressure on the shelf. The numerical method introduced in §2.4 calculates only these values and has a much greater resolution on the shelf than was previously available. The modes calculated are also much closer to orthogonality. In §4.2 the isobath tracing result of Johnson (1989) is derived and some simple examples given.

The field of coastally trapped waves in the vicinity of East Australia has attracted a lot of attention since Hamon (1966) first detected their presence. More systematic observations made in the Australian Coastal Experiment (ACE) and reported by Freeland *et al* (1986) indicated that contrary to expectation significant amounts of low-frequency energy were emerging from the Bass Strait in form of CTWs. Whether these waves arise from wind forcing within the Strait itself or are transmitted waves that originated along the Great Australian Bight has been discussed by (among others) Buchwald and Kachoyan (1987) and Middleton and Viera (1991). Middleton (1991) attempts to resolve this question

by considering the scattering of CTWs through generalised straits by solving the barotropic equations. In §4.3 the isobath tracing result is applied to this geometry and magnitudes of the scattered modes are found without having to explicitly find the solution within the strait.

Another example, considered by Killworth (1989a,b) and Johnson (1989b, 1993) is the scattering caused by a ridge abutting a coastal shelf. Energy can either continue along the coast or be transmitted down the ridge. This more complicated question is tackled in §4.4.

Equations governing the CTW response to wind forcing were derived by Clarke and Van Gorder (1986) who used the orthogonality of the free modes to get a simple first order partial differential equation for the amplitudes. In practical applications of this theory Lopez and Clarke (1989) and Brink (1991) found that a large number of higher modes (up to 30) were needed to specify the alongshore velocities. This was previously impractical. The new method on the other hand accommodates accurate representation of these higher modes with ease. In §4.5 a simple example using harmonic wind stress is given to show the convergence of the pressure and alongshore velocity as more modes are added.

The crucial question concerning all hypothetical models is whether they bear any reference to actual motions in the oceans or atmosphere. The answer to that lies in the *stability* of the flow. Helmholtz (1888) recognised that instabilities would be important in causing vertical mixing and billow clouds in the atmosphere but it was Bjerknes (1937) who realised that the Hadley cell would be unstable to small longitude-dependent disturbances and so could not persist. Instabilities in geophysical flow have been divided up into two main categories, the baroclinic instability which is associated with vertical variations in the velocity and barotropic instability which is associated with horizontal variations. Because of the implied vertical shear in the Hadley cell, it would fall victim to baroclinic instabilities. Mathematical models for baroclinic instabilities were developed by Charney (1947) and Eady (1949). Barotropic instabilities were first considered by Rayleigh (1880) (in the non-rotating case) but their relevance to geophysical flow was only recognised by Lorenz (1972) who considered the stability of planetary Rossby waves in a westerly current.

Chapter 5 moves on to discuss in what circumstances these topographic waves

are stable. Huthnance (1978) showed that all coastally-trapped waves over a monotonic shelf with no background current are stable. Some calculations with different barotropic currents along a shelf were done by Collings and Grimshaw (1986). They found that some shear flows were made unstable by the topography but that most instabilities were just modifications of instabilities that would exist even without topography.

The more interesting case concerns a barotropic shear flow over a ridge. With no shear, waves can exist on both sides of a ridge and travel in opposite directions. The addition of the shear has two main effects: it changes the background potential vorticity upon which these waves depend and it advects the waves. This leaves the possibility that some waves will now travel in the opposite direction and, more importantly for the question of stability, that two waves on opposite sides of the ridge might be brought relatively to rest. As in Taylor (1931) who considered the instability of three layer stratified flow, this can be one of the main preconditions for instabilities to occur.

In the homogeneous limit the problem has a particularly simple form in terms of the barotropic streamfunction. Some necessary conditions for instability to occur are derived in §5.2 and some examples using linear shear are given in §5.4. The equations are also tractable in the long-wave low-frequency limit for the stratified case, §5.3.

These models are only approximately true for real flows. In the real world viscosity, friction, compressibility, thermal effects etc., all play a part in the overall flow. In this thesis it is assumed (except in §4.5) *a priori* that these effects are negligible and that the fluid is always incompressible i.e. that density is conserved by each fluid element. These assumptions are valid for most of the medium to large scale motions in the ocean.

In all the analysis that follows some common assumptions concerning the density and pressure are made. Firstly that the density and pressure fields are perturbations of their hydrostatic or equilibrium values. They can then be written $\rho^* = \rho_0(z)+\rho(\mathbf{x},t)$ and $p^* = p_0(z)+p(\mathbf{x},t)$ where the hydrostatic quantities satisfy $p_{0z} = -g\rho_0$. The second assumption is known as the "Boussinesq" approximation following Boussinesq (1903). In the horizontal momentum equations it is assumed that $\rho$ is negligible in comparison with $\rho_0$ which can be taken as a constant. In

the vertical momentum equations where $\rho$ is multiplied by $g$, full account of the departure from the equilibrium position is taken. The variation with depth of $\rho_0$ allows the introduction of the buoyancy frequency $N^2(z)$ in the density equation. This is generally valid in the oceans where $\rho_0$ does not vary from its mean by more than 2% (Gill, 1982).

The Coriolis frequency $f$ will be assumed constant and equal to $2\Omega \sin\theta_0$ where $\theta_0$ is the base latitude and $\Omega$ the angular speed of the earth. This is equivalent to assuming that the longitudinal length scale relevant for the motion $L$ is much less than $R\tan\theta_0$ where $R$ is the radius of the earth. This is valid for most oceanic flows outside the tropics.

To simplify further the equations of motion in a rational manner requires knowledge of the relative importance of the different terms. This can be found by non-dimensionalising the equations and making order of magnitude estimates.

In general *assume* that the horizontal velocities and lengths can be scaled on typical values $U$ and $L$, and that the vertical length scale is $D$, the depth of fluid. So that the pressure terms should match the Coriolis terms in the horizontal momentum equations, the perturbation pressure $p$ is scaled on $\rho_0 fUL$ to give

$$u_t + \left(\frac{U}{fL}\right)(\mathbf{u}.\nabla)u - v = -p_x, \tag{1.5a}$$

$$v_t + \left(\frac{U}{fL}\right)(\mathbf{u}.\nabla)v + u = -p_y, \tag{1.5b}$$

and where the time scale for the motion has be chosen as $1/f$. It is clear that the importance of the Coriolis terms compared with the inertial terms is measured by $Ro = U/fL$ the "Rossby" number.

In order that the perturbation density and pressure are of the same magnitude in the third momentum equation, the density is scaled on $\rho_0 fUL/gD$. The validity of the Boussinesq approximation is therefore equivalent to the condition that $Ro \ll a^2$. The scaling of the vertical velocity is determined by the density equation in order to bring the buoyancy frequency into the equations. Scaling $w$ then on $f^2UL/DN_0^2$, where $N_0$ is the maximum value of $N(z)$, gives

$$\left(\frac{f}{N_0}\right)^2 \frac{Dw}{Dt} = -p_z - \rho, \tag{1.5c}$$

$$\frac{D\rho}{Dt} - wN^2 = 0. \tag{1.5d}$$

where $D/Dt$ in this context is equal to $\partial/\partial t + Ro(u\partial/\partial x + v\partial/\partial y + B^{-2}w\partial/\partial z)$. This introduces the parameter $B = N_0 D/fL$ which is a measure of the relative importance of the stratification and the rotation. The remaining equation is the incompressibility condition

$$u_x + v_y + B^{-2}w_z = 0, \tag{1.5e}$$

If, in addition, the buoyancy frequency is much greater than the Coriolis frequency the hydrostatic approximation will be valid in (1.5c). This is equivalent to taking the vertical scale $D$ much less than the horizontal scale $L$ (since $f^2 N_0^{-2} = B^2(D/L)^2$) which is valid for almost all geophysical flows.

The density can be eliminated to give the the vertical velocity in terms of the pressure

$$w = -N^{-2}\frac{Dp_z}{Dt}. \tag{1.6}$$

The horizontal velocities can all be written in terms of the pressure

$$\begin{aligned} \left(\frac{D^2}{Dt^2} + 1\right) u &= -p_y - \frac{D}{Dt}p_x, \\ \left(\frac{D^2}{Dt^2} + 1\right) v &= p_x - \frac{D}{Dt}p_y. \end{aligned} \tag{1.7}$$

If the flow is such that $Ro \ll 1$, the "quasi-geostrophic" case, (1.5e) then gives the leading order governing equation for the motion as

$$p_{xx} + p_{yy} + B^{-2}\left(\frac{D^2}{Dt^2} + 1\right)\left(\frac{p_z}{N^2}\right)_z = 0. \tag{1.8}$$

This is the stratified counterpart of (1.1).

Some thought must be given to the boundary conditions on the surface and over topography. The conditions arise as a consequence of the requirement that all fluid particles on the surface or bottom remain there throughout the motion. Additionally, on a free surface the total pressure must be constant. Therefore on the bottom $z = -h$ the condition is

$$\frac{D}{Dt}(z + h) = uh_x + vh_y + B^{-2}w = 0, \ (z = -h) \tag{1.9}$$

On a free surface $z = \eta$, the equivalent condition is that

$$\frac{D}{Dt}(z - \eta) = RoB^{-2}w - \frac{D\eta}{Dt} = 0, \ (z = \eta) \tag{1.10a}$$

Integrate the hydrostatic relation over the depth and use the fact that the *total* pressure is constant on $z = \eta$ to get

$$\left(\frac{fUL}{gD}\right) p - \eta = \text{constant}, \ (z = \eta) \tag{1.10b}$$

Combine equations (1.10a,b) and assume that the disturbance of the free surface is small. Linearise about $z = 0$ and integrate along the surface to get

$$a^2 p_z + B^2 N(0)^2 p = 0, \ (z = 0) \tag{1.11}$$

The equations (1.8), (1.9), (1.11) form the basis for most of the work in this thesis. The scalings used are not always identical depending of course on the particular problem. The homogeneous equations (and 1.1) which are derived assuming a constant density can be recovered from the above by letting $B \to 0$ and expanding in an asymptotic series in powers of $B^2$.

To summarise the assumptions made so far; i) $L \ll R \tan\theta_0$, ii) $Ro \ll a^2$ and iii) $B^2(D/L)^2 = (f/N_0)^2 \ll 1$. In the oceans the depth $D$ ranges from 1–5km and in the mid-latitudes ($\theta_0 > 25^o$) the magnitude of the Coriolis frequency ranges from $7\text{x}10^{-5}s^{-1}$ to $1.4\text{x}10^{-4}s^{-1}$ at the poles. Hence the Rossby radius takes values ranging from 10,000km in the deep ocean to 150km in coastal waters. The motions in this thesis will therefore be assumed to have horizontal length scales much greater than the depth but satisfying the first condition, around 100–1000km. The Rossby number will generally be small and in a number of examples given later the Rossby radius will be taken as infinite, the rigid lid limit. Care though, must be taken in this limit because of the effect it has on the Kelvin wave dynamics.

# Chapter 2

# Coastally trapped waves

## §2.1 Introduction

This chapter concentrates upon the possible wave motions in coastal shelf regions. Large potential vorticity gradients coexist with significant amounts of stratification in such regions and hence both the topographic and buoyancy effects must be included in a realistic model. There is observational evidence for these waves in midlatitudes (see Mysak (1980) for a review) which suggests that they have periods of several days or more (compared with a Coriolis period of about 1/2–1 day). This implies that analysis in which the frequency of the waves is much smaller than the Coriolis frequency will still give physically meaningful results.

In the low-frequency/long-wave limit, Clarke (1976) showed that that waves are non-dispersive i.e. that the energy travels with the phase velocity, and that this limit is consistent with theories of atmospheric forcing by pressure systems with similar periods.

In addition to the barotropic shelf waves (BSWs) obtained by Robinson (1964), two-layer models allow the propagation of an internal Kelvin wave (IKW). An interesting feature of the results in Allen (1975) is the observation that, as stratification or alongshore wavenumber increase and the speeds of the internal Kelvin wave and barotropic waves approach each other, the modes "kiss" and exchange character. One mode deforms into the other over a very small range of $B$. The conditions for which this coupling occurs are discussed in §2.5.

For the continuously stratified case, Huthnance (1978) shows that there exists a countable infinity of discrete modes with frequencies $\omega_n < f$ decreasing to zero. All modes travel in the same direction ($k > 0$) and form a complete set. All pressure fields are therefore expressible as an infinite series of these modes. The fundamental mode is essentially the external Kelvin wave and has maximum phase speed. If the rigid lid approximation is used however, this mode is filtered out.

The difficulty of the analytical problem is mainly due to the fact that the eigenvalue, $\omega$, appears in both the governing equation and boundary conditions in a non-linear way. Analytical solutions have been found only for extreme parameter values with particularly simple topographies. Perturbation results for

large and small values of the stratification parameter, $B$, are obtained, for instance by Middleton and Wright (1990) and Johnson (1991). Analysis in §2.2 and §2.3 show how, in the low frequency limit, this can be systematically extended to give approximations for the eigenvalues and eigenvectors accurate over the whole range of $B$ using Padé approximations.

The numerical schemes employed by Huthnance (1978) (inverse iteration) and by Brink and Chapman (1985) (resonance response to arbitrary forcing term) while flexible in being able to deal with variable stratification, are indirect methods that require a two dimensional grid over the whole domain. The efficiency of these methods is reduced by the search procedure necessary and the restriction of obtaining only one mode at a time. The new method introduced in §2.4 reduces the problem by analysis from a two dimensional problem to a one dimensional eigenvalue problem involving only a line integral across the shelf which can then be reduced to a series of linear equations. This is done by using a Green's function, $G$, for the semi-infinite strip and can be used for any shelf topography, whether it is a piecewise linear approximation or a functional form. If the rigid lid approximation ($a \to \infty$) is valid and the stratification assumed to be uniform ($N(z) \equiv 1$) there is a neat closed form solution for $G$.

If a free surface or non-uniform stratification is required, $G$ can be found as an infinite series (Morse and Feshbach, 1953) with only a slight increase in computing time needed.

This method has the advantages both of vastly increased resolution and of directness and gives all the required modes simultaneously. The resolution of this method is much greater than in previous models and allows a more detailed examination of the waves, in particular their scattering is looked at in detail not previously seen (Chapter 4). Higher modes, as used in theories of wind-forced long waves (Clarke and Van Gorder, 1986), are dealt with much more efficiently than with previous methods (§4.5).

It is possible to extend this method to higher frequencies but as the frequency and wavenumber appear non-linearly the search procedure for finding the phase speed must be changed.

Section 2.5 contains results for various topographies and parameter values and where the conditions leading to kissing modes are plainly seen. Comparisons

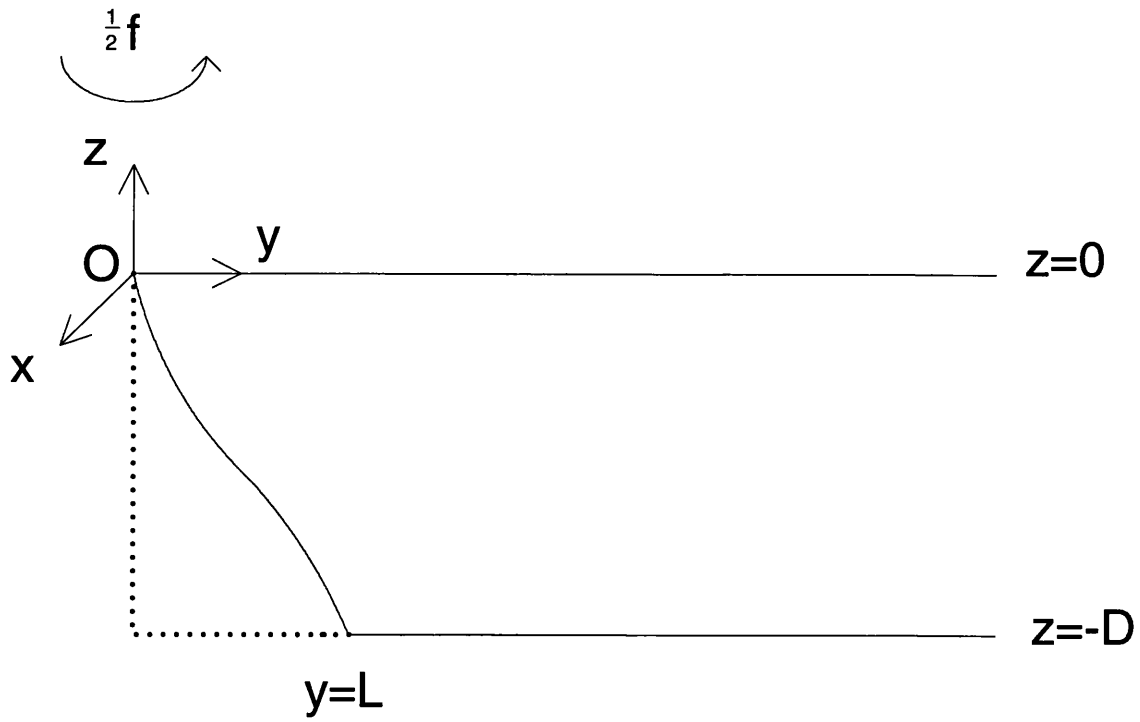


**Figure 2.1**: The domain $A$, with the $z$ coordinate vertically upwards, $y$ increasing out to sea, and $x$ the alongshore coordinate. The width of the shelf is $L$ and the open ocean depth $D$.

of the numerical method and the analytic asymptotic results confirm the accuracy of the numerics and of the Padé approximations. The effects of changing stratification, a free surface and an exponential buoyancy frequency profile are fully explored.

## §2.2 Equations of motion

Consider a semi-infinite ocean of depth $D$ bounded by a monotonic sloping shelf of width of order $L$ (fig. 2.1). Take Cartesian axes $Ox, Oy, Oz$ along the shelf, out to sea and vertically with the shelf profile depending on $y$ alone.

Let the flow be Boussinesq and incompressible with uniform Coriolis frequency $f$, total density $\rho_0(z)+\rho(\mathbf{x},t)$ and pressure $p_0(z)+p(\mathbf{x},t)$. Introduce the buoyancy frequency scaled with the constant $N_0$ chosen so the maximum value of $N(z)$ is unity. Use the same scalings as outlined in the introduction and look for small amplitude waves with (non-dimensional) frequency $\omega$ and wavenumber $k$. Omitting a common factor of $\exp(i\omega t - ikx)$ gives from (1.8) the non-dimensional governing equation

$$-k^2p + p_{yy} + (1-\omega^2)B^{-2}(N^{-2}p_z)_z = 0. \tag{2.2.1}$$

The boundary condition (1.11) at the free surface is

$$a^2p_z + B^2N^2(0)p = 0, \quad (z=0) \tag{2.2.2}$$

where $a = (gD)^{1/2}/fL$, the non-dimensional Rossby radius of deformation. If $z = -h(y)$ is the profile of the coastal boundary (alternatively $y = d(z)$) for $y \leq 1$, the vanishing of the normal velocity at the boundary implies

$$(\omega/B^2)w = -vh'. \quad (z = -h(y), y \leq 1)$$

Substituting in for $v, w$ gives

$$\begin{aligned}(1-\omega^2)cp_z &= -h'B^2N^2(p+cp_y), \quad (z=-h(y), y \leq 1)\\ p_z &= 0, \quad (z=-1, y>1)\end{aligned} \tag{2.2.3}$$

where $c = \omega/k$ is the phase speed. In the far field ($y \to \infty$) $p \to$*constant.*

Now consider the long wave solutions, taking the limit $\omega \to 0, k \to 0$ with $c = \omega/k$ fixed. These waves are non-dispersive satisfying (as in Clarke (1976) and Huthnance (1978) ),

$$p_{yy} + B^{-2}(N^{-2}p_z)_z = 0, \tag{2.2.4a}$$

with

$$h'N^2B^2(p+cp_y) + cp_z = 0, \quad (z=-h(y), y \leq 1), \tag{2.2.4b}$$

$$a^2p_z + B^2N^2(0)p = 0, \quad (z=0), \tag{2.2.4c}$$

$$p_z = 0, \quad (z=-1, y>1). \tag{2.2.4d}$$

The chief advantage of taking this limit is that the eigenvalue of the problem, $c$, now only appears linearly in the boundary condition.

The standard manipulation using Green's theorem shows that the eigenvalues and eigenfunctions are real, the eigenfunctions corresponding to distinct eigenvalues are orthogonal along the slope $z = -h(y)$ and hence can be made orthonormal satisfying $\int_{-1}^{0} p_n p_m \, dz = \delta_{nm}$. The eigenfunctions form a complete set for the expansion of pressure fields specified along the slope.

### §2.2.1 Strong stratification ($B \gg 1$).

Strong stratification suppresses large vertical motions and from (2.2.4$a$) introduces the dynamically important horizontal scale $N_0 D/f$, large compared to the shelf width $L$. On this scale the shelf appears as an almost vertical wall. Introduce the long length scale $Y = y/B$. Then (2.2.4) becomes

$$p_{YY} + (N^{-2} p_z)_z = 0, \tag{2.2.5$a$}$$

with

$$B^{-1} K d' p_z = N^2 (p + K p_Y), \quad \left(Y = B^{-1} d(z)\right), \tag{2.2.5$b$}$$

$$A^2 p_z + p = 0, \quad (z = 0), \tag{2.2.5$c$}$$

$$p_z = 0, \quad (z = -1, Y > 0), \tag{2.2.5$d$}$$

where $K = B^{-1} c$ and $A = B^{-1} a/N(0)$. Let $Z_n$ be the eigenfunctions and $\lambda_n$ the eigenvalues for the vertical structure, satisfying

$$(N^{-2} Z_n')' + \lambda_n^2 Z_n = 0, \tag{2.2.6$a$}$$

$$Z_n' = 0, \ (z = -1, Y > 0)$$

$$A^2 Z_n' + Z_n = 0. \ (z = 0) \tag{2.2.6$b$}$$

Then (2.2.5) has a separated solution of the form

$$p(Y, z) = \sum_{n=0}^{\infty} a_n e^{-\lambda_n Y} Z_n(z) \tag{2.2.7}$$

provided, from (2.2.5b)

$$N^2(z) \sum_{n=0}^{\infty} a_n (1 - K\lambda_n) e^{-\lambda_n d(z)/B} Z_n(z) = B^{-1} K d' \sum_{n=0}^{\infty} a_n e^{-\lambda_n d(z)/B} Z_n'(z). \tag{2.2.8}$$

Expanding $K, a_n$ and $e^{-\lambda_n d(z)/B}$ in terms of $B^{-1}$ and equating powers of $B^{-1}$ gives approximate solutions of successively higher order. Explicit examples are given in §2.3.

### §2.2.2 Weak stratification ($B \ll 1$)

For weak stratification $\omega \ll B \ll 1$ the flow is almost barotropic and solutions follow by expanding (2.2.4) as a series in $B$, writing

$$p(y,z) = p^{(0)} + B^2 p^{(1)} + B^4 p^{(2)} + \cdots \tag{2.2.9a}$$

$$c = c_0 + B^2 c_1 + B^4 c_2 + \cdots \tag{2.2.9b}$$

The expansion proceeds straightforwardly for arbitrary stratification and Rossby radius, $a$, but for definiteness $N(z)$ is taken here to be unity and $a$ to be of order one. Then

$$p_{zz}^{(0)} = 0,\ p_{zz}^{(n)} = -p_{yy}^{(n-1)},\ n \geq 1, \tag{2.2.10a}$$

$$p_z^{(0)} = 0,\ a^2 p_z^{(n)} = -p^{(n-1)},\ (z=0),\ n \geq 1.$$

$$p_z^{(n)} = 0,\ (z=-1, y>1),\ n \geq 0. \tag{2.2.10b}$$

The vertical dependence of the pressure field then follows as

$$p^{(0)} = \phi_0(y),$$

$$p^{(1)} = \phi_1(y) - \frac{1}{a^2} z\phi_0(y) - \frac{1}{2} z^2 \phi_0''(y),$$

and in general

$$p^{(n)} = \sum_{r=0}^{n} \sum_{i=0}^{r} \binom{r}{i} \frac{(-1)^r z^{i+r}}{(i+r)!\ a^{2(r-i)}} \phi_{n-r}^{2i} \tag{2.2.11}$$

where the $\phi_i$ are functions of $y$ alone. The governing equation for each $\phi_i$ comes from expanding the lower boundary condition (2.2.4b) in $B$ and substituting the expression (2.2.11) for the pressure terms.

Two boundary conditions are needed in order to solve for the $\phi_n$, one at $y = 0$ and one at $y = 1$. At $y = 0$, if there is a finite slope at the origin then the pressure must be bounded, however if the wall is vertical near the origin, a no flux condition is necessary. i.e. $p + cp_y = 0$ on $y = 0$. This condition though, cannot be satisfied by any order higher than the first. This implies the existence of a $O(B)$ boundary layer against the vertical wall. The correct boundary condition is then no *net* flux along the wall.

The condition at $y = 1$ is slightly more problematic. In the rigid lid limit consider a circuit $\Gamma$ around the domain which consists of the top and the bottom

boundaries, the vertical line $y = 1-\epsilon$ and which is closed at infinity. The integral of the normal derivative of $p$ around $\Gamma$ is identically zero from Green's theorem. Using the boundary conditions, letting $B \to 0$ and then letting $\epsilon \to 0$ gives

$$\int_{-1}^{0} \frac{dp}{dy}\, dz = 0, \ (y = 1) \tag{2.2.12}$$

which is satisfied at each order. However for finite $a$ this procedure only provides a matching condition to the exponentially decaying solution for $y > 1$. Change the circuit $\Gamma$ to the lines $y = 1-\epsilon$, $y = 1+\epsilon$ and the top and bottom boundaries, and follow the same limiting process to get instead of (2.2.12)

$$\int_{-1}^{0} \frac{d}{dy} p^{inner}\, dz = \int_{-1}^{0} \frac{d}{dy} p^{outer}\, dz, \ (y = 1). \tag{2.2.13}$$

Another matching condition is required to eliminate the outer solution. The net flux across $y = 1$ must be equal on both sides and hence

$$\left[ \int_{-1}^{0} cp_y + p\, dz \right]_{y=1} = 0. \tag{2.2.14}$$

These conditions expanded in a series in $B$ are enough to determine the $\phi(y)$ at all orders. It has been assumed that $h(1) = 1$, if there is a discontinuity in the topography the matching conditions can be altered accordingly.

## §2.3 Asymptotic solutions

**Profile 1.** Let the stratification be uniform, ($N(z) \equiv 1$), the surface rigid $a \gg 1$, and the shelf have the linear profile

$$h(y) = y, \quad y \leq 1 \text{ or } d(z) = -z, \quad -1 \leq z \leq 0. \tag{2.3.1}$$

*a. Strong Stratification*

Equations (2.2.6) can be solved readily to give $\lambda_n = n\pi$ and $Z_n = \sqrt{2}\cos n\pi z$ normalised so that

$$\int_{-1}^{0} Z_n Z_m\, dz = \begin{cases} 1, & \text{if } n = m; \\ 0, & \text{otherwise.} \end{cases} \tag{2.3.2}$$

Expanding (2.2.8) as indicated with $K = K_0 + B^{-1}K_1 + B^{-2}K_2 + \ldots$ and $a_n = a_n^0 + B^{-1}a_n^1 + \ldots$ for each $n$, multiplying by $Z_n$ and integrating with respect to $z$, gives equations for the eigenvalues and the coefficients $a_n$. The lowest order equation gives

$$a_n^0(1 - K_0 n\pi) = 0, \ \forall n \tag{2.3.3}$$

If $K_0 \neq 1/n\pi$ for some $n$ then the solution is identically zero, so for a non-trivial solution, the $m$th eigenfunction has $K_0 = 1/m\pi$ with $a_r^0 = 0 \ \forall r \neq m$. The undetermined coefficients can be found by requiring that the pressure is normalised so that $\int_{-1}^{0} p^2(d(z), z)dz = 1$. Thus the lowest order solution is $p^{(m)}(y, z) = a_m^{(0)}\sqrt{2}e^{-m\pi y/B}\cos m\pi z$, with speed $c^{(m)} = B/m\pi$, which is precisely the $m$th mode IKW. The first deviation from this mode is given by the next term

$$\sum_{n=0}^{\infty} a_n^1(1 - K_0 n\pi)\cos n\pi z = a_m^0(\sin m\pi z + K_1 m\pi \cos m\pi z). \tag{2.3.4}$$

Multiplying by $Z_m(z)$ and integrating gives $K_1 = 0$ and multiplying by $Z_r(z)$, $r \neq m$ implies

$$a_r^1 = \begin{cases} 0, & \text{if } m + r \text{ is even;} \\ -2a_m^0/\pi m, & \text{if } r = 0, m \text{ odd;} \\ -4m^2 a_m^0/\pi(m - r)(m^2 - r^2), & \text{otherwise.} \end{cases} \tag{2.3.5}$$

This gives the first order solution. The second correction follows from the order $B^{-2}$ equation

$$a_m^0 m\pi(z\sin m\pi z + K_2\cos m\pi z) = \sum_{n=0}^{\infty}(1 - \frac{n}{m})\cos n\pi z(a_n^1 n\pi z + a_n^2) + \frac{n}{m}a_n^1 \sin n\pi z \tag{2.3.6}$$

as

$$K_2 = \frac{1}{2m\pi} - \sum_{\substack{n=0 \\ n+m \text{odd}}}^{\infty} \frac{16nm}{\pi^3(m + n)^3(m - n)^2}. \tag{2.3.7}$$

Further terms follow straightforwardly. For the present example the first three eigenfunctions are

$$p(y, z) = \sqrt{2}\left(a_m^0 + \frac{a_m^1}{B}\right)e^{-m\pi y/B}\cos m\pi z + \frac{\sqrt{2}}{B}\sum_{\substack{n=0 \\ n\neq m}}^{\infty} a_n^1 e^{-n\pi y/B}\cos n\pi z + O(B^{-2}),$$

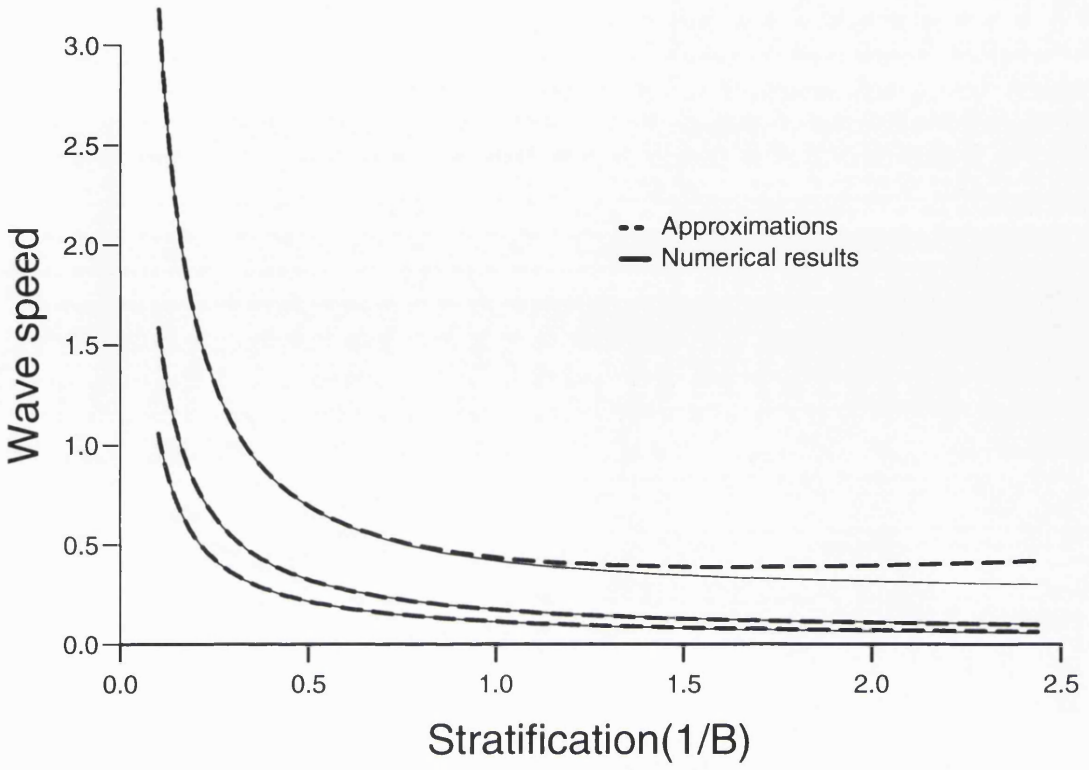


**Figure 2.2**: The comparison of the numerical results and the approximate wave speeds for profile 1. This is the strong stratification limit, $0 < B^{-1} < 2.5$ accurate to $O(B^{-1})$.

$$\text{for } m = 1, 2, 3. \tag{2.3.8}$$

with speeds (fig.2.2)

$$c^{(1)} = 0.3183B + 0.1185B^{-1} + O(B^{-2}),$$

$$c^{(2)} = 0.1592B + 0.01422B^{-1} + O(B^{-2}),$$

$$c^{(3)} = 0.1061B + 0.008124B^{-1} + O(B^{-2}). \tag{2.3.9}$$

*b. Weak Stratification*

For the linear shelf profile (2.3.1), (2.2.4b) for the nth function becomes

$$\phi_n + c_0(y\phi_n')' = \sum_{r=1}^{n} \left\{ \frac{(-1)^{r+1}}{(2r)!} y^{2r} \phi_{n-r}^{2r} + \sum_{i=0}^{r} c_{r-i} \frac{(-1)^{i+1}}{(2i+1)!} (y^{2i+1} \phi_{n-r}^{2i+1})' \right\} \tag{2.3.10}$$

a non-homogeneous Bessel equation of order zero. The solution must remain finite at the origin and at the open ocean satisfy

$$\sum_{r=0}^{n} \frac{(-1)^r}{(2r+1)!} \phi_{n-r}^{2r+1}(1) = 0.$$

The first term satisfies

$$\phi_0 + c_0\phi_0' + c_0 y\phi_0'' = 0,\ 0 \le y \le 1 \qquad (2.3.11a)$$

with (from 2.2.12)

$$\phi_0'(1) = 0, \qquad (2.3.11b)$$

and $\phi_0$ bounded at the origin. This is the barotropic solution, which can be written (up to a constant multiple) as

$$\phi_0(y) = J_0(2\sqrt{y/c_0}),\ 0 \le y \le 1 \qquad (2.3.12)$$

where $J_0(x)$ is the zeroth Bessel function. The boundary condition implies that $2/\sqrt{c_0}$ is a zero of $J_1(x)$ and that therefore the first three modes have wave speeds

$$c_0^{(1)} = 0.2724, c_0^{(2)} = 0.08127, c_0^{(3)} = 0.03865. \qquad (2.3.13)$$

Subsequent solutions follow by variation of parameters. This gives the first correction to the pressure for finite $B$ as

$$EJ_0(2\sqrt{y/c_0}) + \int_0^1 ds\ P(s) \begin{cases} Y_0(2\sqrt{s/c_0})J_0(2\sqrt{y/c_0}), & y < s \\ Y_0(2\sqrt{y/c_0})J_0(2\sqrt{s/c_0}), & y > s \end{cases} \qquad (2.3.14)$$

where $P(s) = (\pi/c_0^2)((c_1 - s/3)\phi_0(s) - c_0 s\phi_0'(s)/3)$, $E$ is an arbitrary constant to be determined by normalisation, and

$$c_1 = \frac{c_0}{3} + \frac{c_0^2}{24\phi_0^2(1)} \int_0^{2/\sqrt{c_0}} J_0^2(z) z^3 dz. \qquad (2.3.15)$$

Evaluating (2.3.15) and combining it with (2.3.13) gives (fig.2.3)

$$\begin{aligned} c^{(1)} &= 0.2724 + 0.2019B^2 + O(B^4), \\ c^{(2)} &= 0.08127 + 0.1382B^2 + O(B^4), \\ c^{(3)} &= 0.03865 + 0.1240B^2 + O(B^4). \end{aligned} \qquad (2.3.16)$$

Higher orders follow similarly.

*c. Arbitrary stratification*

The strong and weak stratification results can be combined efficiently into an approximation to the eigenvalue valid for all values of $B$ by introducing the two point Padé approximation of the form

$$c = \frac{\alpha_0 + \alpha_1 B + \cdots + \alpha_n B^n}{\beta_0 + \beta_1 B + \cdots + \beta_m B^m}. \qquad (2.3.17)$$

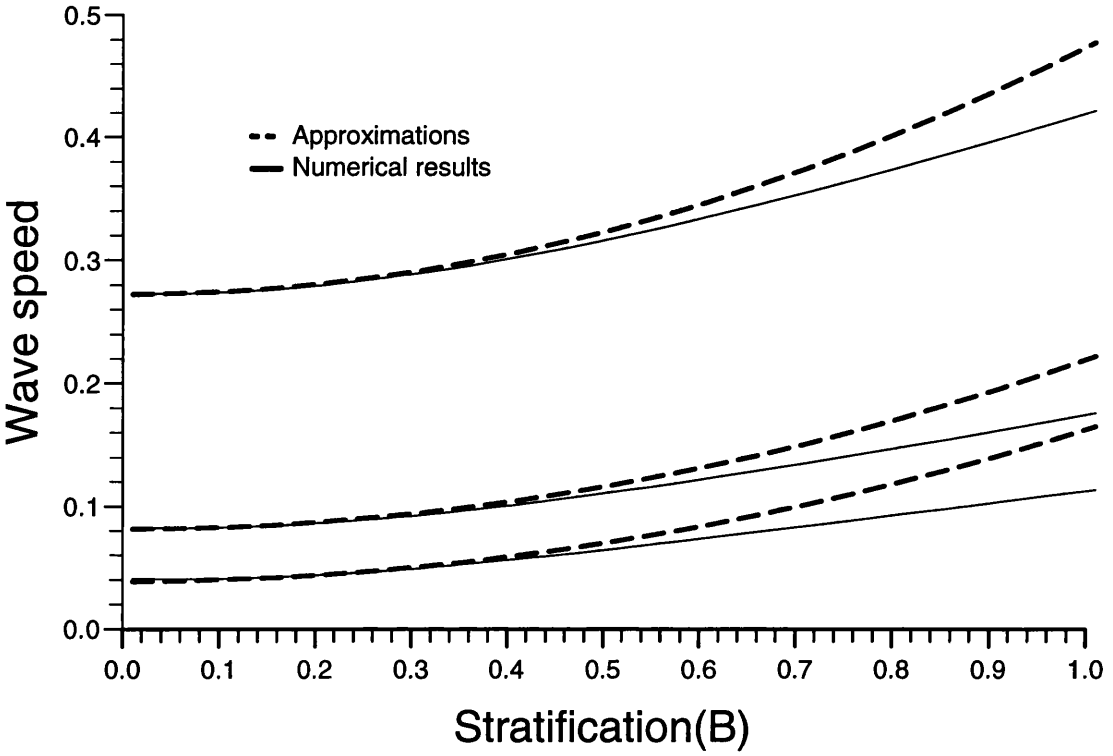


**Figure 2.3**: The comparison of the numerical results and the approximate wave speeds for profile 1. This is the weak stratification limit, $0 < B < 1.0$ accurate to $O(B^3)$. As in the previous figure the asymptotic results are good for surprisingly high values of the expansion parameter

The coefficients $\alpha_i, \beta_i$ are chosen so that the values for c coincide with the previous approximation in the limits $B \to 0, B \to \infty$ and the orders $n, m$ are chosen to accord with the number of known derivatives at the limits. Although convergence is guaranteed at either end, it is by no means sure that the approximation will remain finite for all $B$. Putting in extra coefficients that cannot be determined by the number of known derivatives, introduces a degree of arbitrariness which can be used to ensure there are no zeros in the denominator while still keeping the same accuracy at either end.

For large $B$ the eigenvalues $c$ increase as $B$ and for small $B$ approach a constant. In the above example the first three terms are known for both large and small $B$, thus consider the approximation

$$c = \frac{\alpha_0 + \alpha_1 B + \alpha_2 B^2 + \alpha_3 B^3}{1 + \beta_1 B + \beta_2 B^2}. \tag{2.3.18}$$

Expanding this and matching the various terms gives results accurate to $O(B^2)$ for small $B$ and to $O(B^{-2})$ for large $B$, hence

$$c^{(1)} \approx \frac{0.2724 + 0.4687B + 0.5477B^2 + 0.4041B^3}{1 + 1.7208B + 1.2695B^2}. \tag{2.3.19}$$

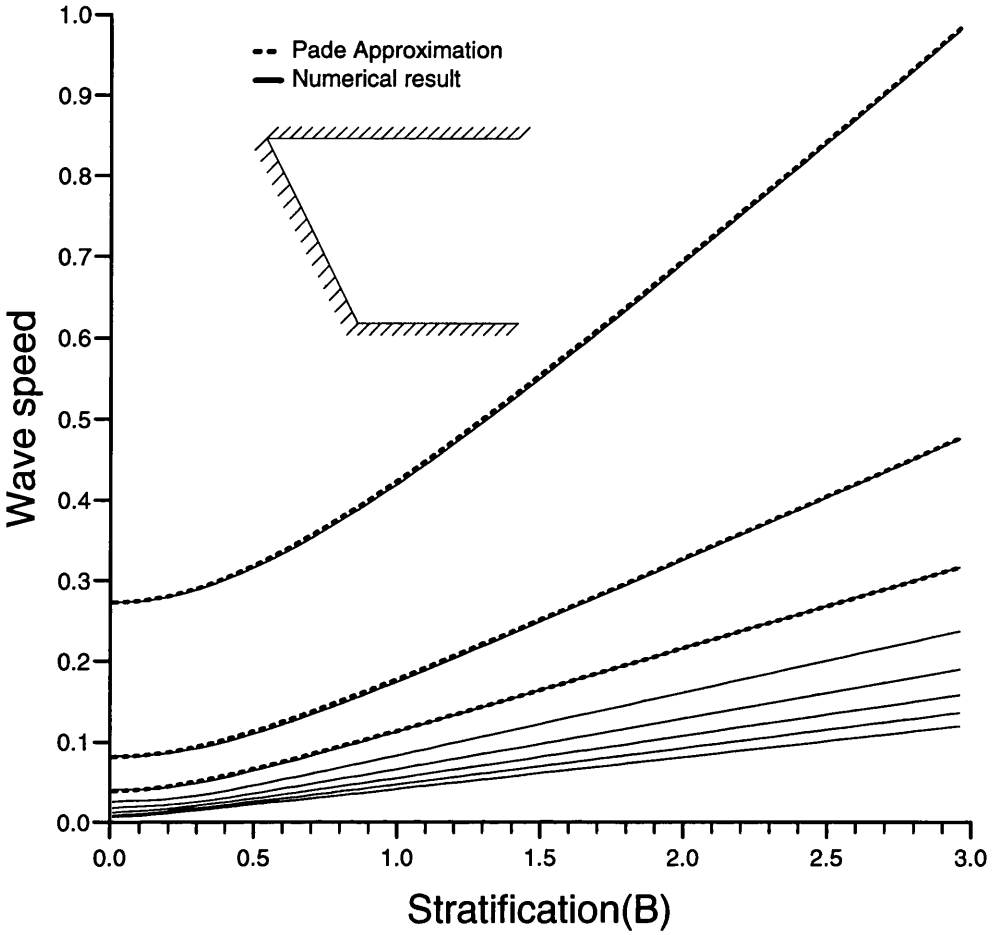


**Figure 2.4**: The first few numerically computed wave speeds and the Padé approximations for profile 1 for increasing stratification, $B$, 0.01-3.0. There is a smooth transition from the barotropic shelf wave modes at small $B$ to the baroclinic IKW modes for large $B$. The waves speeds are almost linear in $B$ for values of the stratification greater than unity and so all wave modes are essentially IKWs after that point. The Padé approximations are correct to third order at both ends. The relative error is around 1% for the first mode and only slightly more for the next two.

Figure 2.4 shows the first three Padé approximations compared with the numerically computed values for a range of $B$.

The pressure at any point can also be expressed in a Padé approximation. For small $B$, $p(y,z) = p^{(0)}(y) + B^2 p^{(1)}(y,z) + O(B^4)$ and for large $B$, $p(y,z) = p_\infty^{(0)}(y,z) + B^{-1} p_\infty^{(1)}(y,z) + O(B^{-2})$. The approximation will now depend on $y, z$ as well as $B$. Keeping this approximation finite for all $y, z$ *and* $B$ is more difficult than for the phase speed but one solution is to take $n$ and $m$ large enough so that all the $\beta_i$ are arbitrary and can be chosen appropriately. As the pressure is completely determined by its value on the shelf, only values there have to be considered.

**Profile 2.** Let the stratification be uniform, ($N(z) \equiv 1$), the surface rigid, ($a \gg 1$) and the shelf have the profile

$$h(y) = (y+1)/2, \quad y \leq 1 \text{ or } d(z) = -2z - 1, \quad -1 \leq z \leq -1/2. \tag{2.3.20}$$

The analysis for this profile is similar to that above so only differences are noted.

For strong stratification, changing to this profile makes no difference to the $O(B)$ term but the second order equation for the $m$th eigensolution,

$$a_m^0 K_1 m^2\pi^2 - \sum_{n=0}^{\infty} a_n^1 (m-n)\pi Z_n(z) = \begin{cases} 0, & -1/2 < z < 0 \\ 2a_m^0 Z_m'(z), & -1 < z < -1/2 \end{cases} \tag{2.3.21}$$

introduces an $O(1)$ term of $-2/m^2\pi^2$ to the eigenvalues of the odd numbered modes. The $O(B^{-1})$ terms proceed similarly but it is noticeable that the forms for even and odd modes are quite distinct.

If $B$ is small there are obviously more alterations. Firstly, the boundary condition at $y = 0$ is a no net flux condition at the coastal wall, i.e. $\int_{-1/2}^{0} p + cp_y \, dz = 0$ on $y = 0$. The governing equation for the $\phi_n(y)$ changes to

$$\phi_n + c_0\phi_n' + c_0(y+1)\phi_n'' = F(\phi_0, \ldots, \phi_{n-1}, y), \quad n = 0, 1, \ldots. \tag{2.3.22}$$

where $F$ is a complicated function similar to the RHS of (2.3.10) and remains a non-homogeneous Bessel equation of zero order. (In fact all piecewise linear profiles give a variation of the Bessel equation.) The homogeneous, barotropic equation has solutions $J_0(2\sqrt{(y+1)/c_0})$ and $Y_0(2\sqrt{(y+1)/c_0})$, $\phi_0(y)$ is a linear combination of these two functions and $c_0$ arises as a solution of a transcendental equation derived from the two boundary equations. The procedure for higher orders is the same as previously and $c_1$ appears in an analogous way. There are IKWs existing for small $B$ which are not found by this procedure because they exist on much smaller scales. Rescaling to consider distances of $O(B)$ from the coast straightforwardly gives first order solutions. The phase speeds are of course simply $B/2m\pi$, $m = 1, 2, \ldots$ and the eigenfunctions $e^{-2m\pi y/B} \cos 2m\pi z$.

Approximations valid for all $B$ can be obtained by introducing Padé approximations as before. Figure 2.5 shows the comparisons between the these and the numerically generated results. This will be discussed more fully in §2.5.

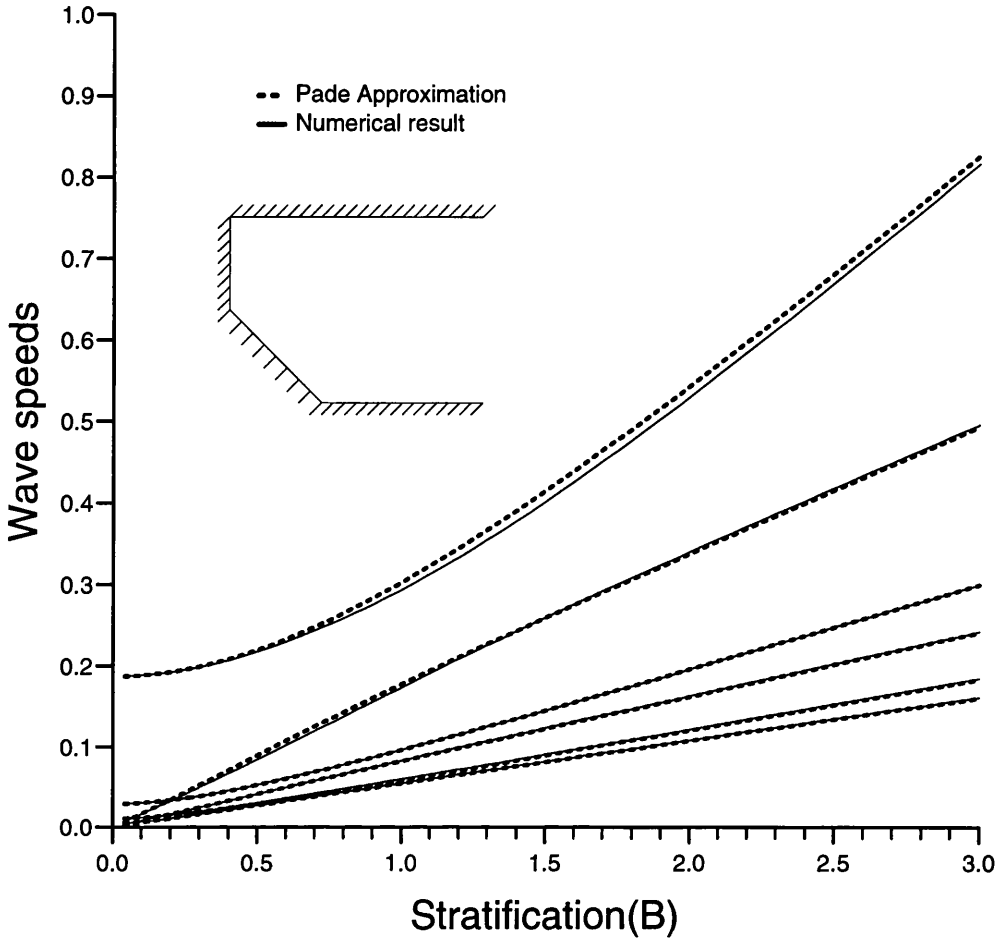


**Figure 2.5**: The first few numerically computed wave speeds and the Padé approximations for profile 2 for increasing stratification, $B$, 0.01-3.0. There is no longer a smooth transition from the barotropic shelf wave modes at small $B$ to the baroclinic IKW modes for large $B$. Hence the Padé approximations cannot fully capture the behaviour of the modes. However away from the "kiss" the accuracy is very good.

## §2.4 Numerical Method

The numerical method presented here relies upon an integral representation of (2.2.4). This requires that a Green's function is found that satisfies (2.2.4a) everywhere except at a point $y_0, z_0$. The divergence theorem then gives an expression for $p(y_0, z_0)$ in terms of an integral along the shelf. The Green's function, $G(\mathbf{r}|\mathbf{r_0})$, does *not* have to satisfy the boundary condition on the shelf, only the conditions on $z = 0, z = -1$. Rescale 2.2.4 by setting $z' = Bz$ and $H(y) = Bh(y)$. Drop the primes to get

$$\mathcal{L}\{p\} = p_{yy} + \left(\frac{p_z}{N^2}\right)_z = 0, \qquad (2.4.1a)$$

$$H'p + c(H'p_y + N^{-2}p_z) = 0, \quad (z = -H(y))$$

or

$$m(y)p - c\mathbf{P}.\mathbf{n} = 0, \quad (z = -H(y)) \tag{2.4.1b}$$

where $\mathbf{P} = (p_y, p_z/N^2)$, $\mathbf{n}$ is the outward normal vector to the slope and $m(y) = H'/\sqrt{1+H'^2}$. The top boundary condition is now

$$a^2 p_z + BN^2(0)p = 0, \quad (z = 0) \tag{2.4.2}$$

For uniform stratification and a rigid lid ($a \gg 1$) a closed form solution for $G(\mathbf{r}|\mathbf{r_0})$ can be found. The function now satisfies Poisson's equation

$$\nabla^2 G = 2\pi\delta(\mathbf{r} - \mathbf{r_0}), \tag{2.4.3}$$

with no normal derivative on $z = 0, -B$. Use the conformal map $w = \sinh(\pi z/B)$ to transform the infinite strip into the half plane. Find $G(\mathbf{r}|\mathbf{r_0})$ by using the method of images to get the fundamental solution

$$G(\mathbf{r}|\mathbf{r_0}) = \log|\sinh\frac{\pi}{2B}(y - y_0 + i(z - z_0))\sinh\frac{\pi}{2B}(y - y_0 + i(z + z_0))|. \tag{2.4.4}$$

This solution behaves like $\pi y/B$ as $y \to \infty$ so subtract $\pi(y + y_0)/B$ from (2.4.4) to get a more appropriate $G(\mathbf{r}|\mathbf{r_0})$.

If the solution for non-uniform stratification and/or a free surface is required then $G(\mathbf{r}|\mathbf{r_0})$ must be found as an infinite series. The $z$-dependence of the homogeneous solution of (2.4.1) can be expressed in terms of orthonormal eigenfunctions $Z_n$ that satisfy

$$(N^{-2}Z_n')' + \lambda_n^2 Z_n = 0, \tag{2.4.5a}$$

$$Z_n' = 0, \ (z = -B) \tag{2.4.5b}$$

$$a^2 Z_n' + BN^2(0)Z_n = 0. \ (z = 0) \tag{2.4.5c}$$

Expand $G(\mathbf{r}|\mathbf{r_0})$ and the $\delta$ function as a series of $Z_n$, i.e.

$$G = \sum_{n=0}^{\infty} F_n(y)Z_n(z), \qquad \delta(\mathbf{r} - \mathbf{r_0}) = \sum_{n=0}^{\infty} \delta(y - y_0)Z_n(z_0)Z_n(z), \tag{2.4.6}$$

where the functions $F_n$ must satisfy the non-homogeneous ordinary differential equations

$$F_n'' - \lambda_n^2 F_n = 2\pi Z_n(z_0)\delta(y - y_0),\ n = 0, 1, 2 \ldots \tag{2.4.7}$$

Use the method of variation of parameters and the conditions that each $F_n(y)$ is bounded as $y \to \infty$ and $F_n'(0) = 0$ to get that

$$F_n(y) = -\pi(e^{-\lambda_n(y+y_0)} + e^{-\lambda_n|y-y_0|})Z_n(z_0)/\lambda_n,\ n = 0, 1, 2 \ldots \tag{2.4.8}$$

and therefore

$$G(\mathbf{r}|\mathbf{r_0}) = -\sum_{n=0}^{\infty} \frac{\pi}{\lambda_n}(e^{-\lambda_n(y+y_0)} + e^{-\lambda_n|y-y_0|})Z_n(z_0)Z_n(z), \tag{2.4.9}$$

as the analogue to (2.4.4). This has exponentially small behaviour as $y \to \infty$ so long as $\lambda_n \neq 0$ for any $n$, (true for any finite $a$). The divergence theorem gives

$$\int\int_A p\mathcal{L}\{G\} - G\mathcal{L}\{p\}\ dA = \int_S (p\mathbf{G} - G\mathbf{P}).\mathbf{n}\ ds \tag{2.4.10}$$

where $S$ is the boundary around the domain $A$ and $\mathbf{G} = (G_y, G_z/N^2)$. As $\mathcal{L}\{p\} = 0$ in $A$ and $\mathcal{L}\{G\} = 0$ everywhere except the point $(y_0, z_0)$, the LHS reduces to $\pi_m p_0$, where $p_0 = p(y_0, z_0)$ and $\pi_m$ is equal to $2\pi$ if the point $(y_0, z_0)$ is an interior point. If the point is on the boundary then $\pi_m$ corresponds to the interior angle at the boundary ($\pi$ if the gradient is continuous there) or twice that angle if the point is on the bottom. This is because the singularity at the image point coalesces with that at the source point. In the free surface case, if the point is on $z = 0$ the value of $\pi_m$ will depend non-trivially on the value of $BN(0)/a$.

There is no contribution from the top or bottom boundaries as $p$ and $G(\mathbf{r}|\mathbf{r_0})$ satisfy the same boundary conditions there. Also $p_y \to 0$ and $G_y \to 0$ as $y \to \infty$. Substitute the boundary condition on $C$(the shelf) to eliminate $\mathbf{P}$, so that

$$\int_C pGm\ ds = c\left\{\int_C p\mathbf{G}.\mathbf{n}\ ds - \pi_m p_0\right\}. \tag{2.4.11}$$

This gives the pressure anywhere in the fluid in terms of the pressure on the shelf. If $\mathbf{r_0}$ is on the boundary though, singularities occur in the line integrals. They

can in fact be removed to give

$$\int_C (p-p_0)Gm\ ds + p_0 \int_C Gm\ ds = c\left\{\int_C (p-p_0)\mathbf{G}.\mathbf{n}\ ds - \frac{p_0}{N^2(0)}\int_{TOP} G_z\ dy\right\}. \tag{2.4.12}$$

The integral along the top is equal to zero in the rigid lid case. If there is a free surface, consideration of Green's theorem around the circuit $z=0, y=0, z=-b, y\to\infty$ shows that the integral is $2\pi$, provided that $(y_0,z_0)$ is not the origin. In that case the integral is found by summation.

As the line integrals are now bounded they can be evaluated using Simpson's Rule with $N$ intervals. This will give an equation for $p_0$ in terms of $p_i, i=1,N+1$, where $p_i$ is the value of $p$ at the ith end point $\mathbf{r_i}=(y_i,z_i)$. As $dz=-m(y)ds$, the integration can be made with respect to $z$ on $[-B,0]$. Choosing the point $(y_0,z_0)$ as each end point successively leaves $N+1$ distinct equations. For $j=1,N+1$

$$c\left\{p_j\left(h\sum_{i=1,i\neq j}^{N+1}\epsilon_i D_{ij}+H_j\right)-h\sum_{i=1,i\neq j}^{N+1}\epsilon_i p_i D_{ij}\right\}= p_j\left\{h\sum_{i=1,i\neq j}^{N+1}\epsilon_i G_{ij}-F_j\right\}-h\sum_{i=1,i\neq j}^{N+1}\epsilon_i p_i G_{ij}, \tag{2.4.13}$$

where $D_{ij}=\mathbf{G}(\mathbf{r_i}|\mathbf{r_j}).\mathbf{n}/m(y_i)$, $F_i=\int_C G(\mathbf{r}(z)|\mathbf{r_i})\ dz$, $G_{ij}=G(\mathbf{r_i}|\mathbf{r_j})$, $H_i=0$ if there is a rigid lid or $H_i=2\pi, i>0$ if there is a free surface, $\epsilon_i$ are the Simpson's rule coefficients and $h$ is the step size. The orthogonality condition is $\sum h\epsilon_i p_i^{(n)} p_i^{(m)}=0$ for distinct $n,m$. Multiply (2.4.13) by $\epsilon_j$ to ensure that the RHS is symmetric in $i$ and $j$. This is a complete $N+1\times N+1$ general eigenvalue problem $\mathrm{A}\mathbf{p}=c\mathrm{B}\mathbf{p}$, $\mathbf{p}=(p_1,p_2,\ldots,p_{N+1})$, where A is a real symmetric matrix and B is a real matrix. The problem of finding the form and speed of low-frequency coastally-trapped waves has been reduced to a linear eigenvalue problem that can be solved using standard algorithms.

For typical oceanic values of $a\approx 10$, the modes are not significantly changed from the rigid lid case. The fundamental external Kelvin wave mode (conventionally mode 0), which depends on finite Rossby radius for its existence, is not present but in any real situation travels much faster than the other modes.

The integral formulation extends to non-zero wavenumbers directly. The governing equation is then Helmholtz's equation. If $z$ is rescaled in (2.2.1) as in (2.4.1), the $Z_n$ are the same as those found above. The Green's function has

exactly the same form as (2.4.9) except that the combination $\sqrt{k^2+(1-\omega^2)\lambda_n^2}$ appears everywhere instead of $\lambda_n$. Equation (2.4.11) follows immediately with the vector $\mathbf{G} = (G_y, (1-\omega^2)G_z/N^2)$. The singularities can be removed as before but an extra term now appears on the RHS of (2.4.12). Equation (2.4.13) follows but with the term $H_j$ now equal to $\pi_m - \int_C \mathbf{G}.\mathbf{n}ds$ which can be evaluated numerically.

However the matrices that result now depend on the values of $\omega$ and $k$ themselves. The eigenvalue problem is no longer linear and so a different search pattern has to be used. Since all the eigenvalues are real, one technique would be to fix $k$ and find all the zeroes of $f(\omega) = \det(kA - \omega B)$. This is more time-consuming than in the low-frequency case but the advantages of increased resolution, directness and one-dimensionality are maintained. This is especially true if some estimate of the frequency and wavenumber is known.

To test the model, consider the case where the shelf is vertical. With a rigid lid the eigenvalues are simply $B/n\pi, n = 1, 2 \ldots$. The numerical results are accurate to 3 decimal places with 20 intervals along the shelf and to 4 decimal places with 40 intervals. Figures 2.2, 2.3 show the comparison with the expansions drawn from the results of the previous section and it is clear that the correspondence is excellent for $B \leq 0.5$ and $B^{-1} \leq 0.7$, the limits of the accuracy of the expansions.

Though not as immediately versatile as the suite of programs developed by Brink and Chapman, the fact that analysis has reduced the problem to only one dimension does allow greater definition and accuracy. It is possible to obtain all possible eigenvalues for a particular case at the same time, an improvement which allows fuller investigation of modes and their scattering. There is also a large increase in resolution over the previous methods for an equivalent number of points. For example, most of the results have been arrived at using 50–60 points across the shelf, while the Brink and Chapman programs use a fixed 17x25 point grid which extends to the far field boundary condition. This implies they have at most 12–13 points across the shelf and so do not resolve any mode higher than mode 6. Higher modes require extra points which the new method accommodates much more efficiently.

For a typical problem, this method takes 6.4 seconds of CPU time for 3 sig. figs. accuracy or 11.5 seconds (4 sig. figs.) for all the eigenvalues, while the Brink

and Chapman program,"BIGLOAD", takes around 39.5 seconds ( 3 sig.figs.) or 67.6 seconds (4 sig.figs.) for only the first five or proportionately longer if more are required. All times are on a Sparc workstation.

### §2.5 Results

The numerical method described in §2.4 was applied to a large number of shelf profiles over the full range of the parameters $B$ and $a$. The structure of the buoyancy frequency was also varied. Analytic solutions for the $Z_n(z)$ functions of (2.4.5) can be found for piecewise constant $N(z)$ as in §2.3 and for $N(z) = \exp(\alpha z)$ in terms of first order Bessel functions (Johnson, 1977). The $Z_n(z)$ are then, for each $n$

$$Z_n(z) = a_n e^{\alpha z/B}(J_1(\beta e^{\alpha z/B})Y_0(\beta) - Y_1(\beta e^{\alpha z/B})J_0(\beta)), \qquad (2.5.1)$$

where $\beta = B\lambda_n/\alpha$ and $a_n$ is a normalisation constant.

To compare the results of §2.3, the numerical method was applied to profile 1 and profile 2 with a rigid lid and uniform stratification. For the linear profile (fig. 2.4) there is a smooth transition from the barotropic shelf wave (BSW) to the internal Kelvin wave (IKW) for each mode and there is no interaction between modes. Comparing this to the Padé approximations shows an exceptional degree of correlation (a maximum of about 1% relative error for the first mode and slightly more for the next two).

For profile 2 (fig. 2.5) the situation is more complicated. Analytically to first order, it is easy to show that for all values of $B$ there are IKWs concentrated at the coastal wall whose phase speeds are like $B/2n\pi$, $n = 1, 2, \ldots$. For small $B$ there are BSWs concentrated on the slope with constant phase speed, independent of $B$, and for large $B$ all the modes are IKWs with speeds $B/m\pi$, $m = 1, 2, \ldots$. This implies that as $B$ decreases, the modes with even $m$ remain essentially IKWs while the odd modes become more like the BSWs. As the phase speeds of the BSWs approach constants as $B$ decreases there has to be some interaction between modes. As the phase speeds of the two modes approach each other, the modes kiss and swap character. Fig. 2.6 shows a close up of the interactions that occur for small values of $B$. This is an extension to the results seen in Allen

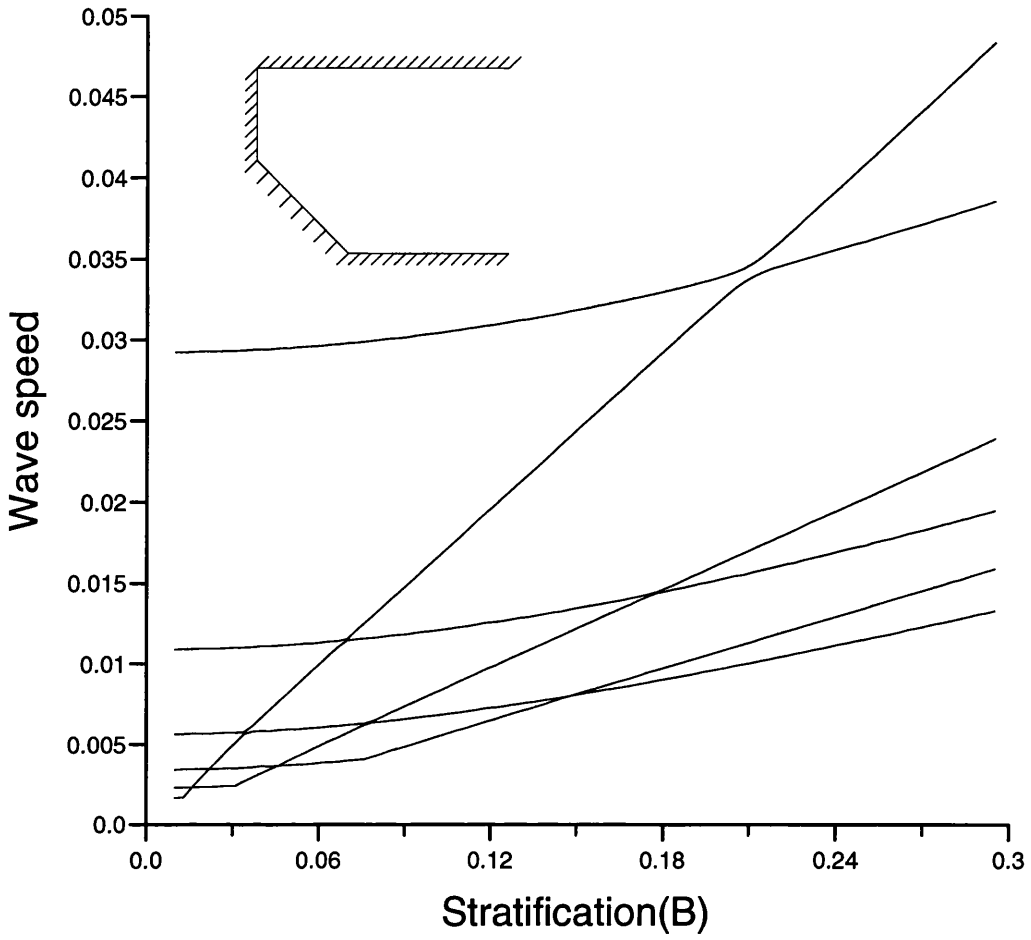


**Figure 2.6**: A closer look at the interactions between the IKW and the BSW modes for profile 2 at small $B$.

(1975) where he proves that the two modes in his problem never meet but do exchange character.

At a kiss the mode changes from predominately an IKW to a BSW. The approximations of course cannot hope to reveal this aspect of the results but can still provide good estimates of where the kiss occurs and the behaviour of the modes everywhere except in the immediate vicinity. However, kissing modes seem to occur only with profiles that allow a clear separation between IKW and BSW modes and mostly among the higher modes. In a real situation it is rare to come across either such a profile or modes higher than the second or third and therefore these kissing modes are unlikely to be of practical relevance.

To fully explore the capabilities of the new method, two other profiles have been used. Profile 3 is a cubic profile with $y = 2z^3 + 3z^2, -1 < z < 0$ and profile 4 is a quartic with $y = 1 - (1 + z)^4, -1 < z < 0$. These are used to provide

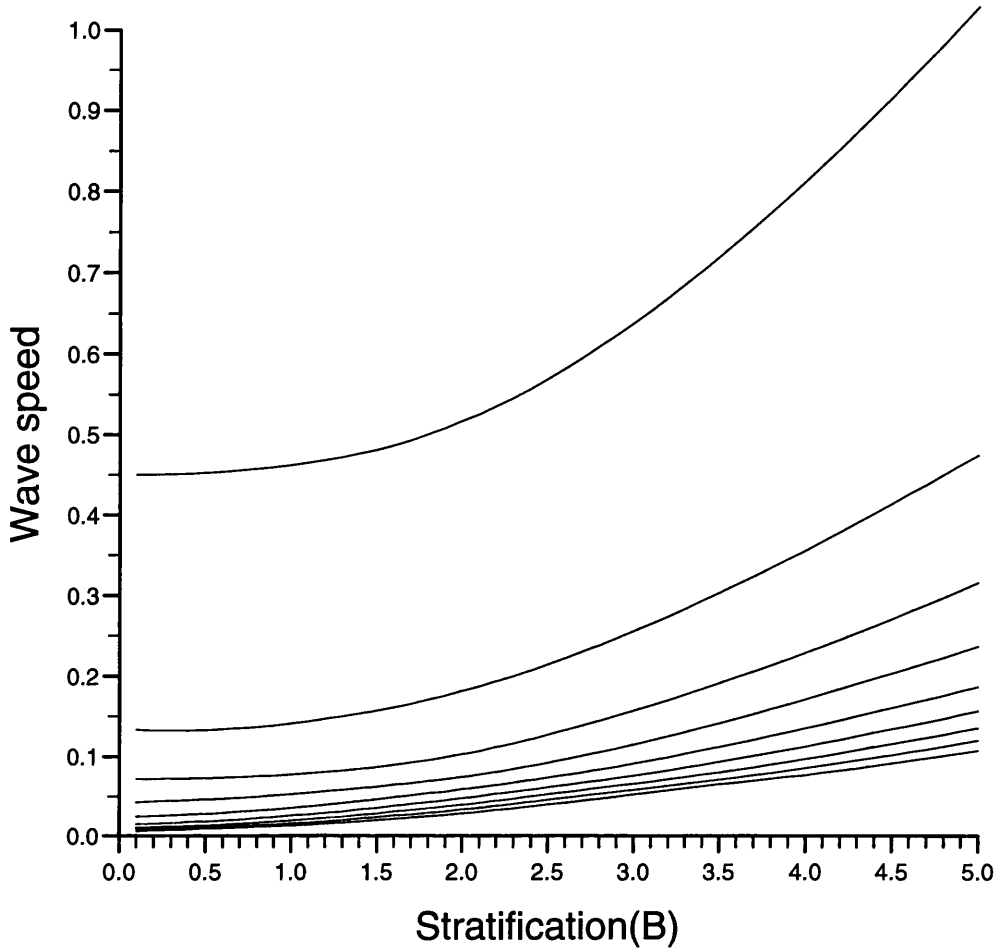


**Figure 2.7**: The waves speeds for profile 4 as the stratification varies. The buoyancy frequency has an exponential profile, $e^z$ and $a = 10$. The external Kelvin wave travels significantly faster than the other modes and is not shown.

more realistic topography and yet still be simple to deal with. The parameters chosen reflect average values for the real ocean and so $B = 1.0$ and $a = 10$ in the cases where they are not varied. Two different stratifications are used, firstly uniform stratification, $N(z) \equiv 1$, and secondly exponential stratification with $N(z) = \exp(\alpha z)$ which models actual buoyancy profiles more accurately.

Using profile 4, fig. 2.7 shows how the wave speeds vary with $B$ in the case of an exponential buoyancy frequency and fig. 2.8 shows how they vary with $a$, the Rossby number. The speed of the EKW is roughly proportional to $a$ and is much greater than the speeds of the other modes for any realistic case i.e. $a \sim 10$. The speeds of the higher modes are not much affected.

One interesting question is how the structure of a mode changes as the profile of the stratification changes. Figures 2.9 and 2.10 show the same mode (mode 1)

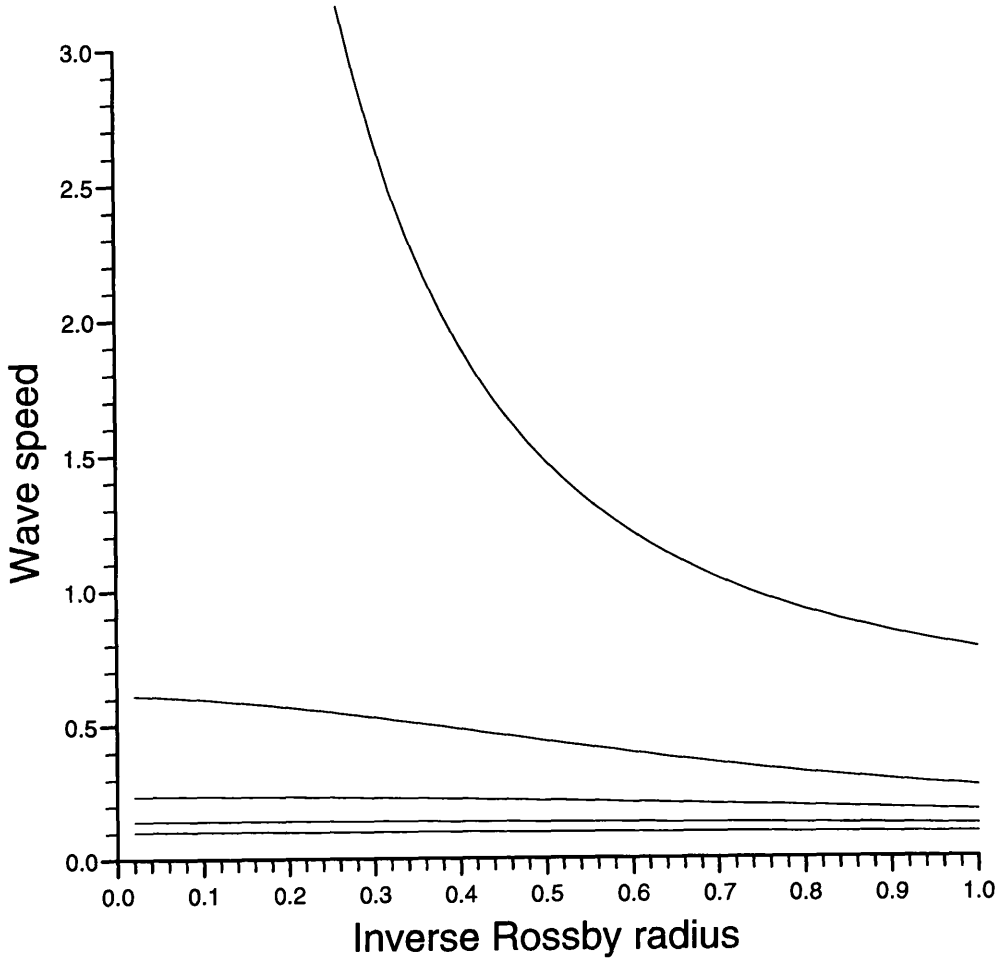


**Figure 2.8**: The wave speeds for profile 4 as the Rossby radius varies with uniform stratification. As $a^{-1} \to 0$ the speed of the external Kelvin wave becomes infinite but the speeds of other modes are not much affected. Even for a realistic value of $a \sim 10$ the EKW travels significantly faster than the other modes.

at the same values of $a$ and $B$ for the two cases $N \equiv 1$ and $N = \exp(10z)$ using profile 3. It is clear that the pressure gradients, and hence velocities, are larger near the surface. The energy of a mode hence concentrates in regions of higher buoyancy frequency.

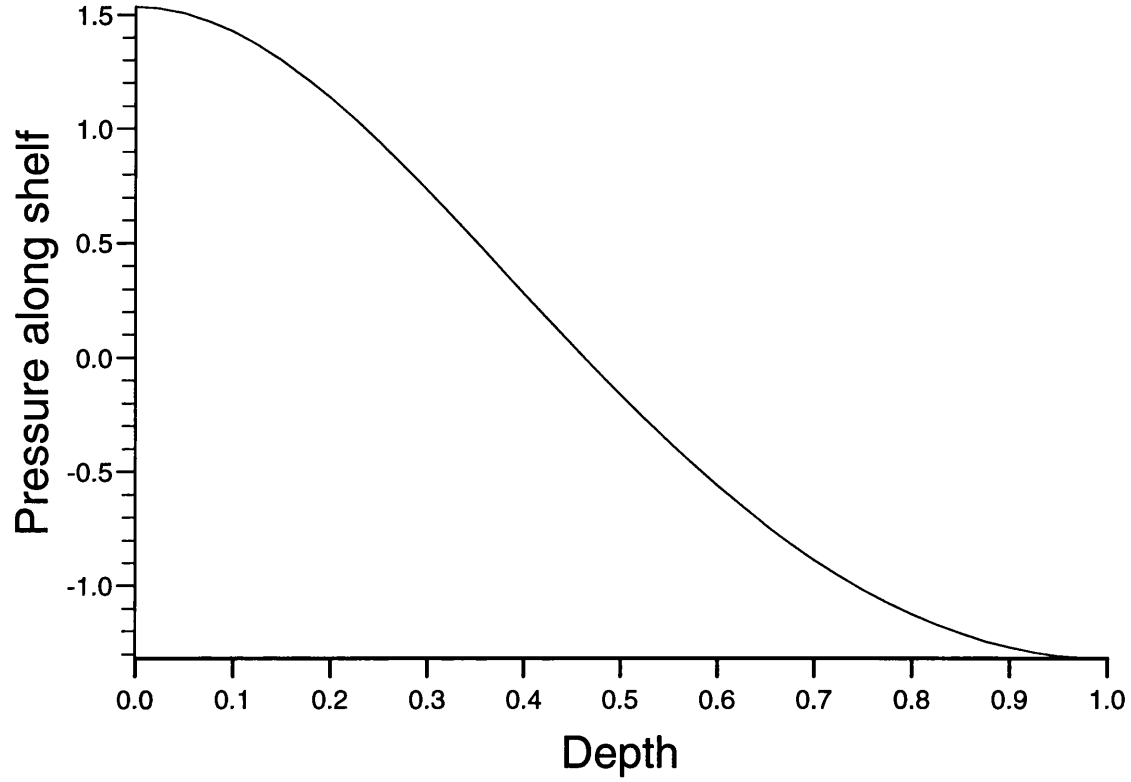


**Figure 2.9**: The value of the pressure along the shelf for profile 3. The stratification is uniform, $B = 1$ and $a = 10$. The pressure gradients are of the same order all the way down.

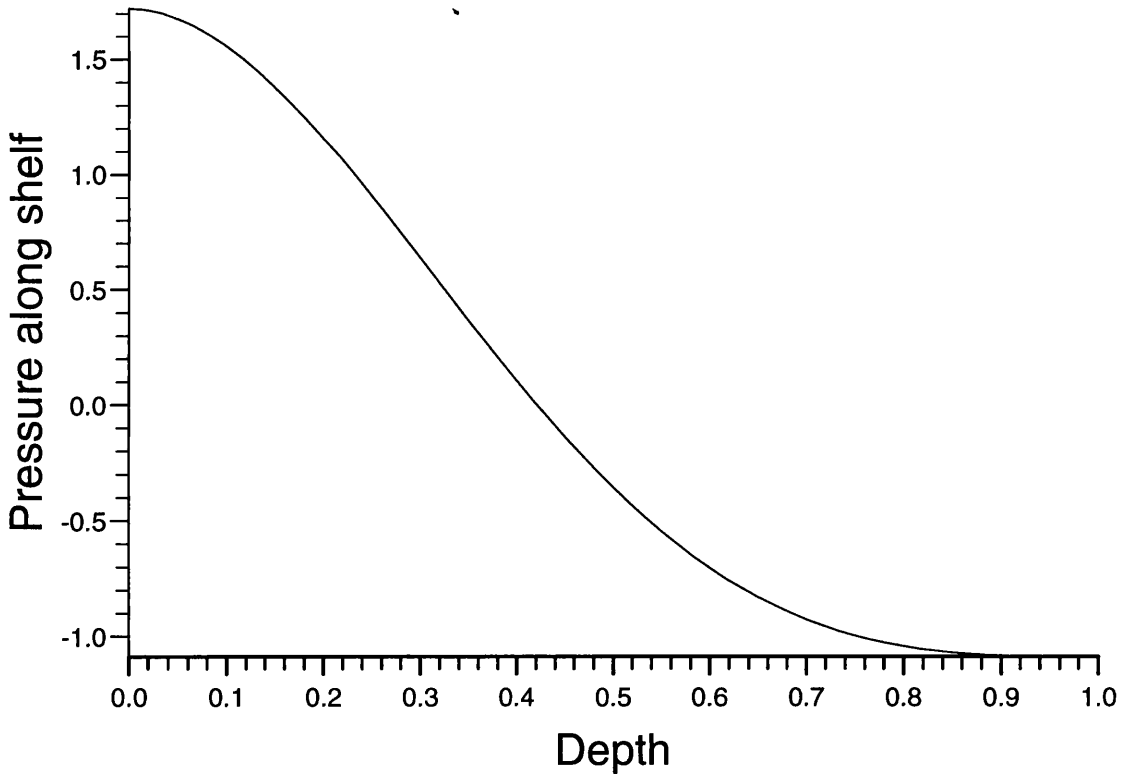


**Figure 2.10**: As fig. 2.9 but with an exponential profile for the stratification, $N(z) = \exp(10z)$. Note that the pressure gradients are concentrated near the surface.

## §2.6 Summary

In this chapter the equations relevant to low-frequency coastally trapped waves have been derived for arbitrary stratification and external Rossby radius. Asymptotic results for both weak and strong stratification were given and combined to give good approximations to the phase speed of the waves at all values of $B$.

A new numerical method was introduced in §2.4 which uses a Green's function to reduce the governing equation and boundary conditions to a one dimensional integral equation. This is then reduced to a set of linear algebraic equations for the values of the pressure on the shelf. This direct method offers increased efficiency and resolution over the methods previously available. There is a particularly simple form for the Green's function in the rigid lid/uniform stratification case.

Results were presented for a number of topographies and the stratification, Rossby radius and buoyancy frequency profile varied. Kissing modes were found but only in quite special circumstances and among the higher modes and so are unlikely to be observed in practice.

The speed of all modes increases with stratification and for large $B$ all modes are essentially IKWs whatever the topography. The variation of the internal Rossby radius does not produce marked differences in any of the modes except the EKW which does not exist in the rigid lid limit. The use of an exponential profile for the buoyancy frequency shows that pressure gradients, and hence velocities, of the wave modes are concentrated, as one might expect, where the buoyancy frequency is greatest.

# Chapter 3

# Other topographic Rossby waves

## §3.1 Introduction

Topographic Rossby waves can propagate along any continuous topographic feature in the ocean, not only continental shelves. Features such as mid ocean ridges and sea mounts can also support these types of waves. Longuet-Higgins (1968) considered barotropic waves guided along a mid ocean discontinuity in depth (a scarp) and Rhines (1969b) considered waves trapped around sea mounts in a homogeneous ocean. The extension to stratified oceans proceeds in an analogous way to coastally-trapped waves (Brink, 1990, Allen and Thomson, 1993) so it is natural to apply the methods of the previous chapter to these cases.

The main differences occur due to the infinite domain now to be considered and in the case of a ridge, the existence of opposite potential vorticity gradients on either side. This allows the propagation of topographic Rossby waves in both directions.

An extra complication arises as the domain is now *concave*. If the topography is taken to be piecewise linear, internal angles must now exist that are greater than $\pi$ radians. As the governing equation for low-frequency waves is essentially the Laplace equation, any motions near such a corner that are sufficiently confined locally not to 'feel' the other boundaries satisfy the classical solution at a corner. This solution behaves like $r^\alpha$ near the apex where $\alpha$ is less than one if the corner has an internal angle greater than $\pi$. Hence there exists an infinite gradient at that point and consequently from (1.7), infinite velocities.

The vertical scale of the flow is of the order $fL/N_0$ so these singularities will become evident when this scale is small compared to the vertical depth $D$, i.e. when $B \gg 1$. This phenomena is then confined to cases of medium to strong stratification. Not all numerical methods are suitable for cases in which this occurs. Section 3.2 extends the method of §2.4 to deal with ridge profiles and shows where it breaks down and how it can be adjusted to account for that. Another method can be used if the topography allows a separated solution. If the topography is stepped, as in the simplest case of a top-hat profile, Fourier expansions in all parts can be matched across a discontinuity in depth. This method is used in §3.3 and is found to accurately model the behaviour at a near-singular point.

Section 3.4 discusses the problems of finding the wave modes that can exist around a seamount where a similar problem can occur. This work is inspired by Sherwin and Dale (1992) who try to model the waves induced by a current around a seamount using the Cox numerical method (Cox, 1984). They found that there was a large numerical error in finding the frequency of the fundamental wave mode and that the error depended on the grid size. By applying the methods of §3.3, a semi-analytical solution is found for the precise conditions used by Sherwin and Dale and hence an explanation for the observed behaviour given.

It is important to note that this singular behaviour is a feature of the problem and not simply an inconsistency of the numerical method. For instance, the problem with Cox code discussed by Hughes (1992), where he notes that if large vertical steps are used then the numerics no longer conserve energy, is a deficiency in the coding. The present problem exists whatever numerical method is used if the topography is piecewise linear.

## §3.2 Topographic waves over a ridge

In this section the equations of motion and methods of solution of §2.2–4 are extended to the ridge case. Consider an infinite ridge of width $2L$ whose profile does not depend on the along-ridge coordinate $x$. Take Cartesian axes $Ox, Oy, Oz$ along the ridge, perpendicular to the ridge and vertically upwards (fig. 3.1). Following §2.2 the governing equation is the same as (2.2.1). The only addition to the boundary conditions is that the pressure has to be bounded as $y \to -\infty$ as well. In the low frequency approximation then, the governing equations and boundary conditions are

$$p_{yy} + B^{-2}(N^{-2}p_z)_z = 0, \tag{3.2.1a}$$

$$h'N^2B^2(p + cp_y) + cp_z = 0, \quad (z = -h(y), |y| \leq 1), \tag{3.2.1b}$$

$$a^2p_z + B^2N^2(0)p = 0, \quad (z = 0), \tag{3.2.1c}$$

$$p_z = 0, \quad (z = -1, |y| > 1), \tag{3.2.1d}$$

$$p_y \to 0, \quad (|y| \to \infty). \tag{3.2.1e}$$

There are a small number of differences to take into account when proving that all the eigenvalues are real. Because the profile function $h(y)$ is no longer

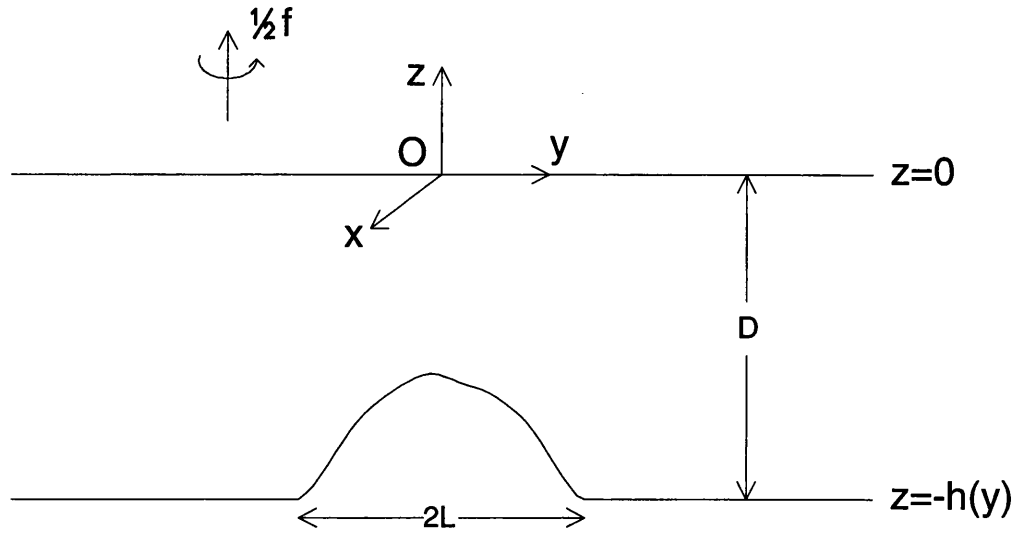


**Figure 3.1**: The domain $A$, with the $z$ coordinate vertically upwards, $y$ increasing out to sea, and $x$ the coordinate along the ridge. The width of the ridge is $2L$ and the open ocean depth $D$.

invertible it is simpler to perform the integrations with respect to $y$, though in some applications (see Chapter 4) it may be more convenient to split the profile into parts where integration with respect to $z$ is possible.

Multiply (3.2.1a) by the complex conjugate of $p$ and integrate over the domain $A$. After integration by parts and use of the boundary conditions the following energy equation results

$$\int\int_A \left\{ |p_y|^2 + \frac{|p_z|^2}{B^2 N^2} \right\} dA + \frac{1}{a^2} \int_{-\infty}^{\infty} |p|^2 \, dy = \frac{1}{c} \int_C h' |p|^2 \, dy. \tag{3.2.2}$$

The LHS is real and positive but $h'$ is now no longer single-signed. Multiply both sides by $c$ and take imaginary parts to show that $c$ must be real. In the coastal shelf case it is also possible to prove that the wave speed is always positive. However since there are opposite potential vorticity gradients on each side of the ridge, waves can propagate in both directions. If the ridge is symmetric the phase speeds will consist of equal and opposite pairs.

The relevant relation for eigenfunctions corresponding to distinct eigenvalues is

$$\int_C h' p_n p_m \, dy = 0, \; n \neq m. \tag{3.2.3a}$$

If the ridge profile can be written as $y = d_A(z)$ for $y \leq 0$ and $y = d_B(z)$ for $y \geq 0$, this relation can be rewritten in the more useful but less compact form

$$\int_{-1}^{-h_0} p_n(d_B(z),z)p_m(d_B(z),z) - p_n(d_A(z),z)p_m(d_A(z),z)\, dz = 0,\ n \neq m, \quad (3.2.3b)$$

where $h_0$ is the minimum depth of water over the ridge. This is not however a suitable inner product since it is not necessarily positive if $n = m$. However the following form

$$\int\int_A \left\{ p_{ny}p_{my} + \frac{p_{nz}p_{mz}}{B^2N^2} \right\} dA + \frac{1}{a^2}\int_{-\infty}^{\infty} p_n p_m\, dy. \quad (3.2.4)$$

can be used to normalise the pressure.

Asymptotic solutions can be found for weak stratification as in §2.3 . In the strong stratification case the limiting profile as $B \to \infty$ is a vanishingly thin ridge at $y = 0$.

As in §2.4 an integral formulation can be found. For the rigid lid/uniform stratification case the fundamental solution (2.4.4) can be used. Unfortunately in the rigid lid limit, no Green's function exists that satisfies $G_y \to 0$ as $|y| \to \infty$. The best that can be done is that the gradient goes to zero at *either* $+\infty$ or $-\infty$. Hence, use the same Green's function as in the shelf case, though through (2.4.10) this introduces the value of the far-field pressure ($p_{-\infty} = constant$) into the equations. This is an extra variable and an extra equation is needed to complete the system. This comes from consideration of the integral of $\nabla^2 p$ over the domain. i.e.

$$0 = \int\int_A \nabla^2 p\, dA = \int_S \frac{dp}{dn}\, ds,$$

and using the boundary conditions to get

$$\int_C h'p\, dy = 0. \quad (3.2.5)$$

The analogue of (2.4.13) for the rigid lid case is then

$$c\left\{ p_j \left( h \sum_{i=1,i\neq j}^{N+1} \epsilon_i h'(y_i) D_{ij} + 2\pi \right) - h \sum_{i=1,i\neq j}^{N+1} \epsilon_i p_i h'(y_i) D_{ij} - 2\pi p_{-\infty} \right\} =$$

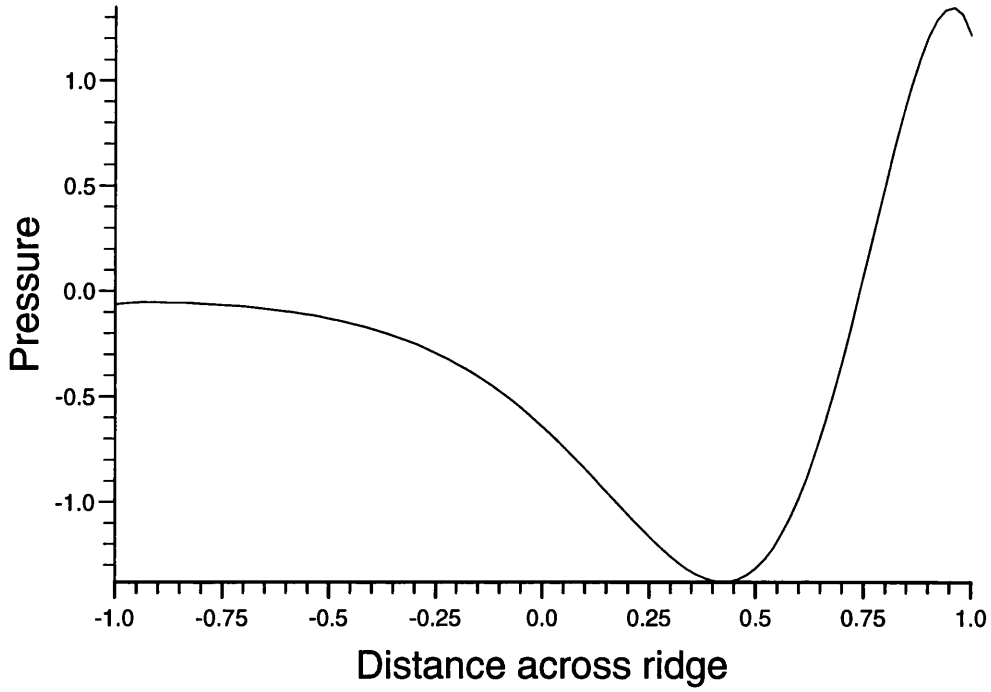


**Figure 3.2**: The pressure across the ridge for second mode when the profile is parabolic, $h(y) = (y^2 + 1)/2$, $B = 1.0$, $a = 10$ and with uniform stratification.

$$p_j \left\{ h \sum_{i=1, i\neq j}^{N+1} \epsilon_i h'(y_i) G_{ij} - F_j \right\} - h \sum_{i=1, i\neq j}^{N+1} \epsilon_i p_i h'(y_i) G_{ij}, \tag{3.2.6a}$$

with

$$\sum_{i=1}^{N+1} \epsilon_i h'(y_i) p_i = 0, \tag{3.2.6b}$$

where the integration is now with respect to $y$.

For the more general case involving a free surface and non-uniform stratification, the eigenfunctions for the vertical structure are the same as those given by (2.4.5) and a Green's function can be constructed in a similar fashion. Instead of the requirement that $F_n'(0) = 0$ for each $n$, it is now necessary that $F_n$ is bounded as $y \to -\infty$. This simplifies the $y$-dependence to give

$$F_n(y) = -\pi e^{-\lambda_n |y - y_0|} Z_n(z_0)/\lambda_n, \; n = 0, 1, 2 \ldots \tag{3.2.7}$$

and hence the Green's function as

$$G(\mathbf{r}|\mathbf{r_0}) = -\sum_{n=0}^{\infty} \frac{\pi}{\lambda_n} e^{-\lambda_n |y - y_0|} Z_n(z_0) Z_n(z). \tag{3.2.8}$$

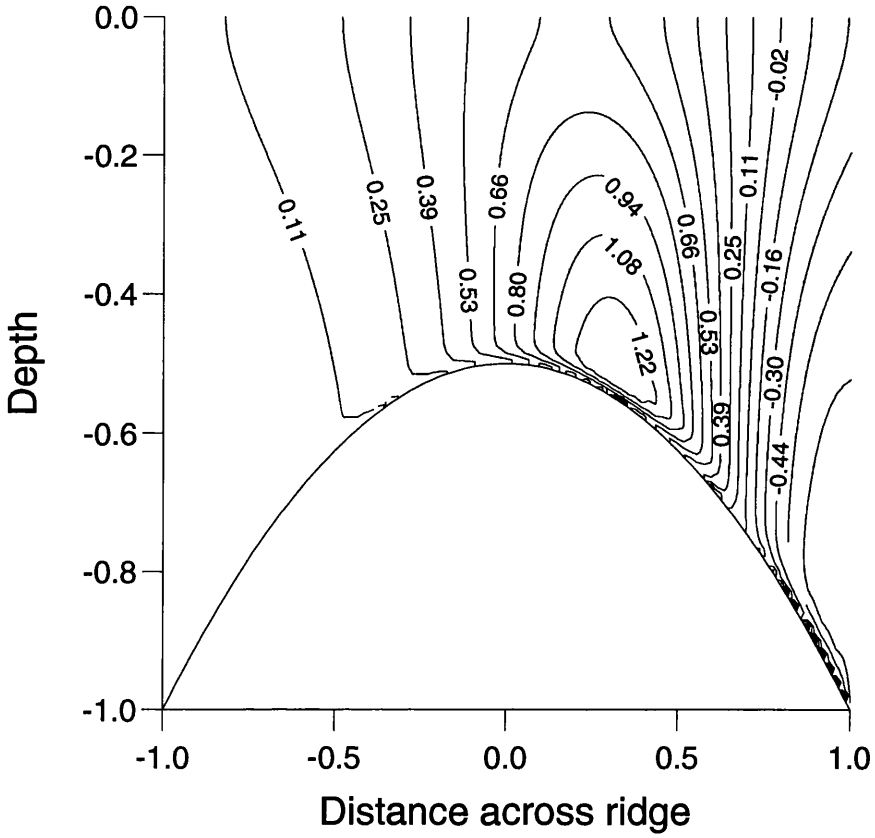


**Figure 3.3**: The pressure field for mode 1 over a parabolic ridge with exponential stratification $N(z) = \exp(3z)$, $B = 2$ and $a = 10$. The mode is effectively barotropic for depths greater than the $e$-folding scale.

With this Green's function the equations (2.4.11), (2.4.12) and (2.4.13) follow immediately (with the understanding that the domain $A$ is now the infinite domain $-B \leq z \leq 0$, $-\infty < y < \infty$ except for the region under the curve $C(y, -h(y))$ and that an extra factor of $h'(y_i)$ appears in each sum).

The structure of the modes differs slightly from the coastal case. The bulk of the energy for positively (negatively) propagating waves is found over the part of the ridge with negative (positive) gradient. On the opposing side there is a small but non-negligible tail (fig. 3.2).

If an exponential profile, say $N(z) = \exp(\alpha z)$ is used then the mode is effectively barotropic for any depth greater than $\alpha^{-1}$. Figure 3.3 shows the pressure field for the first mode over a parabolic ridge when $\alpha = 3$ and it is clear that the vertical velocities (variation of the pressure with depth) are concentrated in the top third of the fluid.

There is a slight complication in working out the pressure if there are corners

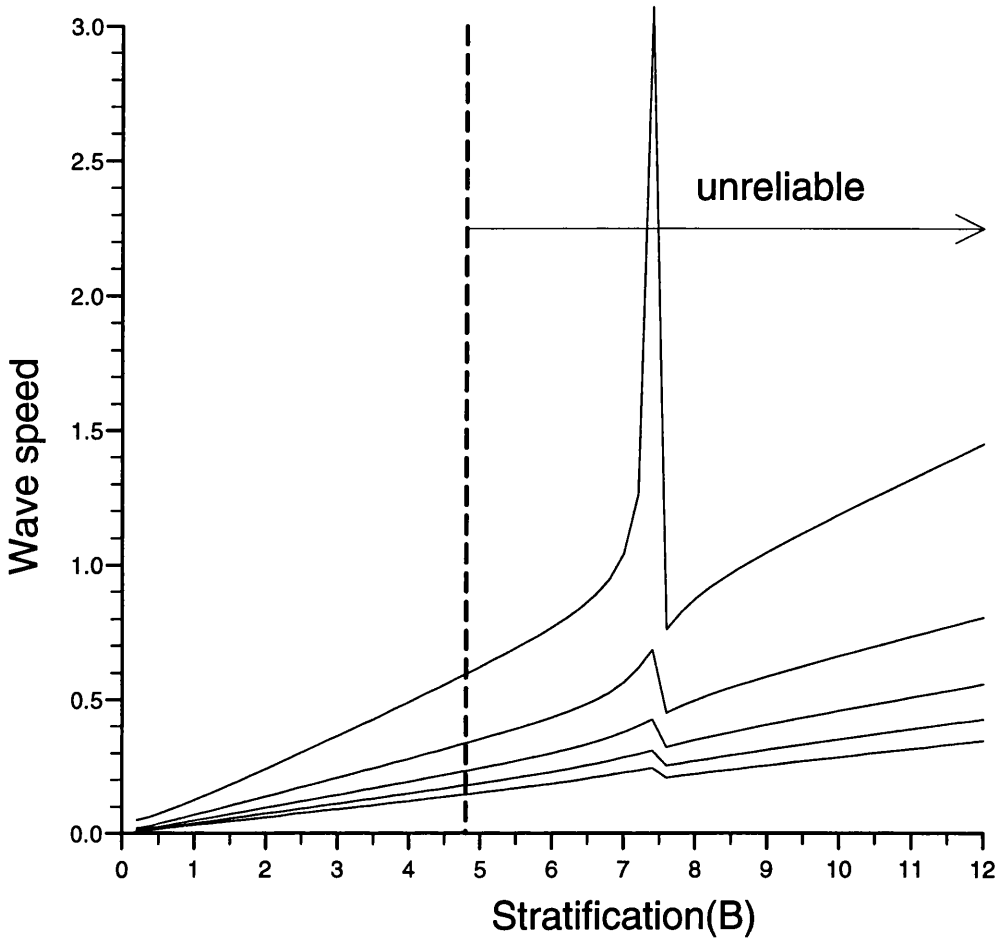


**Figure 3.4**: The variation of the phase speed with stratification for the first few modes as given by the numerical method for a triangular profile (rigid lid/uniform stratification). Due to the singularity appearing at the apex of the ridge the numerical method becomes unreliable for $B > 4$.

with internal angles greater than $\pi$. If the topography is taken as piecewise linear then at such a corner $y_c, z_c$ the lengths over which the pressure will change are much smaller than in other parts of the flow. So rescale $y - y_c$ and $z - z_c$ on $\delta$ and $\delta N(z_c)$ where $\delta << 1$. In the vicinity of the corner the governing equation reduces to Laplace's equation in all cases and the boundary condition on the sides simply becomes $dp/dn = 0$. If the top and bottom boundaries cannot be 'felt' by the fluid at the corner then a solution can be found by separating variables in polar coordinates.

Since the pressure cannot be infinite the solution must be of the form

$$p \approx a_0 + a_1 r^{\alpha} \cos \alpha\theta + \ldots a_2 r^{2\alpha} \cos 2\alpha\theta + \cdots \tag{3.2.9}$$

where $r = \sqrt{(y - y_c)^2 + (z - z_c)^2}$, $\theta$ is the angle going anti-clockwise around the

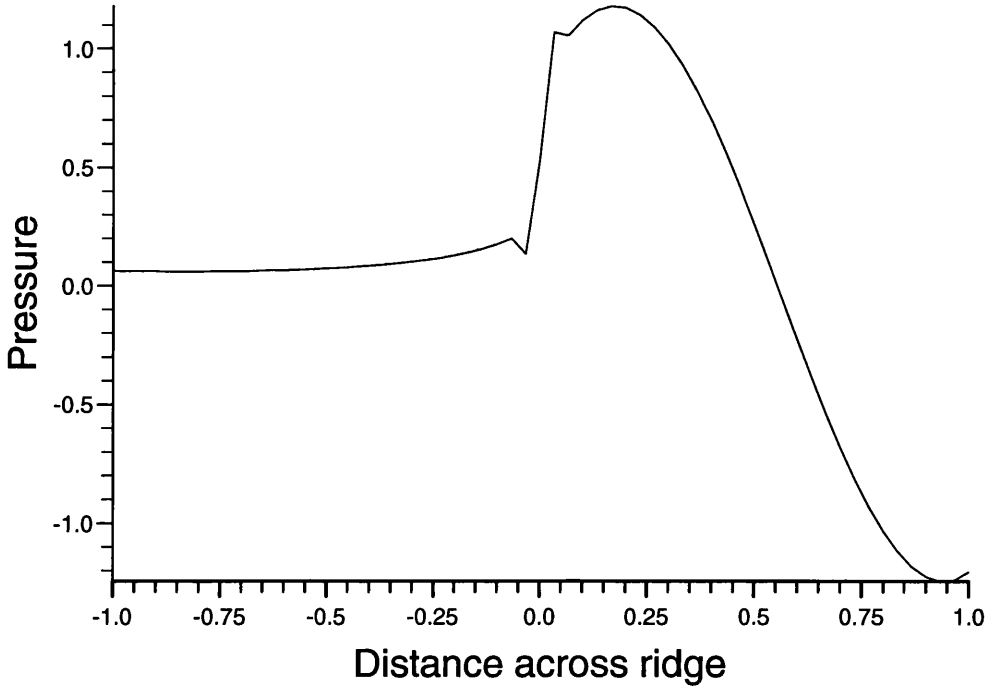


**Figure 3.5**: The pressure across the ridge for first positively propagating mode when the profile is triangular (as in fig. 3.4). The numerical method introduces errors into the pressure function for $B > 4$. Here $B = 6.0$ and it is evident that the results are inaccurate.

corner and $\alpha = \pi/(2\pi - \beta)$ where $\beta$ is the acute external angle. The pressure gradient at this point will be infinite because $\alpha$ is less than one.

As noted above, this analysis is only be valid if the top and bottom boundaries do not affect the fluid at the corner. This will depend on the stratification. The vertical scale of motion is $fL/N_0$, so the assumption is valid if the vertical scale is much less than the depth, $D$ i.e. if $B \gg 1$. For $B \sim 1$ this is not strictly valid but as shown in §3.4, large pressure gradients are still found.

This singularity can affect the working of the numerical method when the topography is taken to be piecewise linear. Figure 3.4 shows that the numerical method becomes unreliable for a triangular profile when $B > 4$. This can be seen in the discontinuities in the pressure field that is produced (fig. 3.5). If however a smooth profile is used (i.e. with a continuous normal vector) there seems to be no problem.

## §3.3 Examples using stepped topography

If the ridge profile is stepped then the equations are separable and the solution can be expressed as an infinite series. The limit of large stratification can be

examined using these expansions further than with the Green's function method outlined in §3.2.

The simplest step profile is the tophat profile

$$h(y) = \begin{cases} 1, & |y| > 1, \\ h, & |y| \leq 1. \end{cases} \tag{3.3.1}$$

In this case the topography is symmetric and it is helpful at this stage to separate the pressure into odd and even parts. Rescale (3.2.1) with $Y = y/B$ and write

$$p(y,z) = \begin{cases} p^o + p^e, & |Y| \leq l, \\ q^o + q^e, & |Y| > l, \end{cases} \tag{3.3.2}$$

where $l = 1/B$, $p^o, q^o$ are the odd functions and $p^e, q^e$ the even. Each of these functions now satisfy Laplace's equation. They all satisfy (3.2.1c) on $z = 0$ and have no normal derivative on the surfaces $z = -h$ and $z = -1$. On the vertical sides (3.2.1b) reduces to

$$\begin{aligned} Kq^o_Y(l,z) + q^e(l,z) &= 0, \ (-1 \leq z \leq -h) \\ Kq^e_Y(l,z) + q^o(l,z) &= 0, \ (-1 \leq z \leq -h) \end{aligned} \tag{3.3.3}$$

where $K = lc$. In addition, the pressure and its horizontal derivative must be continuous at $Y = l$.

Separation of variables and application of the boundary conditions gives that the $z$-dependent functions are similar to the $Z_n(z)$ of (2.4.5). In the uniform stratification case these are $A_n(z) = \cos\alpha_n(z+h)$ for $|Y| \leq l$ and $B_n(z) = \cos\beta_n(z+1)$ for $|Y| > 1$ where $\alpha_n$ and $\beta_n$ are chosen to satisfy the boundary conditions at $z = 0$ i.e.

$$\begin{aligned} \alpha_n \tan\alpha_n h &= B^2/a^2, \ n = 0,1,2,\ldots \\ \beta_n \tan\beta_n &= B^2/a^2, \ n = 0,1,2,\ldots, \end{aligned} \tag{3.3.4}$$

The most general functions which satisfy Laplace's equation and are bounded at infinity are then $e^{-\beta_n|Y|}B_n(z)$. These can be used to construct $q^o(Y,z), q^e(Y,z)$ while cosh and sinh terms are used to create the inner functions. So write

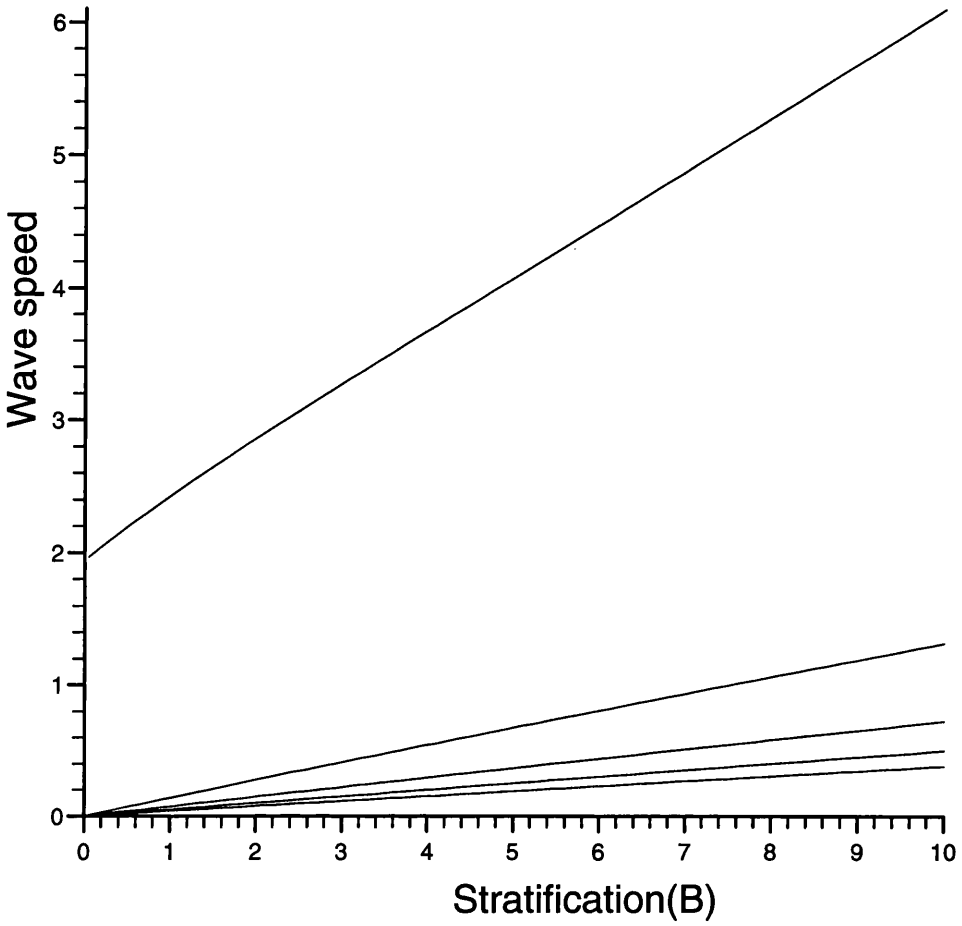


**Figure 3.6**: The variation of the phase speed with stratification for the first few modes for the top-hat profile (uniform stratification, $a = 10$). The matched Fourier mode technique gives accurate solutions even for large stratification even though there is a singularity at the corner (see fig. 3.7).

$$
\begin{aligned}
q^e(Y,z) &= \sum_{n=0}^{\infty} a_n e^{-\beta_n(|Y|-l)} B_n(z), \ (|Y| > l) \\
q^o(Y,z) &= \sum_{n=0}^{\infty} b_n \mathrm{sgn}(Y) e^{-\beta_n(|Y|-l)} B_n(z), \ (|Y| > l) \\
p^e(Y,z) &= \sum_{n=0}^{\infty} c_n \frac{\cosh \alpha_n Y}{\cosh \alpha_n l} A_n(z), \ (|Y| \leq l) \\
p^o(Y,z) &= \sum_{n=0}^{\infty} d_n \frac{\sinh \alpha_n Y}{\sinh \alpha_n l} A_n(z), \ (|Y| \leq l)
\end{aligned} \tag{3.3.5}
$$

where $a_n, b_n, c_n, d_n$ are constants to be determined and the functions $A_n(z), B_n(z)$ have been suitably normalised.

Substitute these definitions into (3.3.3) and the continuity conditions and note that in $z \in [-h, 0]$, the functions $A_n(z), n = 0, 1, 2, \ldots$ are complete and

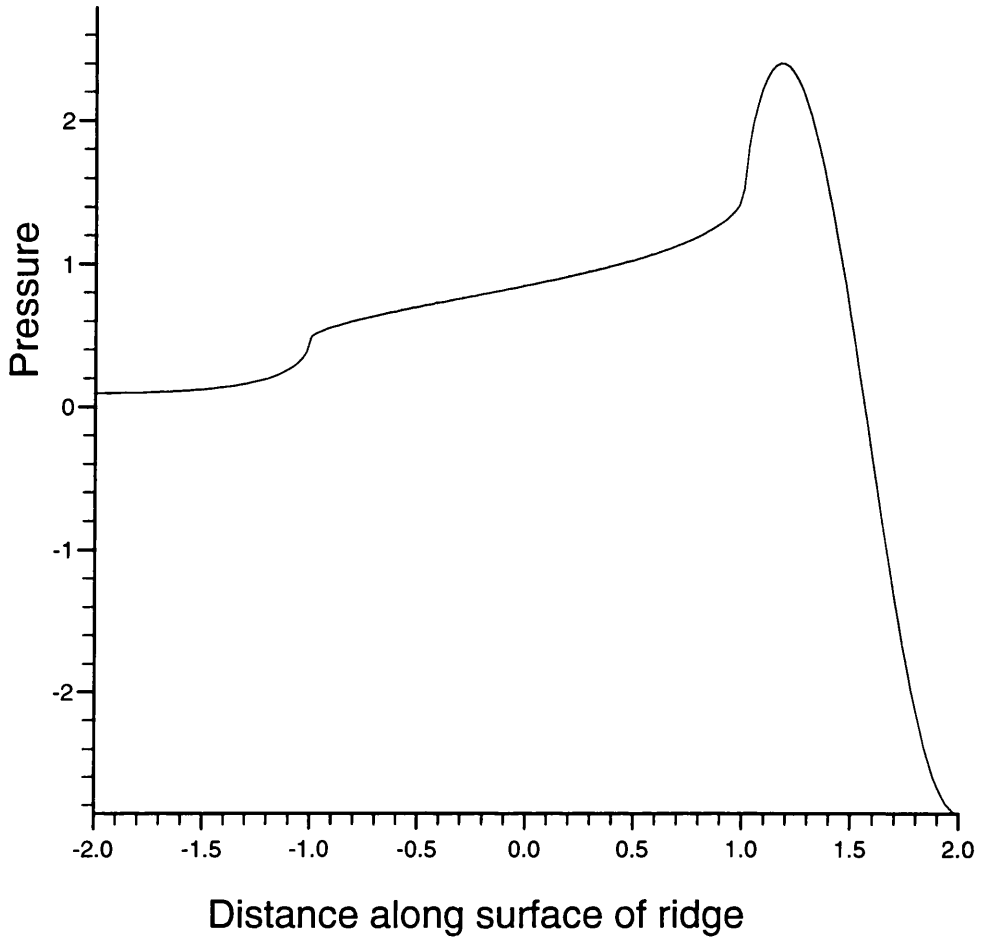


**Figure 3.7**: The pressure along the surface of the ridge for the mode 1 when $B = 10$ (rigid lid/uniform stratification case). The gradient at $y = 1$ is very large and confirms the prediction of (3.2.9).

orthogonal. Multiply each continuity equation in turn by $A_m(z), m = 0, 1, 2, \ldots$ and integrate over the range of validity of $z$ to get; $c_n, d_n, n = 0, 1, 2, \ldots$ in terms of $a_n, b_n$, and two equations for the $a_n, b_n$. For $z \in [-1, -h]$ the functions $C_n(z) = \cos(n\pi(z+1)/(1-h))$ are orthogonal so multiply equations (3.3.3) by $C_m(z)$ and integrate to get another two equations connecting $a_n, b_n$ and the wave speed $K$. If $I_{mn} = \int_{-h}^{0} A_m(z)B_n(z)dz$, and $J_{mn} = \int_{-1}^{-h} C_m(z)B_n(z)$ the equations are

$$\sum_n^\infty I_{mn}a_n(\alpha_m \tanh \alpha_m l + \beta_n) = 0,$$

$$\sum_n^\infty I_{mn}b_n(\alpha_m + \beta_n \tanh \alpha_m l) = 0,$$

$$\sum_n^\infty J_{mn}(K\beta_n a_n - b_n) = 0,$$

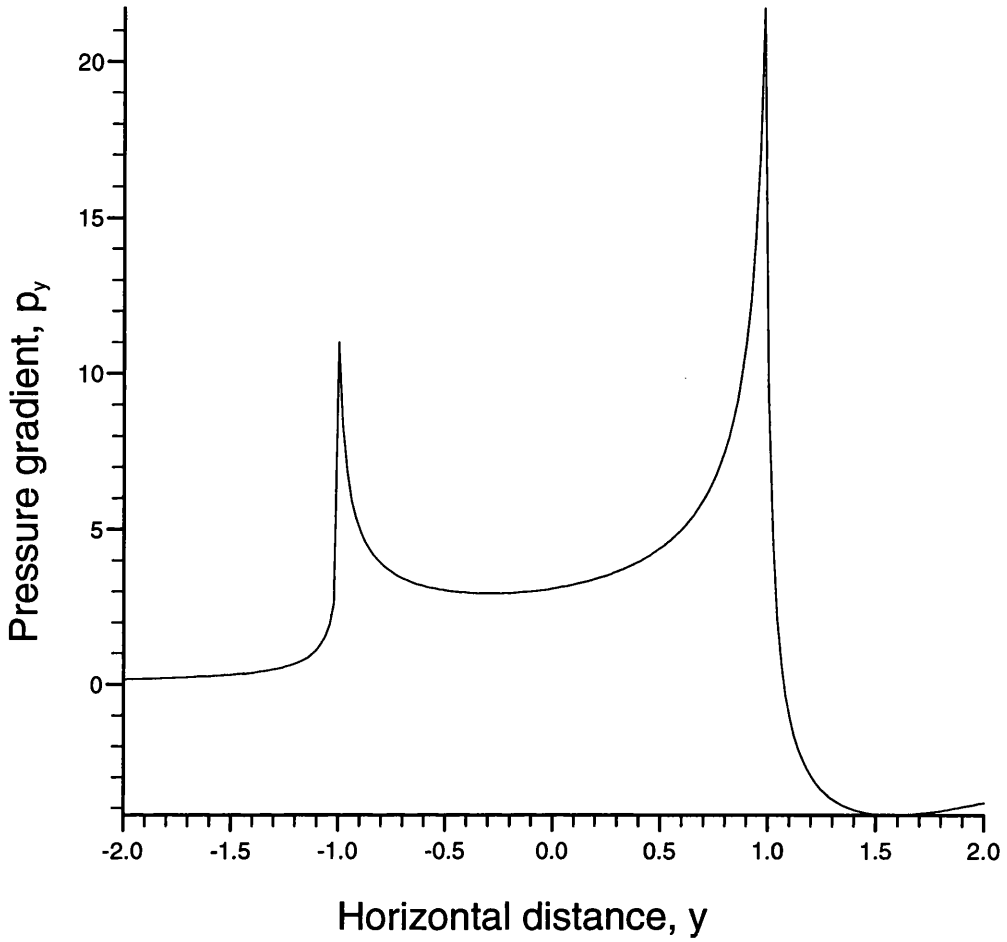


**Figure 3.8**: The horizontal pressure gradient along the top of the ridge at $z = -0.5$. The same parameters as in fig 3.7 are used. The matched Fourier expansions technique accurately reproduces the singularity expected at each corner.

$$\sum_{n}^{\infty} J_{mn}(K\beta_n b_n - a_n) = 0, \tag{3.3.6}$$

where $m = 0, 1, 2 \ldots$.

To solve these equations truncate the expansions at $n = N$ say, and take equations from the first two and second two sets in proportion to the height of the step. They can then be written as $A\mathbf{a} = KB\mathbf{b}$ and $C\mathbf{b} = KD\mathbf{a}$ where $A, B, C$ and $D$ are matrices, and solved using standard linear eigenvalue techniques.

In the barotropic limit there are only two possible modes both very similar to the double Kelvin waves found by Longuet-Higgins (1968), one travelling in each direction. The speeds of all the internal waves go to zero. The following results are from a simple example where uniform stratification is used with $a = 10$ on a top-hat ridge with $h = 0.5$.

As fig. 3.6 shows this technique works accurately even at large stratification

but the singularity that was mentioned in §3.2 is still present. The pressure near the corner (fig. 3.7) is predicted to go as $r^{2/3}$ from (3.2.9) and therefore the pressure gradient should be very large (fig 3.8).

### §3.4 Island trapped waves

Sherwin and Dale (1992) reported on a difficulty found in the Cox code (Cox, 1984) while trying to resolve topographic Rossby waves around a sea mount. The configuration studied as a model for the Anton Dohrn sea mount was a circular cylinder immersed in a uniformly stratified rotating ocean and with a uniform stream across it. This excited a trapped wave around the sea mount whose frequency seemed to be strongly dependent upon the grid size used in the model.

This section applies the semi-analytic method used in §3.3 to finding the frequency of the wave modes for this configuration. The Fourier series used are now in terms of Bessel functions but the same principles apply. In this case there is no need to apply the low-frequency approximation because the azimuthal wavenumbers are quantised by the continuity condition around the sea mount. The solution then provides a basis for examining why the Cox code behaves the way it does.

Consider a semi-infinite ocean of depth $D$ containing an axisymmetric sea mount with radius $L$. Use cylindrical polar coordinates with the origin at the surface directly above the centre of the sea mount. Omitting a common factor of $e^{i\omega t}$, the governing equation for the non-dimensional pressure follows from (1.8) as

$$r^2 P_{rr} + r P_r + P_{\theta\theta} + r^2(1-\omega^2)B^{-2}\left(\frac{P_z}{N^2}\right)_z = 0. \tag{3.4.1}$$

Zero normal velocity on the vertical sides of the cylinder and ocean floor requires

$$i\omega r P_r + P_\theta = 0, \quad (r = 1,\ -1 < z < -h), \tag{3.4.2}$$

and $P_z = 0$ on $z = -1$ and $z = -h$ where $h$ is the depth of water above the mount. For a rigid lid $P_z = 0$ on $z = 0$. Incorporating free surface effects leads to (2.2.2) as before.

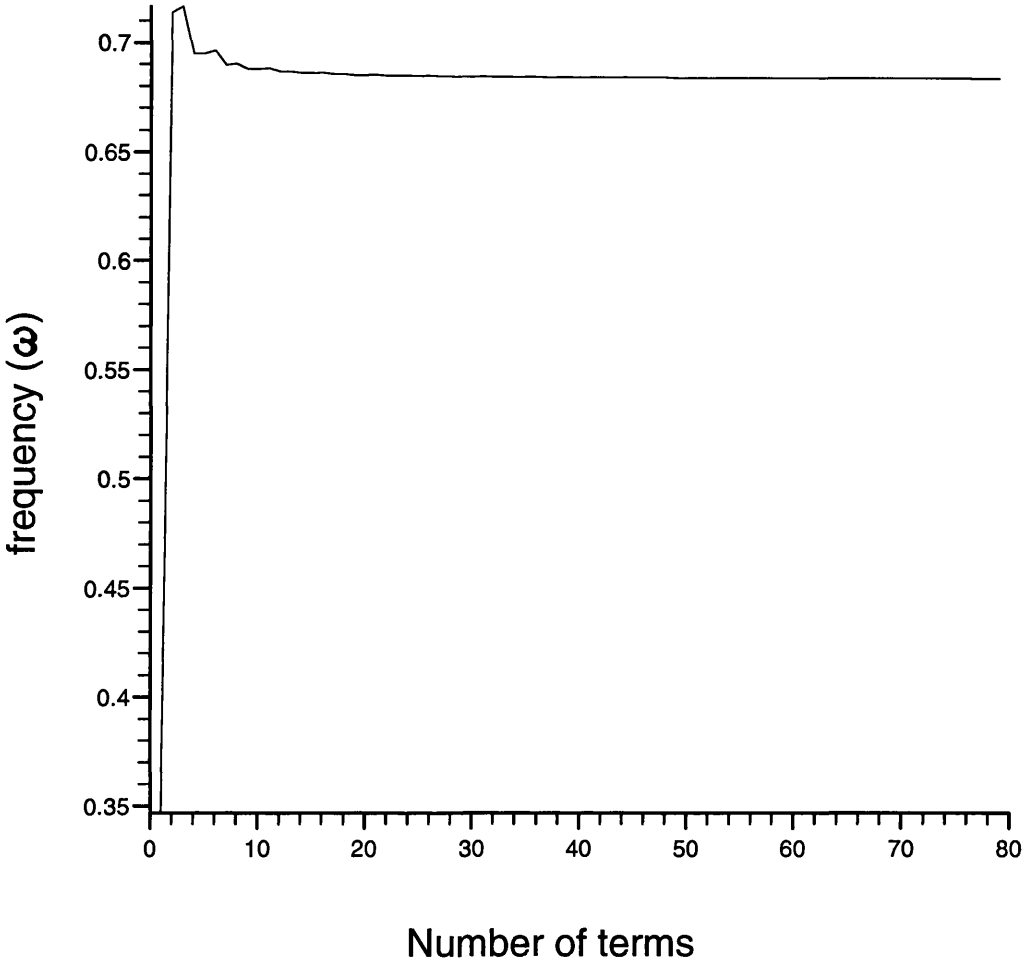


**Figure 3.9**: The frequency $\omega$ of the radial mode 0, azimuthal mode 1 wave for the rigid lid case as a function of the number of terms taken in expansion (3.4.3). Here the stratification parameter is $B = 1.3$ and the depth of fluid above the cylinder is $h = 0.4$. The frequency converges quite rapidly to $\omega = 0.683$, significantly higher than obtained by Sherwin and Dale using the Cox code.

Following Sherwin and Dale assume uniform stratification ($N \equiv 1$) and a rigid lid and look for solutions of the form $P = \Re\{p(r,z)e^{il\theta}\}$ where $l$ must be an integer to ensure continuity. Then separation of variables gives

$$p(r,z) = \begin{cases} a_0 r^l + \sum_{n=1}^{\infty} a_n A_n(z) I_l(\alpha_n r/h), & r < 1, \\ b_0 r^{-l} + \sum_{n=1}^{\infty} b_n B_n(z) K_l(\alpha_n r), & r > 1, \end{cases} \tag{3.4.3}$$

where $A_n(z) = \cos n\pi z/h$, $B_n(z) = \cos n\pi z$, $\alpha_n = n\pi(1-\omega^2)^{1/2}/B$ and $I_l(x)$ and $K_l(x)$ are the modified Bessel functions of order $l$. The pressure and its radial derivative must be continuous across $r = 1$ and these conditions combined with (3.4.2) determine the constant vectors $\mathbf{a} = (a_0, a_1, \ldots)$ and $\mathbf{b} = (b_0, b_1, \ldots)$.

The orthogonality of $A_n(z)$ over $-h < z < 0$ allows $\mathbf{a}$ to be eliminated and gives a set of equations for the components of $\mathbf{b}$. Similarly (3.4.2) can be

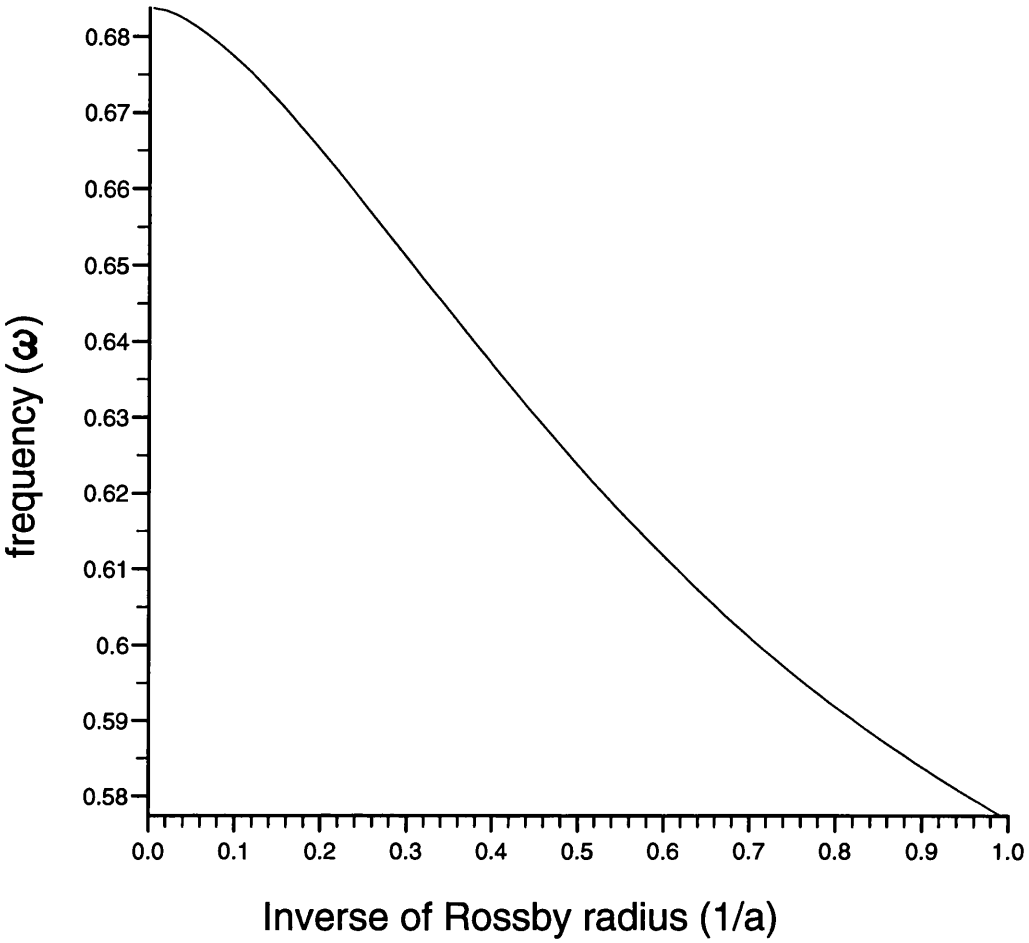


**Figure 3.10**: Variation of the frequency $\omega$ in the free surface case as a function of the Rossby radius of deformation $a$. The rigid lid case is the limit as $a \to \infty$. Here $B = 1.3$, $h = 0.4$ and 40 terms are taken in the expansion.

integrated against a suitable set of orthogonal functions on $-1 < z < -h$ to give another set of equations for the components of $\mathbf{b}$. Combining these gives a matrix equation for $\mathbf{b}$ whose elements depend non-linearly on the frequency $\omega$. A non-trivial solution exists only when determinant of the matrix vanishes. This happens for a countable number of values of $\omega$ which can be found using standard numerical algorithms. The largest $\omega < 1$ for which this occurs at each azimuthal wavenumber is the frequency of the fundamental radial mode.

Using values from Sherwin and Dale gives the stratification parameter $B$ to be approximately 1.3 and the non-dimensional depth above the sea mount $h = 0.4$. Figure 3.9 shows the convergence of the present method for the frequency of the azimuthal mode 1, radial mode 0 as the number of terms in the expansion increases. The variation of the frequency when a free surface is imposed with the

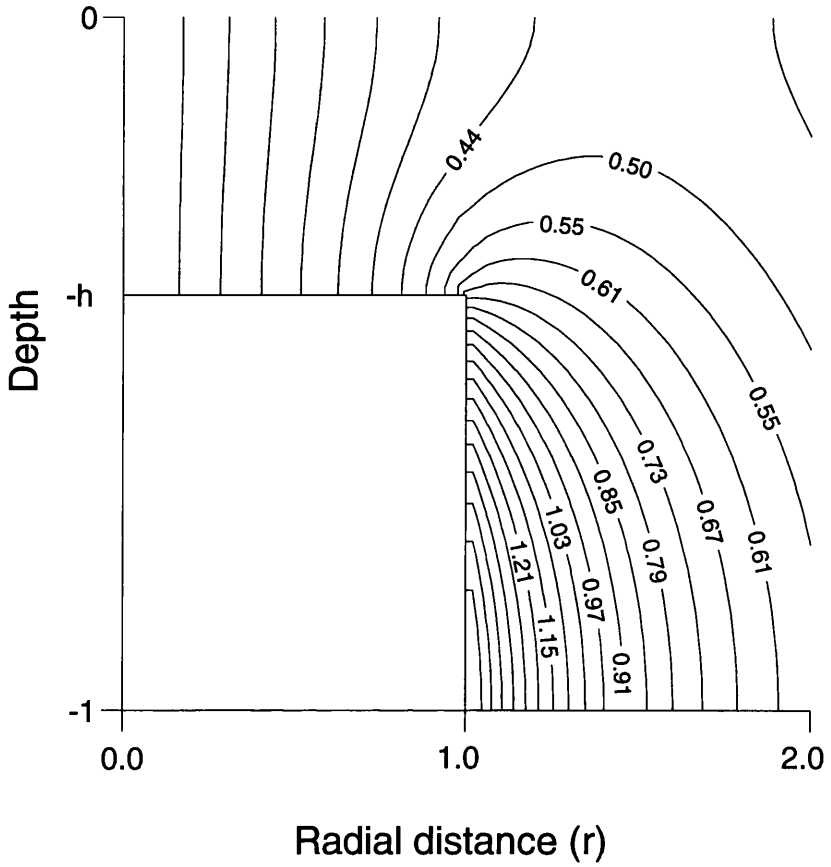


**Figure 3.11**: The pressure contours at $\theta = 0$ for the radial mode 0, azimuthal mode 1. The mode is mostly concentrated along the walls of the cylinder and there are very large pressure gradients at the corner.

non-dimensional Rossby radius of deformation $a = (gD)^{1/2}/fL$ is shown in fig. 3.10. The rigid lid case is given simply as the limit as $a \to \infty$. Here $\omega = 0.683$ as $a \to \infty$. This is significantly higher than frequencies from the Cox code calculations although it is consistent with the trend shown in fig. 25 of Sherwin and Dale when extrapolated to zero grid size.

Figure 3.11 shows pressure contours at $\theta = 0$ and fig. 3.12 shows the pressure along and down the boundary. It is clear that the gradients of the pressure are large near the corner. Figure 3.13 clarifies this by showing the radial pressure gradient along a cross section through the corner for $z = -h$. This is not altogether surprising. As in §3.3 pressure gradients can become very large near the apex. Expand (3.4.1) in the neighbourhood of the corner using polar coordinates $R, \phi$ in a vertical plane centred on $(r, z) = (1, -h)$ with $\phi = 0$ corresponding to $r = 1, z < -h$. If the effects of the top and bottom boundaries are ignored the governing equation is simply Laplace's equation $R(Rp_R)_R + p_{\phi\phi} = 0$. The boundary conditions on the cylinder reduce to the vanishing of the normal derivative

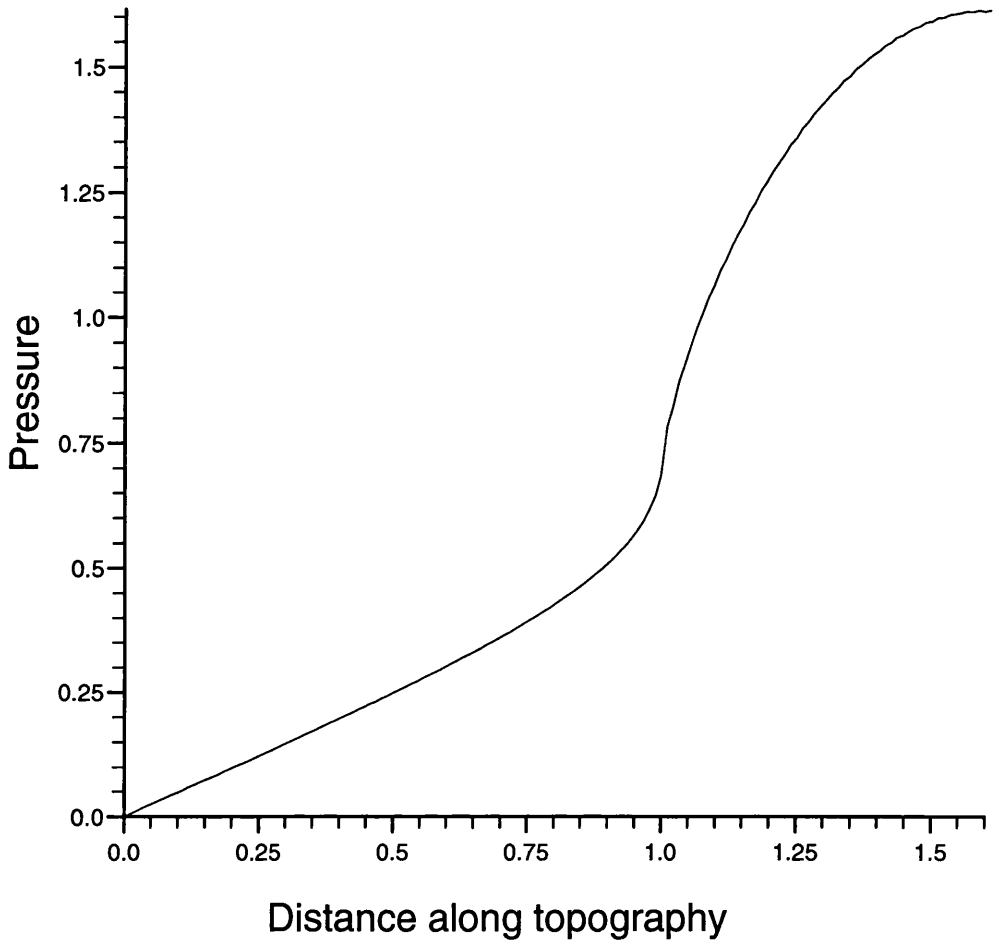


**Figure 3.12**: The pressure along the surface of the sea mount as a function of distance from the axis. The pressure and its derivative are continuous at $s = 1$ though the pressure behaves as $p \sim R^{2/3}$ in the vicinity of the discontinuity. Since the Cox code approximates the derivatives of the pressure, which are infinite, large errors will be introduced at that point.

of $p$ and so at the corner the pressure is of the form

$$p \sim a_0 + a_1 R^{2/3} \cos\frac{2\phi}{3} + \dots , \tag{3.4.4}$$

where $a_0, a_1$ are constants. While the pressure is finite the *derivatives* at the corner are infinite. As mentioned in §3.2, the effects of the top and bottom boundaries can only be neglected if the vertical scale of the motion is much smaller than the depth of fluid, i.e. $B \gg 1$. In this example $B = O(1)$ so the condition is not satisfied. However, the solution near the corner has much the same form as predicted and is similar to that seen in the top-hat ridge case in §3.3.

In working out the velocity components the Cox code approximates the deriva-

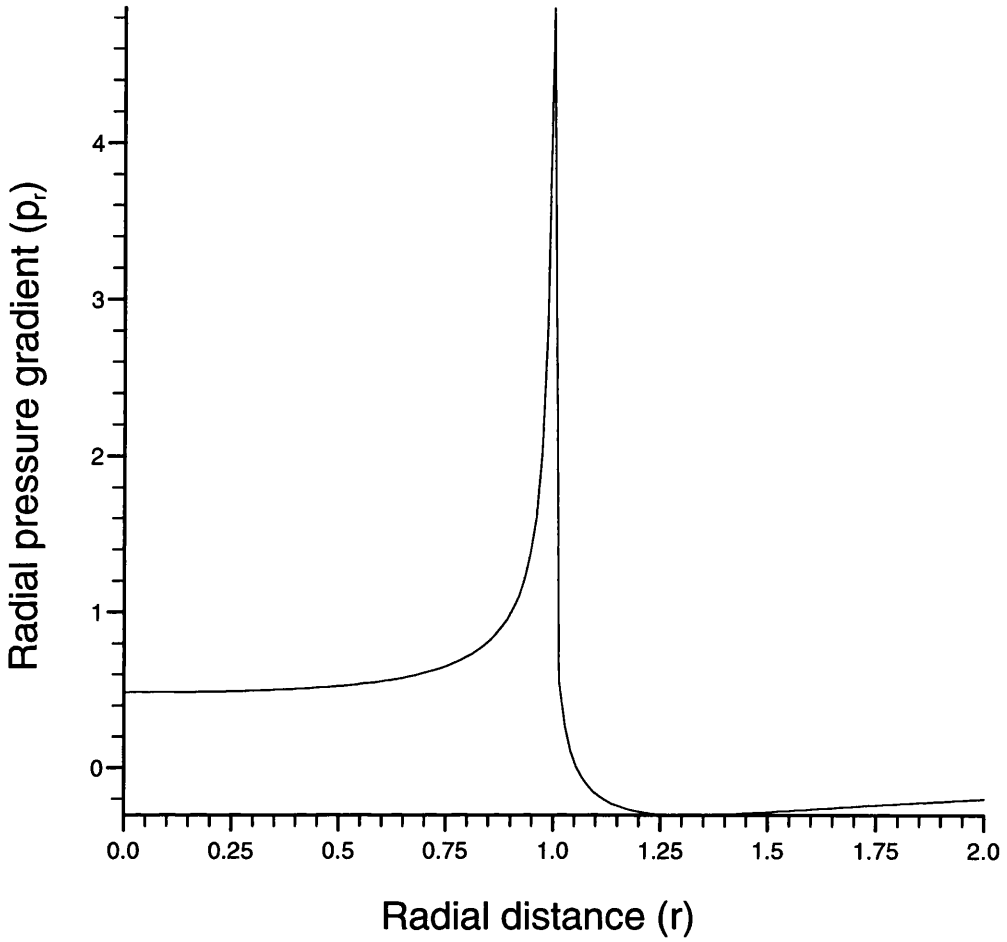


**Figure 3.13**: The radial pressure gradient across the cylinder at a depth of $z = -h$. Gradients become large near the corner.

tives of the pressure by finite differences. When the derivatives are very large or infinite the approximation introduces significant errors into the calculation.

In calculations involving approximations to real ocean topography it is not feasible to remove the singularity at each step. Two practical steps to reduce inaccuracies would be to first smooth the topography to eliminate or minimise sharp corners and secondly to increase the resolution of the model in regions where such corners exist in order to approximate the rapidly varying pressure field more closely.

## §3.5 Summary

The work of Chapter 2 is extended in this chapter to apply to the case of an infinite submerged ridge. The main difference is that the domain is not now closed at one end but suitable Green's functions can still be found. A complication arises

where the topography is modelled by a piecewise linear function. In medium to strong stratification, analysis indicates that very large pressure gradients occur where there is a corner with an internal angle of greater than $\pi$ radians. This can cause problems in determining the modes in such cases.

Examples of another semi-analytic technique using matched Fourier expansions are given in the cases of a tophat shaped ridge. The results for this confirm the existence of large pressure gradients near a corner as the stratification increases. This problem has also been seen in GCM models, specifically in the case of a cylindrical sea mount. The matched Fourier expansion technique is applied to this case and the results compared to those obtained elsewhere.

# Chapter 4

# The scattering and forcing of topographic Rossby waves

## §4.1 Introduction

The main advantage over previous work of the numerical method discussed in §2.4 and §3.2 is its ease of use in applications. There are two main areas to which the theory of low-frequency coastally trapped waves has been profitably applied. These are the scattering of low-frequency energy by topography and the response of coastal waters to low-frequency wind forcing.

Both of these applications rely on the fact that the low-frequency modes are orthogonal over the shelf, (§2.2), or ridge, (3.2.3) and form a complete set there. Hence any pressure distribution over the topography can be expressed as an infinite series of modes and the amplitude of each recovered using the orthogonality relation. The only information about each mode that is required is the pressure on the shelf and the phase speed. A method which restricts itself to finding these values is inherently more efficient. Previous methods, which used a two-dimensional grid over the whole domain, waste time and computing effort determining the pressure in the fluid even though it is completely derivable from the pressure on the shelf using (2.4.11).

In addition because each mode is derived separately in other methods the orthogonality between modes is often rather weak. For instance, in Middleton (1992) the computed inner product for two separate modes is in the range 0.02–0.07 compared with $10^{-5}$–$10^{-15}$ found with the new method.

Johnson (1989a,1991) gave connection formulae relating the incident and transmitted portions of coastally trapped waves as the waves pass through a short (compared to the wavelength) scattering region. These formulae are derived in §4.2 and examples are given there and in the following sections where they are extended to deal with scattering through straits or over ridges.

There is great interest in understanding the flow along the East Australian Coast north of Tasmania. The Australian Coastal Experiment (ACE) as discussed by Freeland *et al* (1986) found, contrary to expectation, that significant amounts of low-frequency energy were emerging from the Bass Straits (between Tasmania and the mainland). There are two possible sources for this energy: wind-forcing in the straits themselves and coastally trapped waves from the Great Australian Bight making their way through the strait. Middleton and

Viera (1991) and Middleton (1991) examined observational data and proposed a model for the whole region in an attempt to determine the question. In §4.3 the connection formulae are applied to scattering of energy through straits and the results compared to the observations in ACE. This has the advantage that the pressure field within the straits does not have to be explicitly calculated.

The example in §4.4 answers a query posed by Killworth (1989a,b) who wondered how much of a Kelvin wave got past a ridge abutting the coastal wall. Killworth considered a two-layer fluid with a vertical coastal wall and found that the amount of energy transmitted across the ridge was roughly proportional to the minimum depth of the ridge. This result for the external Kelvin wave is confirmed for a continuously stratified fluid and is extended to determine the scattering of all the possible modes when more complicated shelf topography is used.

Clarke and Van Gorder (1986) produced a model to determine the response of coastal waters to wind forcing. Lopez and Clarke (1989) and Brink (1991) found that to achieve accuracy a large number of modes had to be used, sometimes up to 30. Until the new method was introduced, the use of so many modes would have been prohibitive. The program would have to be re-run for each mode and for higher modes the number of points needed along the shelf would have meant that a much denser grid would have to have been used. In §4.5 a simple example using harmonic wind stress is used to examine the question of convergence.

## §4.2 Equations of motion

The waves considered in this section have a very low-frequency. Hence alongshore derivatives of the wave field are much smaller than those out to sea or vertically. It is sensible then to consider the equations of motion on two different alongshore length scales, firstly the short scale of order the shelf width $L$, and secondly a long wave scale of order $L/\omega$ where $\omega \ll 1$. Short waves with an alongshore wavelength of order $\omega L$ may also exist but do not have to be taken account of explicitly.

Consider topography as in fig. 4.1, in which two shelves, monotonic but not necessarily parallel, are connected by a scattering region which is of order $L$.

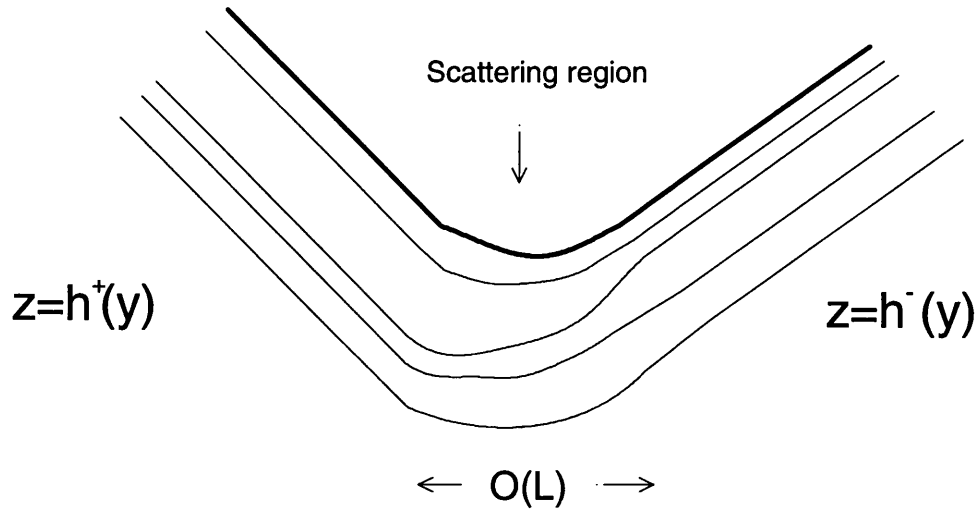


**Figure 4.1**: Two monotonic shelves meet at a scattering region. The length of this region is of the same order as the shelf widths. The profiles of the shelves are given in terms of $y$ measured perpendicular to the coast.

The shelves are straight over a length long compared to $L/\omega$. Over each shelf align the local $x$-axis along the topography, and take the $z$ and $y$ axes vertically and perpendicular to the coast so that they form a right-handed triplet. The topography is given by $z = -h_-(y)$ as $x \to -\infty$ and $z = -h_+(y)$ as $x \to \infty$ or alternatively by $y = d_-(z)$ as $x \to -\infty$ and $y = d_+(z)$ as $x \to \infty$.

Consider a wave of frequency $\omega$ incident upon the scattering region from $x = -\infty$. On the short $x$ scale, omitting a common factor of $e^{i\omega t}$ the horizontal velocities can be written (from 1.7) as

$$u = -(p_y + i\omega p_x)/(1-\omega^2), \tag{4.2.1a}$$

$$v = (p_x - i\omega p_y)/(1-\omega^2), \tag{4.2.1b}$$

and hence in the limit of $\omega \to 0$ with $B$ fixed, the equations reduce to the geostrophic relations. On the short scale therefore, the pressure is constant along a streamline.

The vertical velocity $w$ is of order $\omega$ from (1.5d) and therefore the impermeability condition (1.9) on the topography reduces to

$$uh_x + vh_y = \frac{\partial(p,h)}{\partial(x,y)} = 0, \tag{4.2.2}$$

as $\omega \to 0$. This implies that the pressure on the boundary is a function solely of

the depth and hence gives the isobath tracing result (Johnson 1989a,1991) that *the pressure along an isobath through an $O(L)$ scattering region is constant.* An isobath is a line satisfying $h(x,y)$ =constant. This does not however determine the pressure over any flat portion of the scattering region. In such an area the boundary condition (1.9) reduces to $p_z = 0$ and $p$ is left unspecified.

On the long scale $X = \omega x$, waves can propagate along the straight stretches provided

$$p(X,y,z) = e^{-iX/c_n}\Phi_n(y,z), \tag{4.2.3}$$

where $\Phi_n, c_n$ are the eigenfunctions and phase speeds that satisfy

$$\Phi_{yy} + B^{-2}\left(\frac{\Phi_z}{N^2}\right)_z = 0, \tag{4.2.4a}$$

$$h'N^2B^2(\Phi + c\Phi_y) + c\Phi_z = 0, \quad (z = -h(y)), \tag{4.2.4b}$$

$$a^2\Phi_z + B^2N^2(0)\Phi = 0, \quad (z = 0). \tag{4.2.4c}$$

and which can be determined using the methods in §2.2–4 and §3.2. These modes are complete and orthogonal across the topography and satisfy

$$\int_C \Phi_n\Phi_m dz = \int_C h'(y)\Phi_n\Phi_m dy = \delta_{nm}, \tag{4.2.5}$$

for each $n, m$.

As the pressure is constant along a short length of the isobath, the pressure on the topography after the scattering region is the same as that *before.* Hence, as the pressure on the shelf for the incident wave, $p_m^{(I)}(z)$, is known so is the pressure profile on the other side. Since the modes are complete on the straight stretches the contribution from each wave mode can be ascertained using the orthogonality relationship.

If the $m$th wave mode is incident upon the scattering region the transmitted wave field on the boundary will satisfy

$$p_m^{(I)}(d_-(z),z) = \sum_{n=0}^{\infty} a_{nm}p_n^{(T)}(d_+(z),z), \tag{4.2.6}$$

where $p_n^{(T)}$ are the transmitted wave modes. From orthogonality the coefficients $a_{nm}$, which are measures of the energy carried in each mode, can be determined as

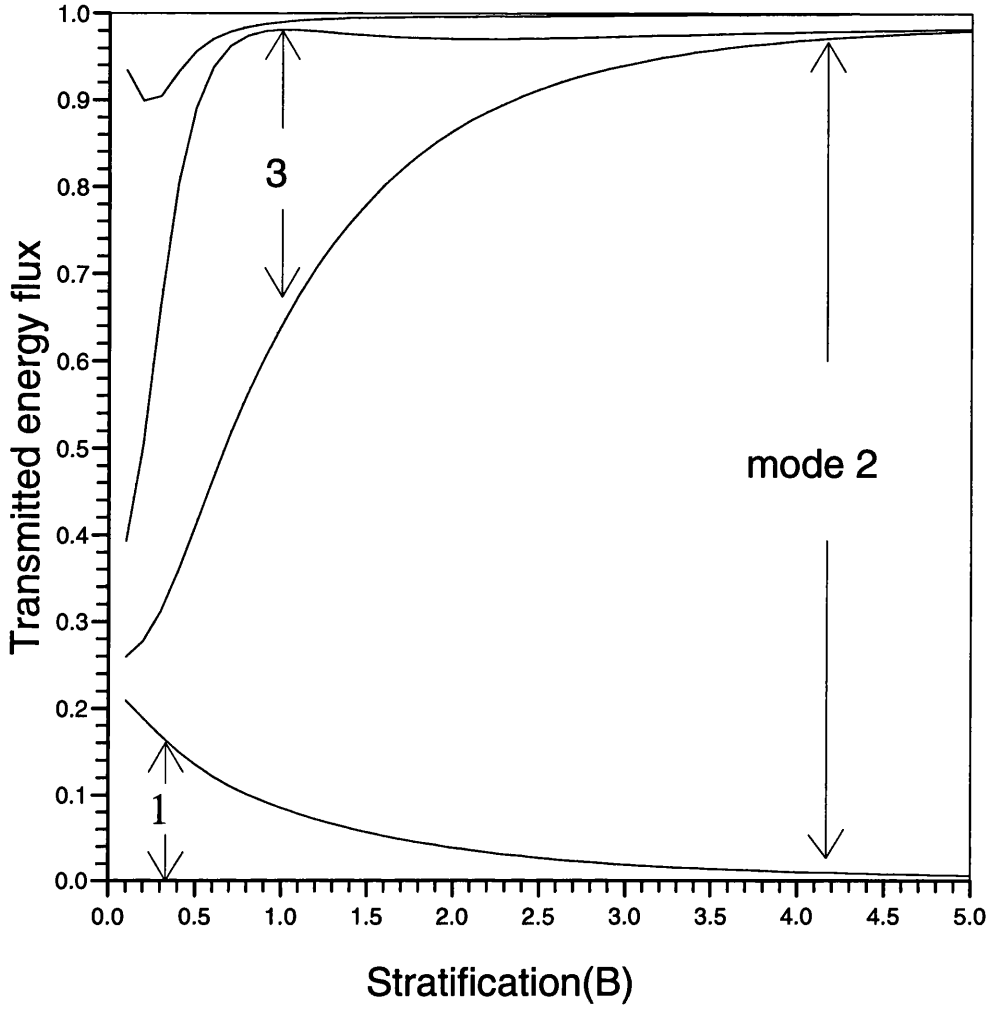


**Figure 4.2**: The scattering of an incident mode 2 wave over the cubic profile as the topography changes to the quartic profile. The quantities plotted are the $a_{nm}^2$ which are proportional to the energy in each transmitted mode.

$$a_{nm} = \int_{-1}^{0} p_m^{(I)}(d_-(z), z) p_n^{(T)}(d_+(z), z) dz. \tag{4.2.7}$$

The advantage of the new method over previous methods in this application is because these values of the pressure on the coast are precisely the eigenvectors of the matrix problem (2.4.13). Hence, if (4.2.7) is evaluated using Simpson's rule it is a trivial matter to calculate $a_{nm}$, especially if the vertical spacings used are the same in both calculations for the $p_n$.

As an example consider the scattering of energy as the shelf shape changes from the cubic profile, $d(z) = 2z^3 + 3z^2$ to the quartic $d(z) = 1 - (1+z)^4$. Figure 4.2 shows how the energy transmitted to each mode at $x \to \infty$ varies with the stratification parameter $B$. The Rossby radius is taken to be $a = 10$ and uniform

stratification is used. If the incident mode is the external Kelvin wave then there is virtually no scattering at all for any value of $B$. In the figure the incident wave is the second mode which scatters mainly to its counterpart and adjacent modes. This result bears out the conclusion in Johnson (1989a) that strong stratification suppresses all scattering.

For the scattering as a *ridge* changes shape, there is the possibility that some energy is reflected as waves concentrated on the opposite side. The topography given by $z = -h(y)$ can be decomposed into a series of monotonic profiles $y = d_n(\mathbf{z})$ for $y_{n-1} \leq y \leq y_n$ $n = 1, 2, \ldots N$, and the isobath tracing result followed through. If the minimum depth of the ridge changes in the scattering region then some of the isobaths must necessarily double-back. A discussion of the complications that then arise follows this simple example.

Take two symmetric ridges which have the same minimum depth, $h_0$, and assume that all the isobaths from $x = -\infty$ arrive at $x = \infty$. The topography can then be written as

$$y = \begin{cases} -d(z), & -1 \leq y \leq 0, \\ d(z), & 0 \leq y \leq 1. \end{cases} \tag{4.2.8}$$

The result of isobath tracing gives as the analogue of (4.2.6)

$$\sum_{n=0}^{\infty} a_{nm} p_n^{(T)}(-d_+(z), z) = p_m^{(I)}(-d_-(z), z) + \sum_{n=0}^{\infty} b_{nm} p_n^{(R)}(-d_-(z), z), \quad z < -h_0,$$

$$\sum_{n=0}^{\infty} a_{nm} p_n^{(T)}(d_+(z), z) = p_m^{(I)}(d_-(z), z) + \sum_{n=0}^{\infty} b_{nm} p_n^{(R)}(d_-(z), z), \quad z < -h_0, \tag{4.2.9}$$

where the functions $p_n^{(R)}$ are the pressure fields for the reflected waves opposite the incident wave. Each set of modes on the different ridges is independently orthonormal and so two sets of equations for the vectors $\mathbf{a} = (a_{0m}, a_{1m} \ldots)$ and $\mathbf{b} = (b_{0m}, b_{1m} \ldots)$ result

$$\mathbf{a} = \mathbf{c} + M\mathbf{b}, \tag{4.2.10a}$$

$$\mathbf{b} = M^T \mathbf{a}, \tag{4.2.10b}$$

where the components of the matrix $M$ are

$$m_{ij} = \int_{-1}^{-h_0} \left\{ p_j^{(R)}(d_-(z), z) p_i^{(T)}(d_+(z), z) - p_j^{(R)}(-d_-(z), z) p_i^{(T)}(-d_+(z), z) \right\} dz,$$

and

$$c_i = \int_{-1}^{-h_0} \left\{ p_m^{(I)}(d_-(z),z) p_i^{(T)}(d_+(z),z) - p_m^{(I)}(-d_-(z),z) p_i^{(T)}(-d_+(z),z) \right\} dz.$$

As above, it is very simple to evaluate these integrals if the method used to find the pressure gives the values on the shelf evenly spaced in $z$. Then Simpson's rule can be applied with no difficulty. This does however imply that the integrations in the numerical method must be performed with respect to $z$. Hence it rules out the possibility of using a ridge profile that is flat at the top (i.e. $h'(0) = 0$).

Equations (4.2.10) combine to give a simple matrix equation for the amplitudes which can be solved using LU-decomposition and back substitution. Returning to the situation where some of the isobaths double-back, say those on the incident side of depth greater than $h_1$ but less than $h_0$, note that (4.2.9) and (4.2.10a) still hold. There is an additional equation which matches the pressure along the higher isobaths i.e.

$$p_m^{(I)}(-d_-(z),z) + \sum_{n=0}^{\infty} b_{nm} p_n^{(R)}(-d_-(z),z) = p_m^{(I)}(d_-(z),z) + \sum_{n=0}^{\infty} b_{nm} p_n^{(R)}(d_-(z),z), \quad -h_1 > z > -h_0. \tag{4.2.11}$$

This implies two extra terms in (4.2.10b) to give

$$\mathbf{b} = M^T \mathbf{a} + E\mathbf{b} + \mathbf{d}, \tag{4.2.12}$$

where

$$e_{ij} = \int_{-h_0}^{-h_1} \left\{ p_j^{(R)}(-d_-(z),z) p_i^{(R)}(d_-(z),z) - p_j^{(R)}(d_-(z),z) p_i^{(R)}(-d_-(z),z) \right\} dz,$$

and

$$d_i = \int_{-h_0}^{-h_1} \left\{ p_m^{(I)}(-d_-(z),z) p_i^{(R)}(d_-(z),z) - p_m^{(I)}(d_-(z),z) p_i^{(R)}(d_-(z),z) \right\} dz.$$

These equations can be solved as previously by eliminating the vector $\mathbf{a}$.

The method can be extended to various other more complicated topographies simply by tracing each isobath through the scattering region. This is done for the cases of a strait and for a ridge abutting a coastal shelf in the following two sections.

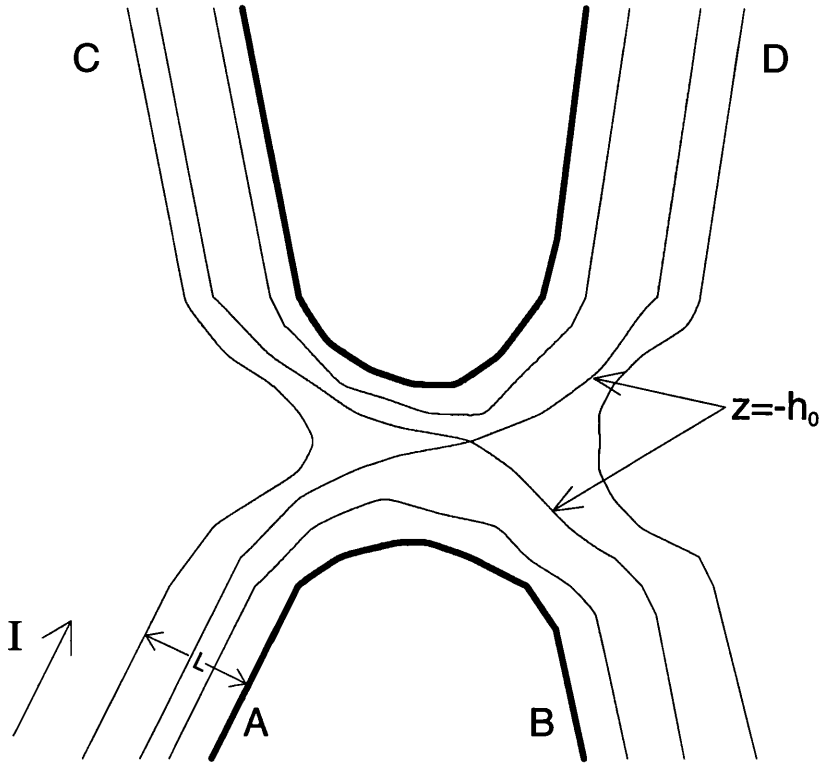


**Figure 4.3**: A coastally trapped wave from A is incident upon a strait. Some energy is passed through the strait to produce a coastally trapped wave field at B while the rest continues up the coast at C. The main factor determining the proportion of energy transmitted through is the depth of the separating isobath, $h_0$.

## §4.3 Scattering through straits

Consider first the strait topography given in fig. 4.3. The depth and the horizontal length are scaled on the outer depth, $D$, and shelf width, $L$, at $A$. The width and length of the scattering region are of order $L$. There is an isobath at $z = -h_0$ which divides those isobaths which cross the strait and those which remain on the same side. The existence of areas of closed streamlines wholly within the strait or scattering region does not affect the result of this section and plays no role in the scattering of energy.

Let the shelves at points $A, B, C$ and $D$ vary slowly enough in the alongshore direction so that the low frequency theory is valid. For directness, the four profiles given by the functions $y = d_A(z), d_B(z), d_C(z)$ and $d_D(z)$, where $y$ is taken to be perpendicular to the shelf, are assumed to be monotonic. Consider the flow field driven by a low-frequency wave $I$ incident from $A$. The energy associated with isobaths higher than $h_0$ passes through the strait and determines the pressure field

for the higher isobaths at $B$. The pressure on the lower isobaths at $C$ is similarly determined. Since there is no energy incident from $D$, the pressure along isobaths originating at $D$ is identically zero. Hence the transmitted pressure distribution at $B$ and $C$ is completely determined and depends solely upon the depth of the dividing streamline. As the mode structure at $B$ and $C$ is known, orthogonality can be used to determine the amplitudes of each mode.

Denote the pressure field at $A, B$ and $C$ by $p^{(A)}(y,z), p^{(B)}(y,z)$ and $p^{(C)}(y,z)$ respectively. If the wave mode incident from $A$ is the $m$th mode then the isobath tracing result gives

$$\sum_{n=0}^{\infty} b_{nm} p_n^{(B)}(d_B(z), z) = \begin{cases} p_m^{(A)}(d_A(z), z), & z > -h_0, \\ 0, & z < -h_0, \end{cases} \tag{4.3.1a}$$

$$\sum_{n=0}^{\infty} c_{nm} p_n^{(C)}(d_C(z), z) = \begin{cases} 0, & z > -h_0, \\ p_m^{(A)}(d_A(z), z), & z < -h_0. \end{cases} \tag{4.3.1b}$$

Use orthogonality at $B$ and $C$ to give the amplitudes

$$b_{nm} = \int_{-h_0}^{0} p_m^{(A)}(d_A(z), z) p_n^{(B)}(d_B(z), z)\, dz, \tag{4.3.2a}$$

$$c_{nm} = \int_{-1}^{-h_0} p_m^{(A)}(d_A(z), z) p_n^{(C)}(d_C(z), z)\, dz, \tag{4.3.2b}$$

As an example take the three profiles at $A$,$B$ and $C$ to be the cubic, quartic and linear profiles respectively. Denote the EKW mode at $C$ by $C_0$, the second mode at $B$ by $B_2$ etc. Firstly, assume uniform stratification and that $a = 10$ and $h_0 = 0.5$. In figures 4.4 and 4.5 the distribution of energy between $B$ and $C$ is indicated by the thick line. In both cases there is very little change in the amount of energy passing through the strait as the stratification varies although over each profile the distribution within the modes does vary quite considerably. There is a tendency for the energy that passes through the strait to be scattered into lower modes and for the energy that passes by to be scattered into higher modes. This of course, will depend crucially on the shelf profiles at $B$ and $C$.

Figures 4.6 and 4.7 show how the energy associated with the transmitted modes varies with the height of the dividing isobath. In fig. 4.6 the incident wave at $A$ is the external Kelvin wave mode (mode 0). The energy transmitted through the strait is almost exactly linearly proportional to the depth and most

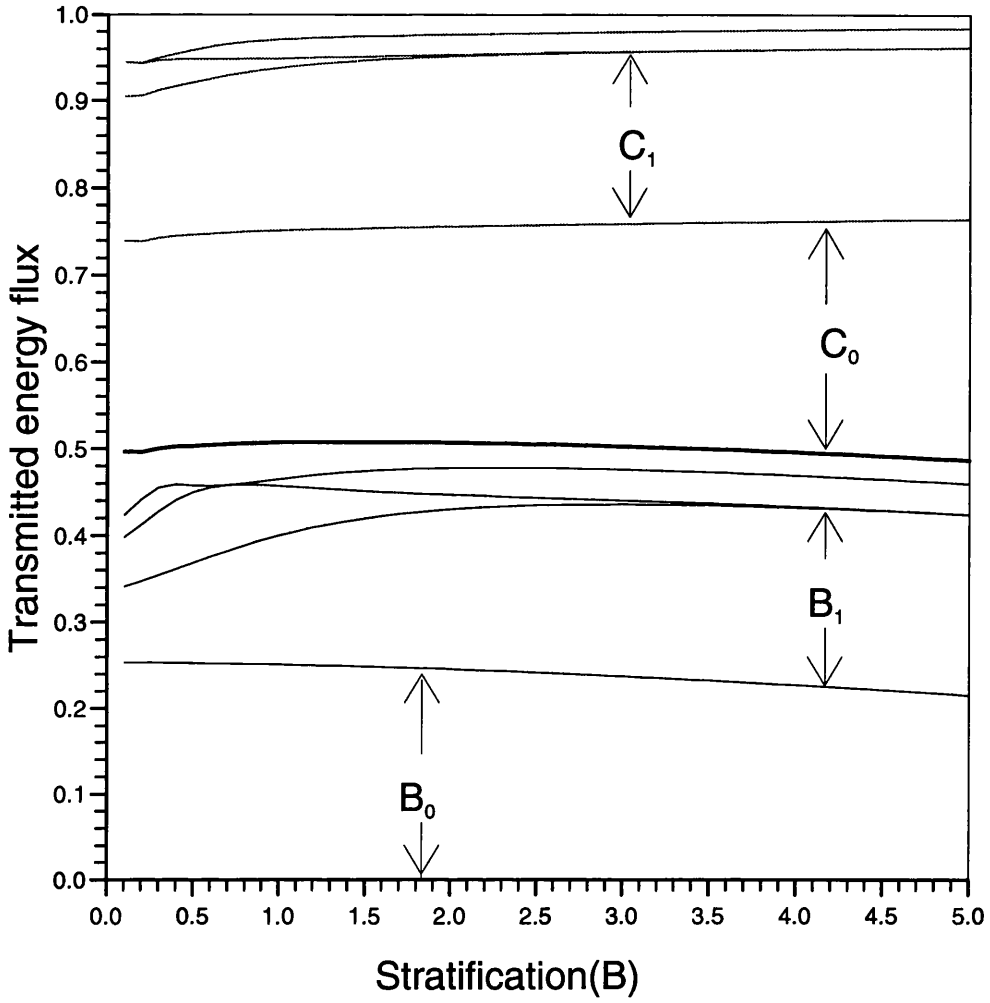


**Figure 4.4**: The scattering of an external Kelvin wave mode (mode 0) incident upon the strait. Uniform stratification, $a = 10$ and $h_0 = 0.5$. The distribution of energy among the modes at $B$ and $C$ is found by plotting $b^2_{nm}$ and $c^2_{nm}$. The mode $B_0$ refers to the external Kelvin wave mode at B etc. The total amount of energy passing through the strait, indicated by the thicker line, does not vary significantly with stratification, although the distribution of energy among the modes on each side does.

of that energy remains as the EKW mode at $B$. However in fig. 4.7 the incident wave is the second mode and the energy transmitted depends far more upon the complicated structure of the mode.

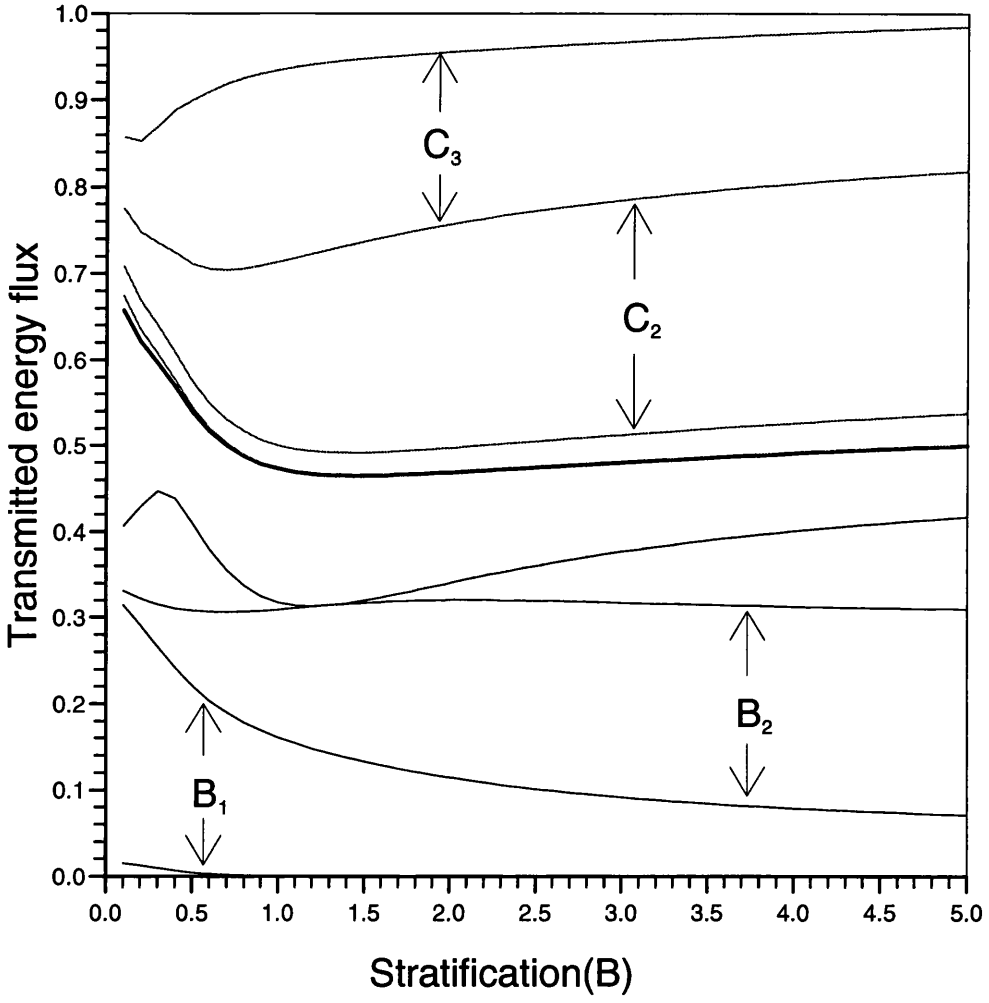


**Figure 4.5**: The scattering of a mode 2 wave incident from $A$ with the same parameters as in fig. 4.4 . With these profiles there is a tendency for the energy at $C$ to be scattered into higher modes than the energy at $B$.

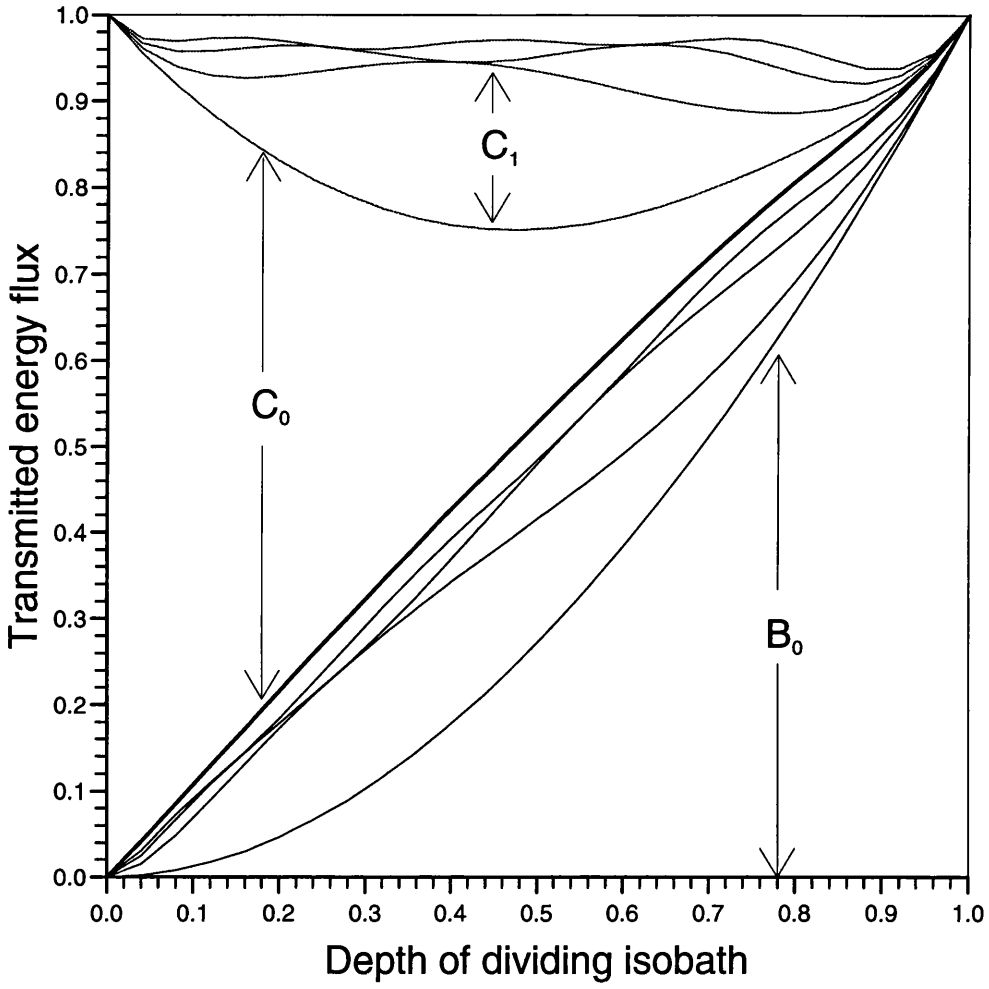


**Figure 4.6**: The scattering of a mode 0 wave through the strait. The energy transmitted through the strait (the bottom modes in the diagram) is almost exactly proportional to the depth of the dividing streamline, $h_0$.

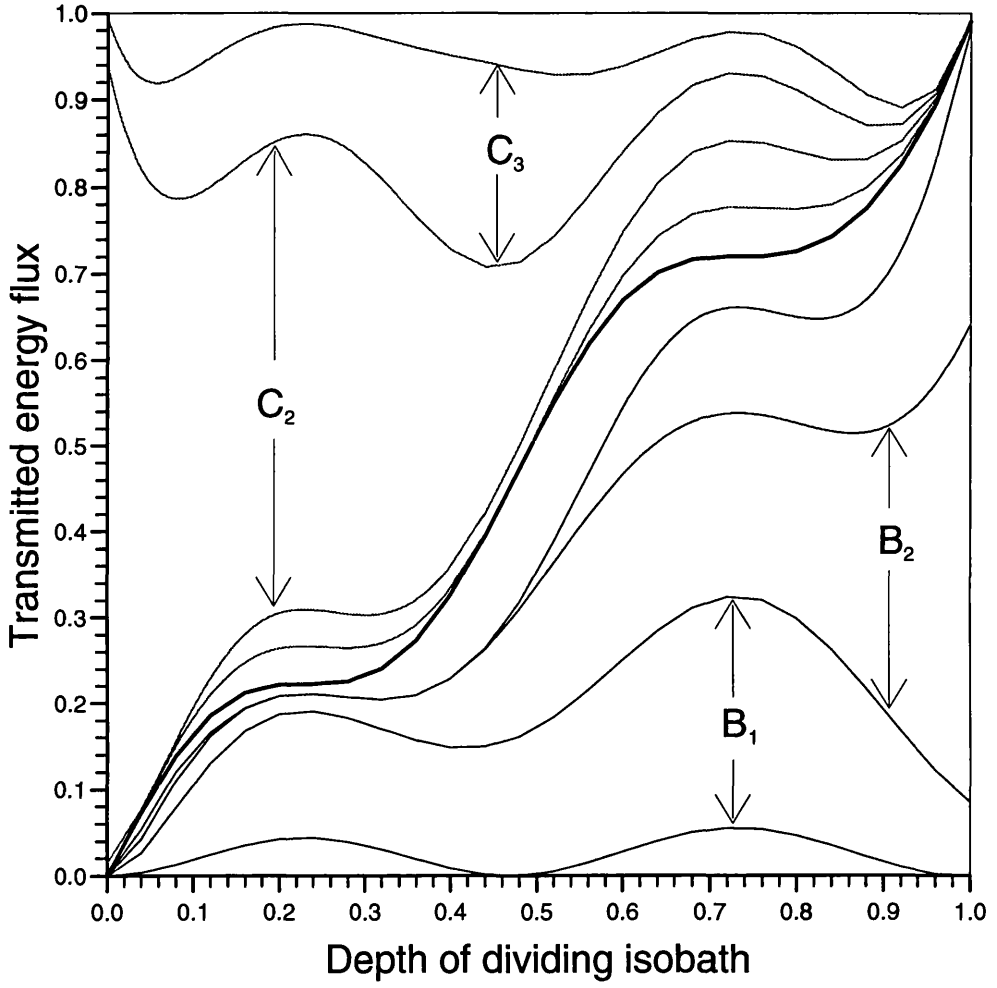


**Figure 4.7**: The scattering of a mode 2 wave through the strait. The total energy transmitted through the strait increases with the depth of the dividing streamline but because of the more complicated structure of the incident wave it is not simply proportional as in the previous figure.

It is also of interest to see what effect the structure of the buoyancy frequency profile has on the energy passing through the strait. Assume that $N(z) = \exp(\alpha z)$, $B = 1.0$, $a = 10$ and take $h_0 = 0.5$. Figure 4.8 shows the scattering of an incident mode 1 wave as the parameter $\alpha$ varies. As the stratification becomes more concentrated at the surface more of the mode energy is transmitted through the strait. There is also a tendency for the energy passing through the strait to to distributed more towards the higher modes as $\alpha$ increases.

Of more practical interest is the situation at the Bass Strait. Figure 4.9 (from Middleton, 1991) shows the topography in the vicinity. The depth of the dividing streamline is around 70m compared to the open ocean depth of 3-4km. Hence only very few of the isobaths cross the strait. This might be expected to scatter energy preferentially into the higher modes as was seen in Freeland *et al* (1986).

To apply the preceding theory to this example, assume that no energy is carried by the incident wave around the island and that the low-frequency pressure field on isobaths to the east of Tasmania is identically zero. This is a fair assumption given the topography to the south of the island and backed up by the lack of observational evidence for waves there. Take the length scale to be 100km and the Coriolis parameter $f$ =-9.15x10$^{-5}s^{-1}$, (negative in the Southern hemisphere).

The stratification on the shelves is modelled by an exponential buoyancy frequency profile with $\alpha = 4.0$ and $N_0 = 0.01s^{-1}$. The values of the non-dimensional parameters are then $B = 3.8$, $a = 19.0$ and $h_0 = 0.02$. The topography is approximated by the quartic profile on all three shelves.

The results in table 4.1 confirm that no matter which mode is incident, the energy that passes through the strait is predominately contained in modes 1,2 and, to a lesser extent, mode 3. There is very little energy ($\sim 2\%$) transmitted to the fundamental mode in any case. The greatest penetration of energy through the strait occurs when either mode 1 or mode 2 is incident.

With such a relatively shallow strait it is not surprising that the majority of the incident wave energy continues along the coast. This energy tends to remain in the same mode.

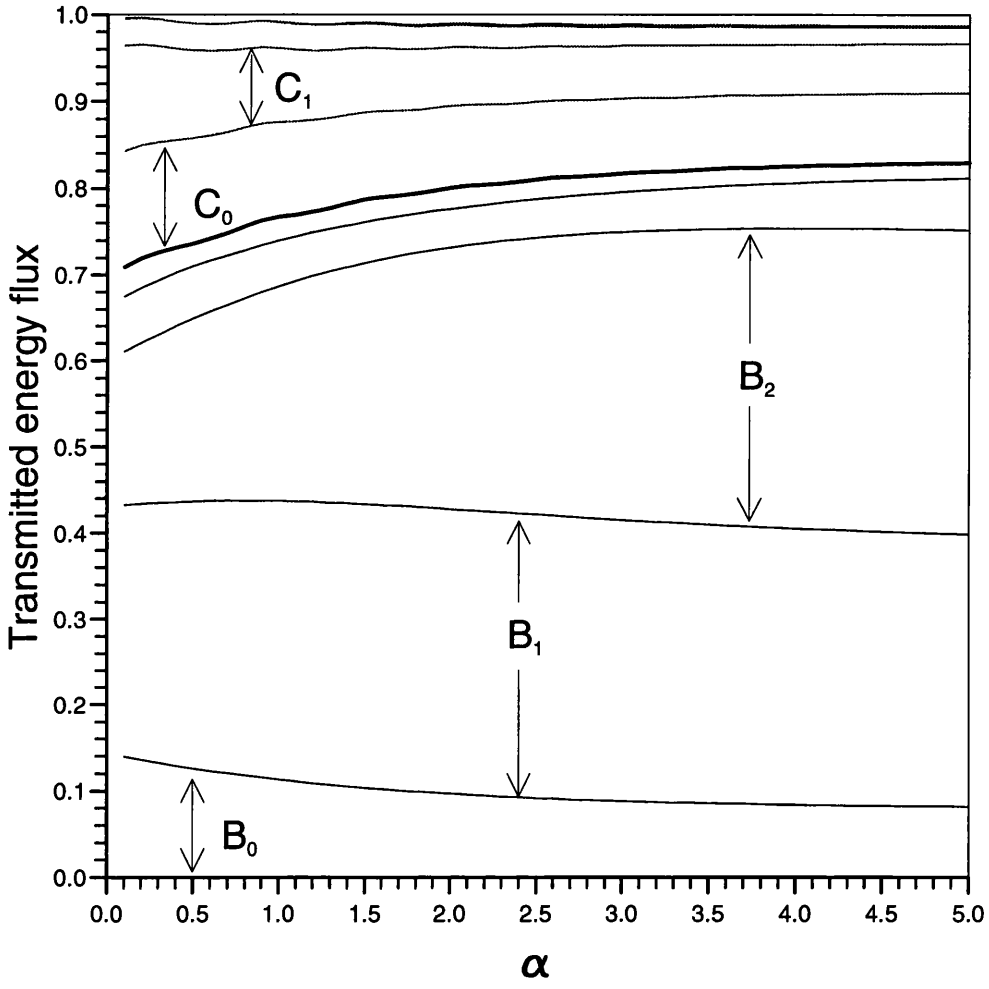


**Figure 4.8**: The scattering of a mode 1 wave through the strait as the structure of the buoyancy frequency profile changes. $N(z) = \exp(\alpha z)$ and $\alpha$ ranges from 0.1 to 5. As alpha increases more energy is concentrated near the surface and hence more energy passes through the strait.

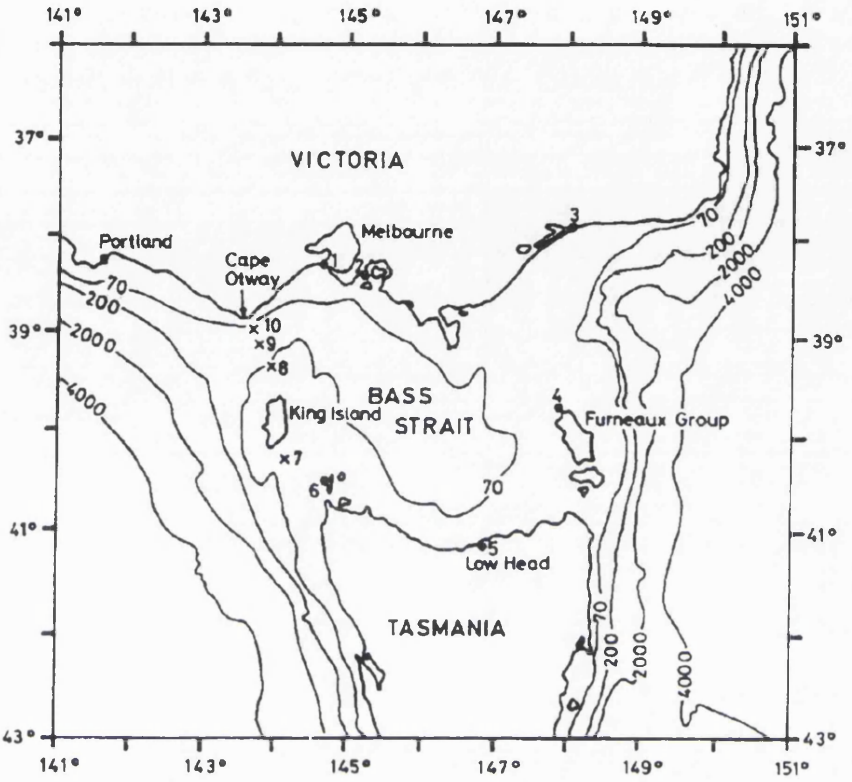


**Figure 4.9**: The topography in the vicinity of the Bass Strait. The depth of the dividing streamline is about 70m compared to an open ocean depth of 3–4km.

| Incident mode | Total energy passed through the strait (%) | Distribution of energy among modes at $B$ (%) | | | | Distribution of energy among modes at $C$ (%) | | | |
|---|---|---|---|---|---|---|---|---|---|
| | | 0 | 1 | 2 | 3 | 0 | 1 | 2 | 3 |
| 0 | 2.0 | 2.2 | 23.1 | 22.3 | 16.8 | 97.9 | 0.5 | 0.5 | 0.4 |
| 1 | 21.7 | 2.2 | 23.0 | 22.4 | 17.0 | 0.6 | 78.8 | 6.2 | 4.7 |
| 2 | 21.1 | 2.2 | 22.5 | 22.3 | 17.3 | 0.6 | 6.1 | 79.0 | 4.7 |
| 3 | 16.8 | 2.1 | 21.5 | 22.7 | 17.3 | 0.4 | 4.3 | 4.4 | 83.2 |

**Table 4.1:** This table shows the estimated amount of energy scattered through the Bass Strait by incident waves from the Great Australian Bight using the parameters given in the text. The distribution of energy among the modes on the far side of the strait (at $B$) shows that energy is scattered preferentially into mode 1 and mode 2.

## §4.4 Scattering of waves incident upon a ridge

Consider a straight coast aligned along the $y$-axis with a ridge perpendicular to the coast aligned along the $x$-axis although the analysis that follows is still valid whatever angle the ridge makes with the coast. Assume for simplicity that the depth of the water is equal on both sides of the ridge.

Scale the depth and horizontal lengths on the dimensions of the shelf at $A$ in fig 4.10 . The profile of the coastal shelf does not need to be the same on either side of the ridge, so denote the profiles at $A$ and $D$ by $x = d_A(z)$ and $d_D(z)$ respectively. The ridge is assumed to have a profile which can be written $y = d_B(z)$ for $y \leq 0$ and $y = d_C(z)$ for $y \geq 0$. There is a dividing isobath at a depth of $h_0$.

The isobath tracing result can now be applied to this geometry. There is a complicating factor when the problem involves a ridge in that the pressure field for the waves on the ridge has a 'tail' on the opposite side, $C$, that is not determined by the incident wave mode. It can be found by matching the pressure along the lower isobaths to that at $D$. The equations that arise are matrix equations that must be solved using standard linear algebra techniques.

Assume that a $m$th mode wave is incident upon the ridge from $A$. The isobath tracing result can be used to determine the pressure on the ridge at $B$ and on the higher isobaths at $D$. No energy is incident from $x = \infty$ along $C$ so the pressure on $C$ consists solely of the tails of the outward propagating modes. This pressure has to be matched on the isobaths at $D$.

Denote the pressure field at $A, B$ and $D$ by $p^{(A)}(x,z), p^{(B)}(y,z)$ and $p^{(D)}(x,z)$ respectively. So at $B$ and $D$

$$\sum_{n=0}^{\infty} b_{nm} p_n^{(B)}(d_B(z), z) = p_m^{(A)}(d_A(z), z), \quad z < -h_0,$$
$$\sum_{n=0}^{\infty} d_{nm} p_n^{(D)}(d_D(z), z) = p_m^{(A)}(d_A(z), z), \quad z > -h_0. \tag{4.4.1}$$

where the modes at $B$ consist only of the outward propagating waves. The matching condition at $C$ implies

$$\sum_{n=0}^{\infty} b_{nm} p_n^{(B)}(d_C(z), z) = \sum_{n=0}^{\infty} d_{nm} p_n^{(D)}(d_D(z), z), \quad z < -h_0. \tag{4.4.2}$$

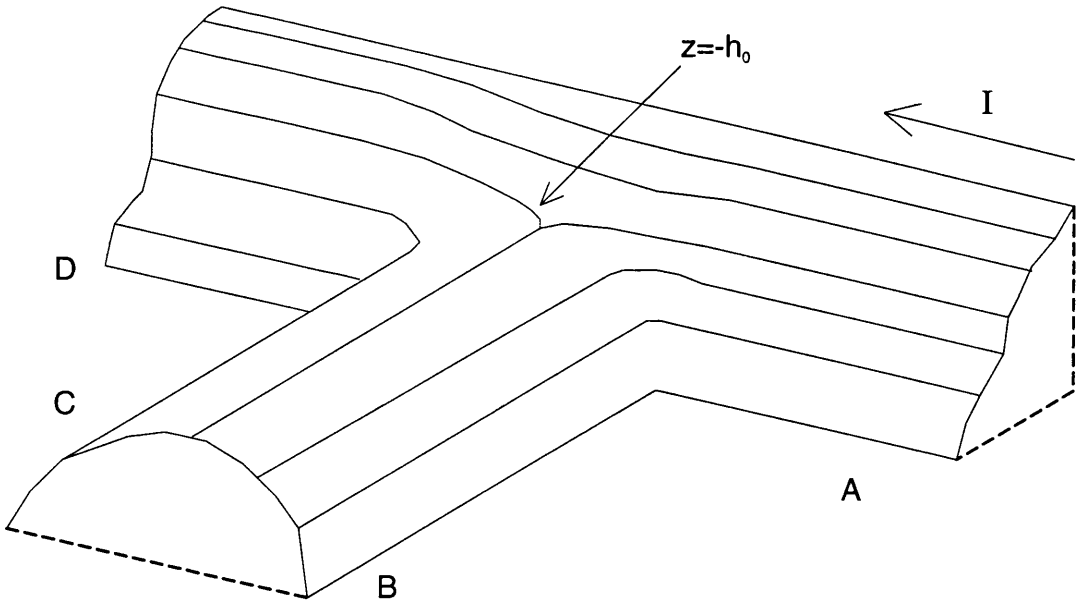


**Figure 4.10**: Waves from $A$ are incident upon a ridge. Energy is scattered into wave fields concentrated at $B$ and at $D$. The depth of the dividing isobath is $h_0$.

Orthogonality of the modes at $D$ implies (in vector notation, $\mathbf{d} = (d_{0m}, d_{1m}, \ldots)$ and $\mathbf{b} = (b_{0m}, b_{1m}, \ldots)$)

$$\mathbf{d} = \mathbf{a} + M\mathbf{b}, \tag{4.4.3}$$

where the components of the matrix $m_{ij} = \int_{-1}^{-h_0} p_j^{(B)}(d_C(z), z) p_i^{(D)}(d_D(z), z)\, dz$ and $a_i = \int_{-h_0}^{0} p_m^{(A)}(d_A(z), z) p_i^{(D)}(d_D(z), z)\, dz$. Similarly, orthogonality on the ridge implies

$$\mathbf{b} = \mathbf{c} - M^T\mathbf{d}, \tag{4.4.4}$$

where $c_i = \int_{-1}^{-h_0} p_m^{(A)}(d_A(z), z) p_i^{(B)}(d_B(z), z)\, dz$. Substitute (4.4.3) into (4.4.4) to get a simple equation for $\mathbf{b}$

$$(I + M^T M)\mathbf{b} = \mathbf{c} - M^T\mathbf{a}. \tag{4.4.5}$$

This can be solved using LU-decomposition and back substitution. The components of $\mathbf{d}$ can be recovered from (4.4.3).

As an example assume that the profiles at $A$ and $D$ are the cubic and quartic profiles used previously. Further assume that the ridge has the symmetric profile $|y| = 1 - (z+1)^2/(1-h_0)^2$ where $h_0$ is the depth of the dividing isobath.

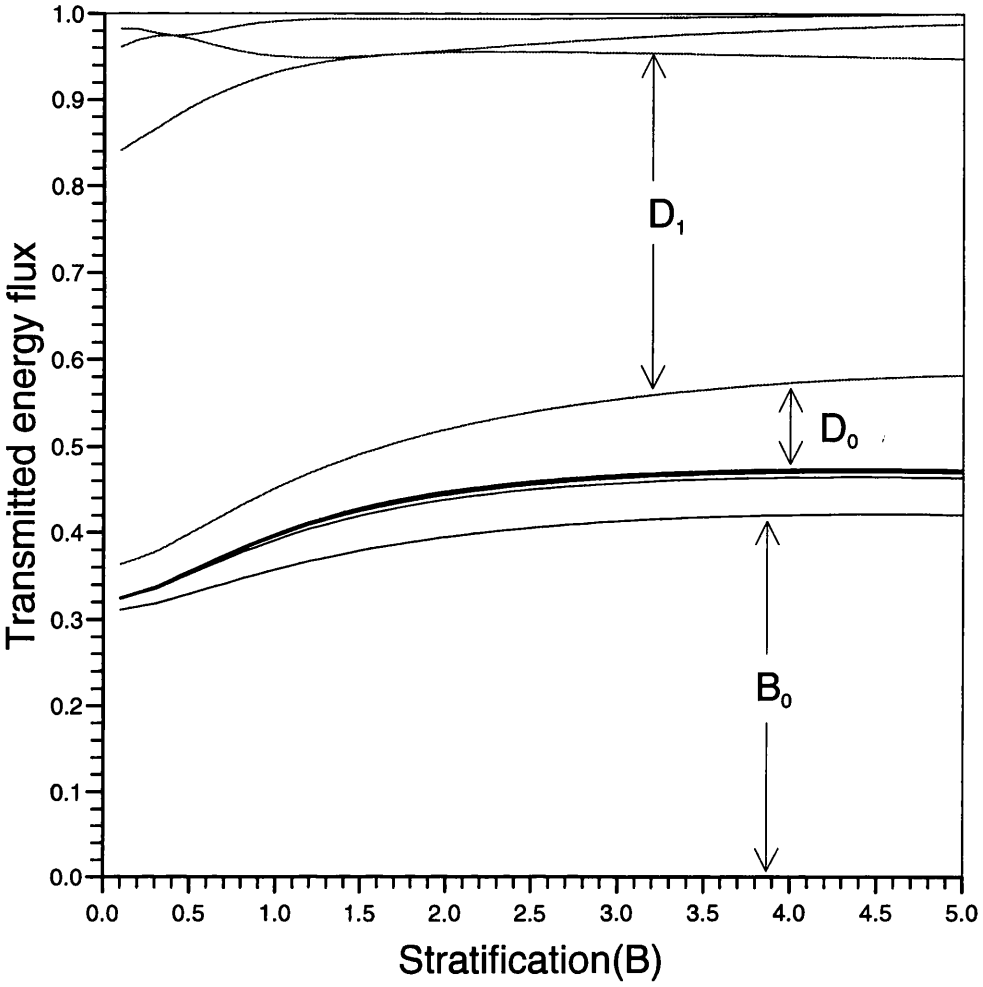


**Figure 4.11**: The scattering of an incident mode 1 wave by a ridge abutting the shelf. The amount of energy crossing the ridge decreases with increasing stratification. Interestingly, most of the energy that is propagated along the ridge is in the fundamental mode and conversely the energy at $D$ is in the form of a mode 1 wave.

Figure 4.11 shows how the energy from an incident mode 1 wave at $A$ is scattered by the ridge as the stratification varies. The modes are labelled $B_0, B_1 \ldots$ and $D_0, D_1 \ldots$ for the fundamental mode 0, mode 1 ... on the ridge and on the shelf at $D$ respectively. The depth of the dividing isobath is $z = -0.5$ and $a = 10$.

As the stratification increases, the amount of energy transmitted past the ridge decreases to 50% in the limit as $B \to \infty$. Most of the energy at $D$ remains as a mode 1 wave but on the ridge only mode 0 is present.

Figure 4.12 shows how the amount of energy distributed varies with the depth of the dividing isobath (the minimum depth of the ridge). For an incident mode 0 wave the amount of energy that passes over the ridge is roughly proportional to the minimum depth. This supports the hypothesis of Killworth (1989a,b)

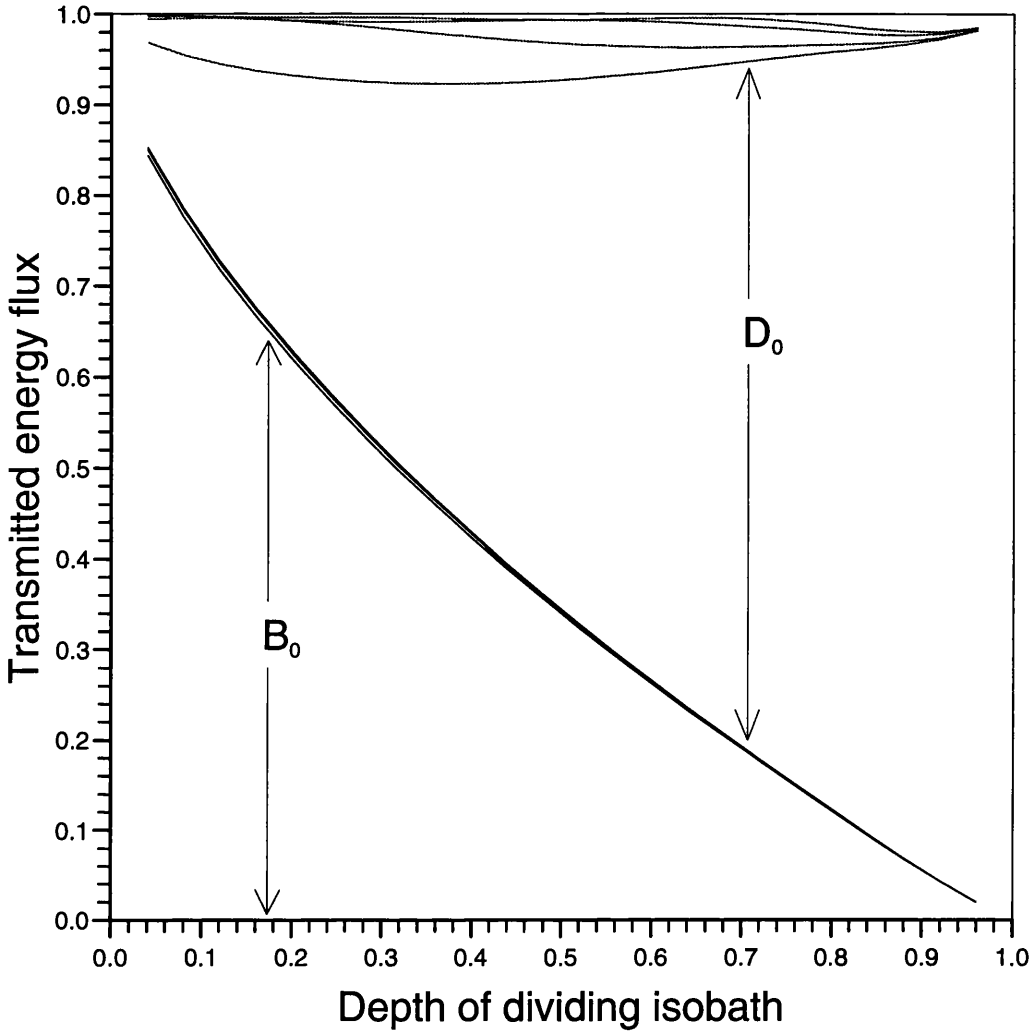


**Figure 4.12**: The scattering of an incident mode 0 wave by a ridge abutting the shelf as the height of the ridge varies. The amount of energy that passes the ridge is roughly proportional to the depth of the dividing isobath. All the energy transmitted along the ridge is in the fundamental mode.

who presented large numerical computations for one- and two-layer flows with a vertical shelf. It also agrees with analytical results of Johnson (1991,1993). Most of the energy at $D$ is also in the form of the external Kelvin wave.

The situation where the mode 1 wave is incident on the ridge is more interesting. There is now a zero in the incident pressure field on the shelf. Recall that each mode number is characterised by these zeros on the shelf, i.e. mode 0 has no zeros, mode 1 has 1 zero etc. and that the zeros for adjacent modes interlace. This is true for both ridge and coastal waves.

The zero in the incident pressure field in fig. 4.13 occurs at a depth of around 0.46. The point at which the mode 1 wave ceases to be important to the pressure

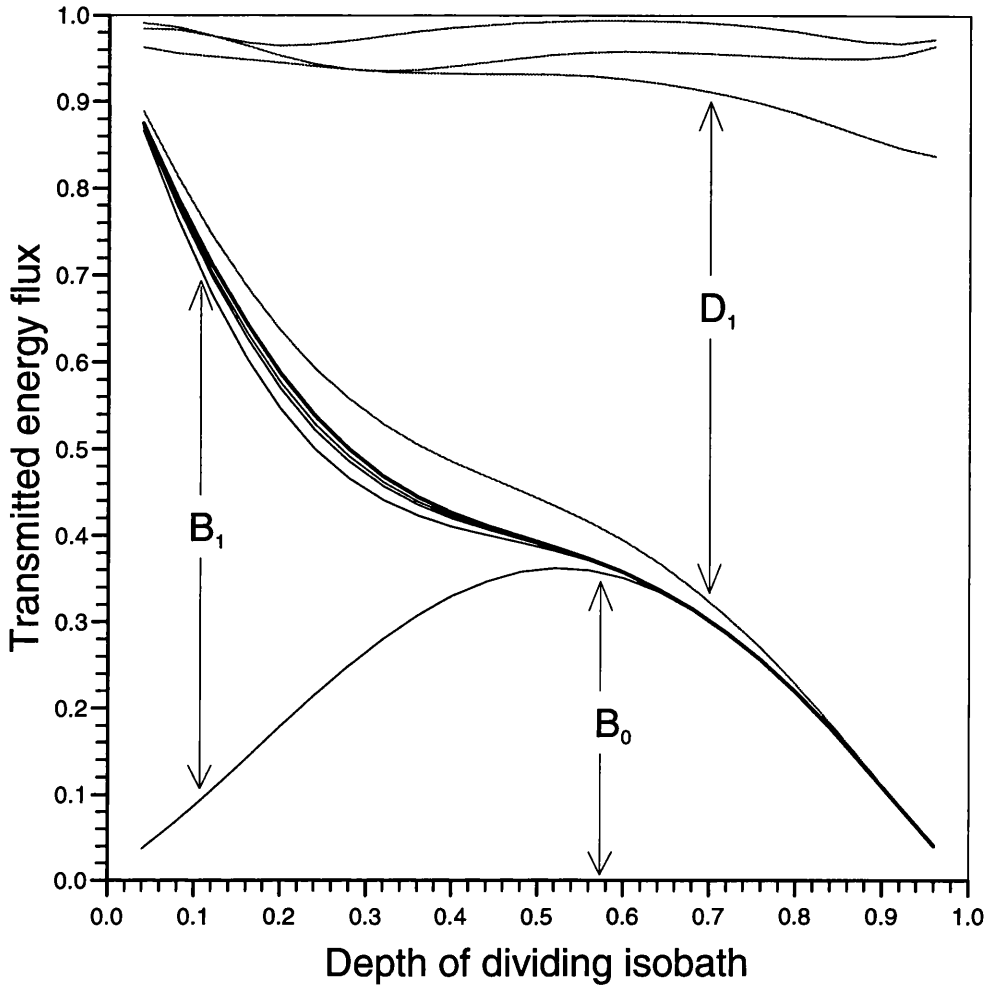


**Figure 4.13**: The scattering of an incident mode 1 wave by a ridge abutting the shelf as the height of the ridge varies. The position of the zero in the incident pressure field is crucial in determining which mode is propagated along the ridge. For this incident mode the only zero lies at a depth of 0.46.

field on the ridge occurs at approximately the same depth i.e there is no mode 1 component of the pressure on the ridge if the minimum depth is larger than $\sim$ 0.46.

Obviously, if there is a zero of pressure on the ridge then there must be a mode 1 component. From this data it appears that the converse is also correct. The situation is clearer if a higher incident mode is used. In fig. 4.14 a mode 3 wave is incident. This has 3 zeros on the shelf at depths of 0.16, 0.50 and 0.83. These points correspond almost exactly to the points in the diagram at which the mode 3, mode 2 and mode 1 components respectively cease to become important. More generally, *the mode n component of the pressure field on the ridge is only significant if there are n zeros lower than the depth of the dividing streamline in*

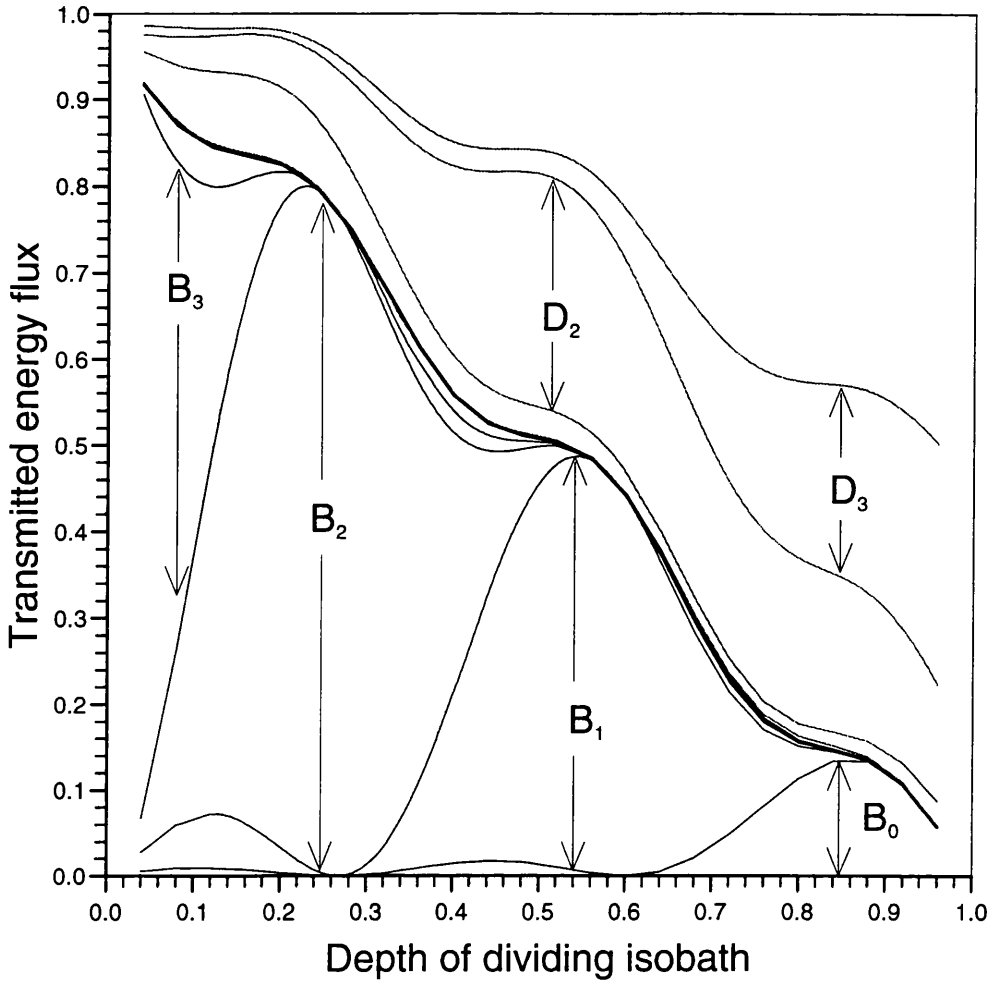


**Figure 4.14**: The scattering of an incident mode 3. The zeros in the incident pressure field are at 0.16, 0.50 and 0.83. This is crucial in determining which mode is propagated along the ridge. The zeros correspond almost exactly with the points at which the higher modes disappear. (Some smoothing using spline curves has been used).

*the incident pressure field.*

This appears to be quite general in that it does not depend upon the particular topographies used or on the other variables. These factors are however important in determining the distribution of energy among the modes at $D$. The difference between the behaviour of the transmitted modes on the shelf and on the ridge is explained by noting that outwardly propagating modes on the ridge are concentrated on the near incident side and so they are strongly constrained by the incident pressure field. At $D$ the modes spread evenly across the shelf.

## §4.5 Wind-forcing of waves along a coast

The equations and boundary conditions concerning the forcing by the wind of low-frequency coastally trapped waves in a stratified, frictional ocean were derived by Clarke and Brink (1985). They include the effects of the bottom friction coefficient $r$, given by the usual (dimensional) relationship $\tau_B^x = \rho_0 r u_B$ between the bottom stress and alongshore velocity at the bottom, but neglect the effects of wind stress curl. The governing equation is simply the time-dependent form of (2.2.4a)

$$p_{yyt} + B^{-2}\left(\frac{p_{zt}}{N^2}\right)_z = 0, \tag{4.5.1}$$

The terms representing the friction and wind stress only appear in the boundary conditions. The rigid lid condition holds on the surface due to the neglect of wind stress curl. The wind stress then only has an effect through the boundary condition at the line $y = b$ which is an artificial boundary needed to separate the turbulent viscous flow very close to the coast from the inviscid flow in the interior. The terms representing bottom friction also appear when considering the boundary condition on the topography. The boundary conditions are then

$$B^{-2}\frac{p_{zt}}{N^2} + h_y(p_{yt} - p_x) + R((rp_y)_y - h_y r p_y z) = 0, \ z = -h, \tag{4.5.2a}$$

$$hp_{yt} + Rrp_y - hp_x = T\tau^x(x,t), \ y = b, \tag{4.5.2b}$$

$$p_z = 0, \ z = 0, \tag{4.5.2c}$$

where $\tau^x$ is the alongshore component of the wind stress, and the two non-dimensional parameters $R = r_0/Df$ and $T = \tau_0/D\rho_0 fU$ measure the importance of the bottom friction and alongshore wind-stress respectively.

Following Clarke and Van Gorder (1986) and Brink (1991) the pressure field can be written

$$p(x,y,z,t) = \sum_{n=0}^{\infty} \phi_n(x,t) F_n(y,z), \tag{4.5.3}$$

where the functions $F_n(y,z)$ are the free CTW modes as calculated in §2.4 etc, which form a complete set for the pressure specified on the shelf. Using orthogonality, the amplitudes $\phi_n$ satisfy the first order equation

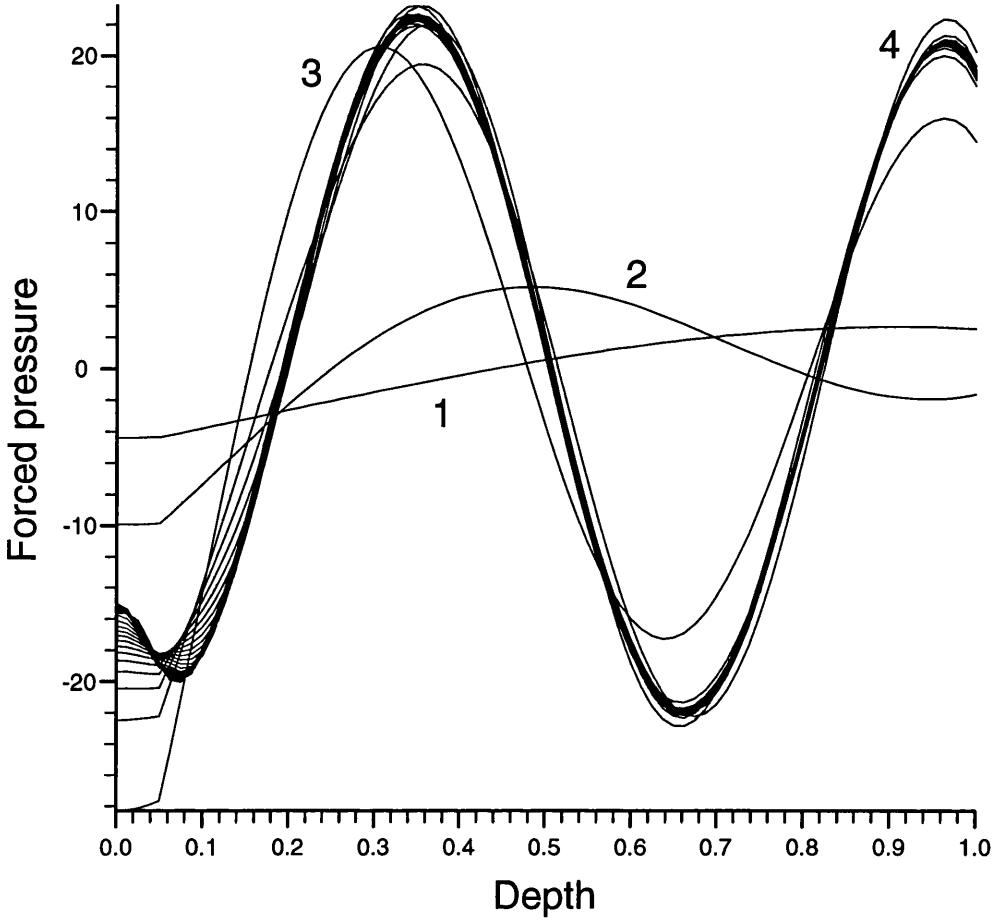


**Figure 4.15**: The convergence of the pressure along the shelf for the wind-forced mode as the number of modes used increases. Up to 40 modes are used but 7–10 modes would be sufficient. The harmonic wind forcing has $\omega_0/k_0 = 0.1$ compared with the phase speed of the third free wave mode of 0.11.

$$-\frac{1}{c_n}\frac{\partial \phi_n}{\partial t} - \frac{\partial \phi_n}{\partial x} + R\sum_{m=0}^{\infty} a_{mn}\phi_m = Tb_n\tau^x(x,t),\ n = 1,2,\ldots \tag{4.5.4}$$

with

$$a_{mn} = \int_{-h(b)}^{0} rh^{-1}F_{my}(-b,z)F_n(-b,z)\,dz + \int_{b}^{1} F_n(y,-h(y))\frac{d}{dy}[rF_{my}(y,-h(y))]\,dy,$$

$$b_n = \frac{1}{h(b)}\int_{-h(b)}^{0} F_n(b,z)\,dz, \tag{4.5.5}$$

where $a_{mn}$ and $b_n$ are the frictional coupling and wind forcing coefficients respectively.

If bottom friction is ignored the equations for the $\phi_n$ uncouple. Further, if a harmonic wind stress is imposed the solution for each $\phi_n$ is very simple.

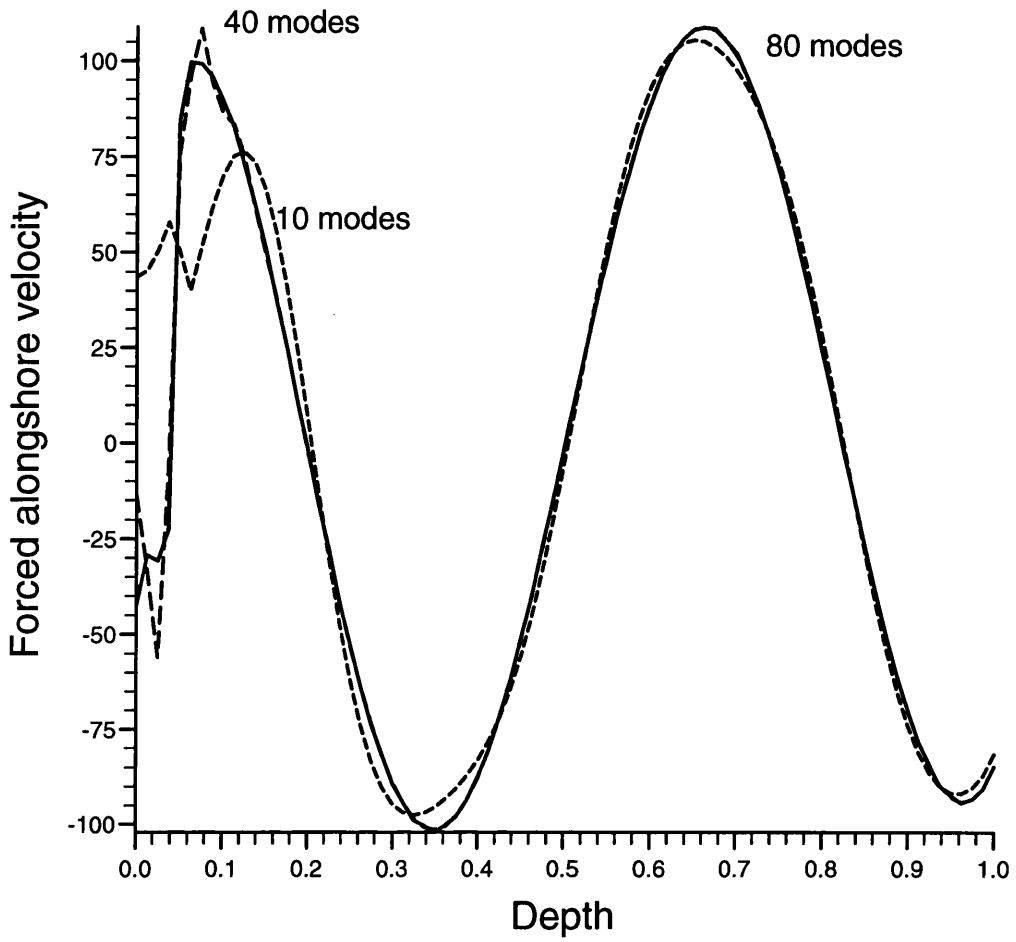


**Figure 4.16**: The convergence of the alongshore velocity on the shelf for the wind forced mode using the same parameters as in the previous figure. The convergence after 10 modes is not very good and even after 40 modes there are inaccuracies near the surface. Many more modes are needed to approximate the velocity than for the pressure.

Take the limit $R \to 0$, let $\tau^x = \cos(\omega_0 t - k_0 x)$ and look for solutions proportional to $\sin(\omega_0 t - k_0 x)$. Then for each $n = 1, 2, \ldots$

$$\phi_n(x,t) = \frac{T c_n b_n}{c_n k_0 - \omega_0} \sin(\omega_0 t - k_0 x). \tag{4.5.6}$$

This implies that the wind-forced mode will resemble most closely the modes for which $c_n \sim \omega_0/k_0$. For an example, take a linear shelf and choose $\omega_0/k_0 = 0.1$. Figure 4.15 shows how the pressure along the shelf varies for the forced mode as the number of terms in expansion (4.5.3) increases. The free mode closest to this is the third mode which has phase speed 0.11. The figure shows the result with up to 40 modes but for the pressure 7–10 would seem to be sufficient.

To calculate measurable quantities, such as the alongshore velocity, requires

differentiation and use of the boundary conditions. The tangential pressure gradient for each mode can be approximated using finite differences while the normal pressure gradient is known from (2.4.1b). The alongshore velocity on the shelf is given by

$$u = -p_y = -\sum_{n=1}^{\infty} \phi_n \frac{\partial}{\partial y} F_n(d(z), z), \tag{4.5.7}$$

where

$$\frac{\partial}{\partial y} F_n(d(z), z) = \frac{-1}{B^2 N^2 + d'^2} \left( \frac{B^2 N^2 F_n}{c_n} + d' \sqrt{1 + d'^2} \frac{dF_n}{ds} \right) \tag{4.5.8}$$

Figure 4.16 shows the convergence for the alongshore velocity on the shelf for the same example given above. The summation for the pressure converges much faster than that for the velocity. Possibly 40 or more modes would be necessary to give the required accuracy for the velocity. Previously this would have been impractical and hence it was necessary to use further approximations such as those used by Lopez and Clarke (1989). However with the new numerical method it is simpler to just use more modes.

## §4.6 Summary

In this chapter the main applications of the numerical methods derived in previous chapters were looked at. Principally the isobath tracing result of Johnson (1989) is used to examine the scattering of topographic Rossby waves as the topography changes. Simple geometries are considered as well as more complicated ones, such as the scattering through straits and over ridges abutting a coast.

The fraction of energy of an incident EKW that is transmitted through a strait is roughly proportional to the fractional (minimum) depth of the strait but the portion of energy transmitted for higher incident modes depends strongly on the structure of the mode. Stratification does not significantly affect the total amount of energy transmitted though it does affect its distribution among the modes. If the buoyancy frequency profile is taken to be exponential then the amount of energy transmitted can be altered significantly.

Results from a model of the Bass Strait confirm observational evidence of low-frequency wave energy passing through from the Great Australian Bight. The energy is mostly contained in modes 1 and 2 in agreement with previous studies

and observations.

As in the previous example the main factor determining the scattering of a wave incident on a ridge abutting a shelf is the height of the ridge. Stratification and topography are the main factors determining the distribution of energy among the transmitted modes on the shelf. The components of the outwardly propagating pressure field on the ridge are determined by the number of zeros in the incident pressure field below the dividing isobath.

The theory concerning the wind-forcing of low-frequency motions is used to examine the number of free CTW modes needed to satisfactorily model the wind-forced pressure and alongshore velocity. Many more modes than have been used previously are needed to model the velocities accurately.

# Chapter 5

# The stability of shear flow over topography

## §5.1 Introduction

Horizontal shear flow along an infinite ridge is an exact solution of the Euler equations for a continuously stratified, rotating ocean and is relatively common in real flows. It is therefore a flow whose stability is of some practical interest and is unusually amenable to analysis.

As seen in §3.2 topographic waves can propagate along a ridge due to the variation of background potential vorticity. This will depend on the rotation, topography and the shear. These waves always travel with higher potential vorticity to their right so waves can exist on both sides of the ridge and travel in opposite directions. In the absence of shear it is easily shown (from 3.2.2) that these modes are always stable. However, on physical grounds it might be expected that the presence of an opposing shear flow which could bring two opposite waves relatively to rest could be destabilising. It should be remembered that the shear flow has two effects on these waves, it alters the background potential vorticity as well as advecting so can fundamentally alter the wave-modes that are present without shear.

In the absence of topography the stability of this flow depends on the Rayleigh criterion (Drazin and Reid, 1981) i.e. whether $u_0''$ changes sign. A more general condition is derived in §5.2 for the barotropic case along with an extension to the Fjørtoft condition, that $u_0''(u_0 - c)$ must be somewhere negative.

Previous literature has considered separately the effects in a stratified fluid of shear and topography. Moreover the particular results for a ridge have not been remarked on previously. Collings and Grimshaw (1980a,b) and Collings (1986) deal with the effect of linear shear on barotropic shelf waves and the instability of these waves in the presence of more general horizontal shear flow. They show that topography can destabilise an otherwise stable shear flow along a coastal shelf, though they consider in the main the modification of already unstable modes due to topography. Barotropic and baroclinic instability of shear flow are considered by Killworth (1980) in rotating, stratified flow but only in the absence of topographic effects.

The equations, after a suitable non-dimensionalisation, depend on $\mu = Lf/U$ and $F = N_0 D/U$ where $N_0$ is the buoyancy frequency, $D, L$ are typical length

scales, $f$ is the Coriolis parameter and $U$ is the typical shear flow velocity. $F$ measures the importance of stratification in the flow and $\mu$ is an inverse Rossby number which measures the importance of rotation. The first case that is considered here is the barotropic limit ($F \ll 1$) with top-hat or multi-step topography. The second case where analytic results can be obtained is the long-wave, low-frequency limit.

If a rigid lid is assumed the formulation in the barotropic case is particularly simple in terms of the barotropic stream function. This is detailed in §5.2 and a number of results that in the general case are rather complicated, are proved very straightforwardly.

The rest of the chapter restricts itself to considering linear shear flow. For this case it can only be the topography which destabilises the flow as $u_0''$ is identically zero and so does not satisfy the Rayleigh condition in the absence of topography. The general equations are derived from first principles in §5.3 and are shown to give the barotropic case as the first term in an asymptotic expansion in $F$. The long wave limit is then discussed and some examples using simple ridge profiles are given in §5.4. The profiles used here are a simple top-hat profile and a multi-step profile which are chosen to minimise the complexity of the algebra while still allowing most of the interesting features of the problem to exist. In the long wave case, it is necessary for a complete picture to consider a free surface. This allows the external Kelvin wave mode to exist which dominates the stability of the flow.

## §5.2 Equations of motion: Barotropic formulation

The essential principle used in this formulation is the conservation of potential vorticity written in terms of the barotropic stream function. The governing equations are (following Pedlosky, 1979)

$$\frac{D}{Dt}\left(\frac{\xi^* + f}{h^*}\right),$$
$$\nabla.(h^*\mathbf{u}^*) = 0, \tag{5.2.1}$$

where $\mathbf{u}^* = (u^*, v^*)$ is the horizontal velocity vector, $\xi^* = v_x^* - u_y^*$ is the vorticity, $z^* = -h^*(y^*)$ is the depth profile and $f$ is the Coriolis parameter. Consider the

perturbation field to the shear flow $-Uu_0(y^*)$, where $U$ is a typical velocity scale. Scale $x, y$ with a typical length scale $L$ (see the next section for the complete details), define $\psi$, the stream function in terms of the non-dimensional horizontal perturbation velocity components $u, v$ and the depth $h$,

$$\psi_y = -hu, \quad \psi_x = hv, \tag{5.2.2}$$

This is only possible if there is a rigid lid on the top surface but this does not make a substantial difference to the results. Write the vorticity and velocity in terms of $\psi$ to arrive at the governing equation

$$\left(\frac{\partial}{\partial t} - u_0\frac{\partial}{\partial x}\right)\left(\nabla^2\psi - \frac{h'}{h}\psi_y\right) + \left(\frac{u_0' + \mu}{h}\right)'\psi_x = 0, \tag{5.2.3}$$

where $\mu = Lf/U$ is an inverse Rossby number.

Consider a wave travelling along the topography with wavenumber $k$ and frequency $\omega$ and look for solutions proportional to $\exp(i\omega t - ikx)$. Equation (5.2.3) then becomes

$$\left(\frac{\psi'}{h}\right)' - \frac{k^2}{h}\psi - \left(\frac{u_0' + \mu}{h}\right)'\frac{\psi}{c + u_0} = 0, \tag{5.2.4}$$

where $c = \omega/k$ is the speed of the wave.

This equation can be used to generate necessary conditions for instability. Multiplying (5.2.4) by the complex conjugate of $\psi$, integrating over the range of $y$ and using the boundary condition that $\psi \to 0$ as $y \to \pm\infty$ gives the energy equation

$$\int_{-\infty}^{\infty} \frac{(|\psi'|^2 + k^2|\psi|^2)}{h} dy = -\int_{-\infty}^{\infty} \frac{|\psi|^2}{c + u_0}\left(\frac{u_0' + \mu}{h}\right)' dy. \tag{5.2.5}$$

The LHS is clearly real and positive so taking the imaginary part of (5.2.5) gives as a necessary condition for instability that

$$\int_{-\infty}^{\infty} \frac{|\psi|^2}{|c + u_0|^2}\left(\frac{u_0' + \mu}{h}\right)' dy = 0. \tag{5.2.6}$$

This implies that $((u_0' + \mu)/h)'$ must change sign over the range of $y$. This is simply Rayleigh's criteria for instability for this flow. The counterpart of the Fjørtoft condition can be found by taking the real part of (5.2.5) and using (5.2.6) to show that

$$\int_{-\infty}^{\infty} \frac{|\psi|^2}{|c+u_0|^2} u_0 \left(\frac{u_0'+\mu}{h}\right)' dy < 0, \tag{5.2.7}$$

which therefore implies that $u_0((u_0'+\mu)/h)'$ must be somewhere negative.

These conditions are also true for a coastal shelf and imply that if the shelf profile is monotonic then linear shear, $u_0 = y$, is always stable. For a trench where $h' > 0$ for $y < 0$ and $h' < 0$ when $y > 0$, then so long as $1 + \mu > 0$ the Fjørtoft condition implies that *negative* linear shear is stable. Conversely for a ridge *positive* linear shear is stable.

Negative $\mu$ must also be considered even though at first sight it seems as though the waves would be travelling the wrong way and would not be opposed by the shear flow. The shear flow has two effects. As well as advecting the flow it also changes the background potential vorticity upon which the waves rely. Thus even with negative rotation the waves will be opposing the shear flow so long as $1+\mu > 0$. If $\mu < -1$ then the waves will go the 'wrong' way and the conclusions drawn in the previous paragraph will be reversed.

## §5.3 Equations of motion: Stratified case

Consider an infinite ocean of depth $D$ with a submerged ridge of width of order $2L$ (as in fig. 3.1). Take cartesian axes $Ox^*, Oy^*, Oz^*$ along the ridge, out to sea and vertically and let the ridge profile depend on y alone. Assume a uniform Coriolis frequency $f$ and let the flow be Boussinesq and incompressible with total density $\rho_0^*(z^*)+\rho^*(\mathbf{x}^*,t)$ and pressure $p_0^*(z^*)+p^*(\mathbf{x}^*,t)$. Introduce the buoyancy frequency

$$N_0^2 N^2(z^*) = -\frac{g}{\rho_0^*}\frac{d\rho_0^*}{dz^*}, \tag{5.3.1}$$

with the constant $N_0$ chosen so the maximum value of $N(z^*)$ is unity. The shear flow has been chosen to be positive when it opposes the direction of the ridge waves on both sides of the ridge. Consider a small perturbation to the linear shear flow $-Uy^*/L$ with frequency $\omega U/L$ and introduce scalings

$$(x^*, y^*, z^*, t^*) = (Lx, Ly, Dz, Ut/L),$$

$$(u^*, v^*, w^*) = (-Uy + \epsilon u, \epsilon v, (\epsilon\omega U^2/N_0^2 DL)w),$$

$$p^* = -fUL\rho_0^* y^2 + U\epsilon\rho_0^* p, \;\; \rho^* = (\epsilon\rho_0^* U/gD)\rho, \tag{5.3.2}$$

where $\epsilon$ is the (small) magnitude of the disturbance velocity. The scalings are such that the pressure terms match the inertial terms in the Euler equations and that the buoyancy terms match the density terms in the density equation.

The non-dimensional equations become

$$\frac{Du}{Dt} - (\mu+1)v = -p_x, \tag{5.3.3a}$$

$$\frac{Dv}{Dt} + \mu u = -p_y, \tag{5.3.3b}$$

$$(\omega U/LN_0)^2 \frac{Dw}{Dt} = -p_z - \rho, \tag{5.3.4}$$

$$\frac{D\rho}{Dt} - \omega N^2 w = 0, \tag{5.3.5}$$

$$u_x + v_y + (\omega/F^2)w_z = 0, \tag{5.3.6}$$

where $D/Dt = \partial/\partial t - y\partial/\partial x$ and $F = N_0 D/U$ measures the importance of stratification in the dynamics. The flow is hydrostatic with

$$\rho = -p_z, \;\; w = -\frac{1}{\omega N^2}\frac{D(p_z)}{Dt}, \tag{5.3.7}$$

provided the incident frequency, $\omega U/L$, is small compared to the buoyancy frequency, $N_0$. Cross-differentiating gives as the governing equation

$$p_{xx} + p_{yy} + F^{-2}\left(\frac{D^2}{Dt^2} + \mu(\mu+1)\right)\left(\frac{p_z}{N^2}\right)_z - 2v_x = 0. \tag{5.3.8}$$

Consider a disturbance with wavenumber $k$ and look for solutions proportional to $\exp(i\omega t - ikx)$. Equation (5.3.8) can then be written in terms of $p$ alone.

$$-k^2 p + p_{yy} + F^{-2} r\left(\frac{p_z}{N^2}\right)_z + \frac{2k^2}{r}((c+y)p_y + \mu p) = 0. \tag{5.3.9}$$

where $c = \omega/k$ is the wave speed and $r(y) = \mu(\mu+1) - k^2(c+y)^2$.

The free surface boundary condition is

$$a^2 p_z + N^2(0)F^2 p = 0, \;\; (z=0) \tag{5.3.10}$$

where $a = \sqrt{gD}/U$ is the external radius of deformation. The vanishing of the normal velocity at the lower boundary $z = -h(y)$ implies

$$(\omega/F^2)w = -vh'. \quad (z = -h(y)) \tag{5.3.11}$$

which becomes in terms of the pressure alone

$$(c+y)rp_z = -h'F^2N^2((c+y)p_y + \mu p), \quad (z = -h(y)) \tag{5.3.12}$$

In the far field ($|y| \to \infty$) $p \to$ *constant*.

*a. Weak stratification ($F \ll 1$).*

For weak stratification the flow is almost barotropic and analytical solutions follow by expanding (5.3.9) as a series in $F$, writing

$$p(y,z) = p^{(0)} + F^2p^{(1)} + O(F^4),$$
$$c = c_0 + F^2c_1 + O(F^4). \tag{5.3.13}$$

For clarity take $N(z)$ as identically unity, $a$ as infinite (i.e. a rigid lid) and assume that $\mu$ is of order one. Then (5.3.9) gives to $O(F^2)$

$$p^{(0)}_{zz} = 0, \tag{5.3.14a}$$
$$r_0p^{(1)}_{zz} = k^2p^{(0)} - p^{(0)}_{yy} - \frac{2k^2}{r_0}((c_0+y)p^{(0)}_y + \mu p^{(0)}), \tag{5.3.14b}$$
$$r_0p^{(2)}_{zz} = 2k^2c_1(c_0+y)p^{(1)}_{zz} + k^2p^{(1)} - p^{(1)}_{yy} - \frac{2k^2}{r_0}((c_0+y)p^{(1)}_y + \mu p^{(1)} + c_1p^{(0)}_y)$$
$$-\frac{4k^4c_1}{r_0^2}(c_0+y)((c_0+y)p^{(0)}_y + \mu p^{(0)}). \tag{5.3.14c}$$

Further terms follow similarly.

Expanding the boundary conditions in the same way gives $p^{(n)}_z = 0$ on $z = 0$ and on $z = -h(y)$

$$p^{(0)}_z = 0, \tag{5.3.15a}$$
$$(c_0+y)r_0p^{(1)}_z = -h'((c_0+y)p^{(0)}_y + \mu p^{(0)}), \tag{5.3.15b}$$
$$(c_0+y)r_0p^{(2)}_z + c_1r_0p^{(1)}_z - 2c_1k^2(c_0+y)^2p^{(1)}_z = -h'((c_0+y)p^{(1)}_y + \mu p^{(1)} + c_1p^{(0)}_y). \tag{5.3.15c}$$

Equations (5.3.14a), (5.3.15a) together imply that $p^{(0)}$ is a function of $y$ alone, so set $p^{(0)} = q_0(y)$. Integrating (5.3.14b) once and substituting into (5.3.15b) gives the governing equation for the barotropic limit,

$$q_0'' - k^2 q_0 + \frac{2k^2}{r_0}((c_0+y)q_0' + \mu q_0) = -\frac{h'}{h}\left(q_0' + \frac{\mu q_0}{c_0+y}\right). \tag{5.3.16}$$

This equation is equivalent to (5.2.4) with linear shear as can be seen by writing $\psi = h((c_0+y)q_0' + \mu q_0)/r_0$ and $\psi' = h((1+\mu)q_0' + k^2(c_0+y)q_0)/r_0$ and noting that the elimination of $q_0$ implies (5.2.4) and that the elimination of $\psi$ implies (5.3.16). If (5.3.14b) is integrated again, the first order pressure can be written as

$$p^{(1)} = q_1(y) - \frac{z^2}{2r_0}\left(q_0'' - k^2 q_0 + \frac{2k^2}{r_0}((c_0+y)q_0' + \mu q_0)\right), \tag{5.3.17}$$

and the governing equation for $q_1(y)$ follows from (5.3.14c) and (5.3.15c).

*b. Long-wave limit ($\omega, k \ll 1$).*

Now to consider the stability of long waves, take both $\omega$ and $k \ll 1$ while keeping $c = \omega/k$ constant. Equation (5.3.9) then reduces to a form of Laplace's equation (so long as $\mu(\mu+1) > 0$ )

$$p_{yy} + \mu(\mu+1)F^{-2}\left(\frac{p_z}{N^2}\right)_z = 0, \tag{5.3.18}$$

subject to (5.3.10) and with

$$\mu(\mu+1)(c+y)p_z = -h'F^2N^2((c+y)p_y + \mu p), \ (z = -h(y)) \tag{5.3.19}$$

As in §5.2 these equations can be used to derive the standard instability conditions. Multiplying by the complex conjugate of $p$, integrating over the domain $A$ and using the boundary conditions gives

$$\int_A \left\{|p_y|^2 + \mu(\mu+1)\frac{|p_z|^2}{F^2N^2}\right\} dA + \int_{-\infty}^{\infty} \mu(\mu+1)\frac{|p|^2}{a^2}dy = \int_{-\infty}^{\infty} \frac{\mu h'|p|^2}{c+y}dy. \tag{5.3.20}$$

Taking imaginary parts shows that for instability it is necessary that $h'$ changes sign. Further, provided $\mu(\mu+1) > 0$, taking real parts shows that it is necessary

for $yh'$ to be positive over an appreciable amount of $y$. These are identical to the conditions (5.2.6) and (5.2.7) for the barotropic case.

## §5.4 Specific examples

**Top-Hat profile.** Let the ridge have the linear top-hat profile

$$h(y) = \begin{cases} 1, & |y| > 1, \\ h, & |y| \leq 1. \end{cases} \tag{5.4.1}$$

This implies that $h'(y) = 0$ almost everywhere and simplifies the equations enormously.

*a. Weak Stratification*

The lowest order equation (5.3.16) is now

$$\left(\frac{q_0'}{r_0}\right)' + \frac{k^2}{r_0^2}(2\mu - r_0)q_0 = 0, \tag{5.4.2}$$

almost everywhere with the condition at infinity that $q_0$ should be bounded. The jump conditions at $y = \pm 1$ are derived from integrating (5.3.16) and are that $q_0$ is continuous and that

$$[h((c_0 + y)q_0' + \mu q_0)]_-^+ = 0, \ y = \pm 1. \tag{5.4.3}$$

These imply that the pressure and mass flux are continuous across the jump.

Equation (5.4.2) has the general solution

$$q_0 = A_0(k(c_0 + y) - (1 + \mu))e^{ky} + B_0(k(c_0 + y) + 1 + \mu)e^{-ky}, \tag{5.4.4}$$

where $A_0, B_0$ are constants. Using the boundary conditions then gives

$$q_0 = \begin{cases} h(1 - \lambda e^{2k})(k(c_0 + y) - (1 + \mu))e^{ky}, & y < -1, \\ (k(c_0 + y) - (1 + \mu))e^{ky} + \lambda(k(c_0 + y) + 1 + \mu)e^{-ky}, & |y| < 1, \\ h(\lambda - e^{2k})(k(c_0 + y) + 1 + \mu)e^{-ky}, & y > 1, \end{cases} \tag{5.4.5}$$

where

$$\lambda = -\frac{\Delta(k(c_0 - 1) - (1 + \mu))e^{-2k}}{k(c_0 - 1) + \Delta(1 + \mu)} = -\frac{(k(c_0 + 1) - \Delta(1 + \mu))e^{2k}}{\Delta(k(c_0 + 1) + 1 + \mu)}, \tag{5.4.6}$$

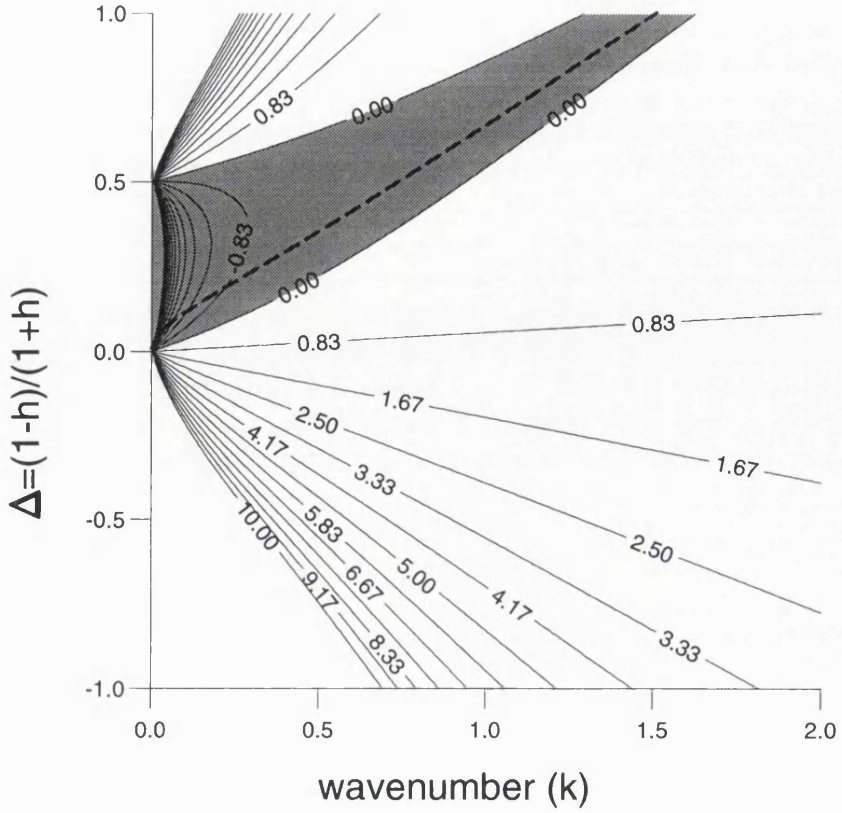


**Figure 5.1**: The variation of $c_0^2$, the zeroth order approximation to the phase speed for the weak stratification case. This figure shows the variation against $\Delta = (1-h)/(1+h)$, where $h$ is ratio of the height of the ridge ( or depth of the trench) to the open ocean depth, and $k$, the wavenumber, for $\mu = 0.5$. Regions of instability are shaded. As expected from (5.2.7) there is no instability for $\Delta < 0$, corresponding to a trench. The dotted line shows the points where the equivalent waves that would exist without the shear flow would be relatively brought to rest by the shear.

and $\Delta = (1-h)/(1+h)$, with the condition that, for the solution to exist

$$c_0^2 = \frac{\Delta^2 e^{-4k}(k+1+\mu)^2 - (k-\Delta(1+\mu))^2}{k^2(\Delta^2 e^{-4k}-1)}, \tag{5.4.7}$$

giving the speed of the fundamental mode. There are no other modes for this profile in the barotropic limit. The wave speed for the fundamental mode is either purely real or purely imaginary with the two regions separated by a neutral curve in $(k, \Delta, \mu)$ space (figs. 5.1 and 5.2).

It is instructive to consider the waves that would be present if the advection by the shear flow is ignored. The shear flow alters the background potential vorticity from $f/h$ to $(U/L+f)/h$, so for this linear shear problem the "equivalent" waves can be found by assuming a new rotation parameter $(U/L+f)$. The dotted line in the figures represents the points where the phase speed of the equivalent waves

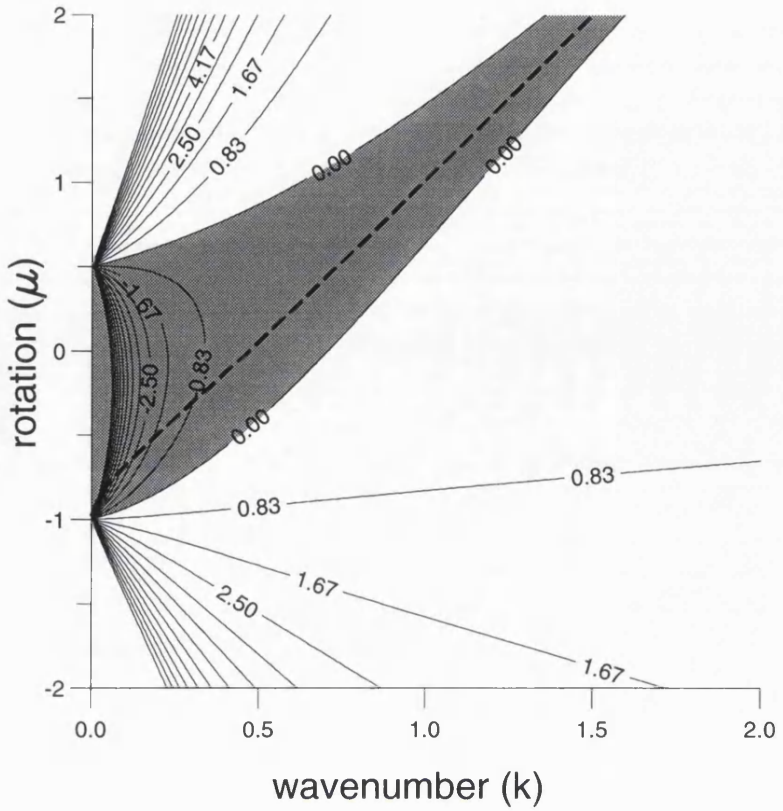


**Figure 5.2**: The variation of $c_0^2$ against $\mu$ and $k$ for fixed $\Delta = 0.5$. The dotted line shows the points where the equivalent waves that would exist without the shear flow would be brought to rest.

is exactly equal and opposite to that of the shear flow and hence where the two opposing waves would be brought to rest. This line lies very close to the line of largest growth rate (for fixed $k$) and indicates that, as in the stratified shear flows considered by Taylor (1931), this might be the mechanism for instability.

*b. Long wave limit*

Consider first uniform stratification $N(z) \equiv 1$ and suppose that $\mu(\mu+1) > 0$. Rescaling the horizontal coordinate $Y = ly$, where $l = \sqrt{\mu(\mu+1)}/F$, in (5.3.18) gives

$$p_{YY} + p_{zz} = 0, \tag{5.4.8}$$

with the rescaled boundary condition

$$(K+Y)p_z = -H'(Y)((K+Y)p_Y + \mu p), \quad (z = -H(Y)), \tag{5.4.9}$$

where $K = lc$ and $H(Y) = h(ly)$. If the profile is now chosen to be the top-hat

profile (5.4.1) then the boundary conditions become $a^2 p_z + F^2 p = 0$ on $z = 0$ and $p_z = 0$ on the horizontal surfaces and $\mu p + (K + Y)p_Y = 0$ on the vertical walls at $Y = \pm l$.

Following the method used in §3.3 separate the odd and even parts of the pressure. Write

$$p = \begin{cases} p^o + p^e, & |Y| \le l, \\ q^o + q^e, & |Y| > l, \end{cases} \tag{5.4.10}$$

where $p^o, q^o$ are the odd functions and $p^e, q^e$ the even. Continuity at $Y = \pm l$ of the pressure and its derivatives together with the boundary conditions imply that

$$\begin{gathered} p^e(l,z) = q^e(l,z),\ p^o(l,z) = q^o(l,z),\ (-h \le z \le 0) \\ p^e_Y(l,z) = q^e_Y(l,z),\ p^o_Y(l,z) = q^o_Y(l,z),\ (-h \le z \le 0) \end{gathered} \tag{5.4.11a}$$

$$\begin{gathered} \mu q^e(l,z) + K q^o_Y(l,z) + l q^e_Y(l,z) = 0,\ (-1 \le z \le -h) \\ \mu q^o(l,z) + K q^e_Y(l,z) + l q^o_Y(l,z) = 0.\ (-1 \le z \le -h) \end{gathered} \tag{5.4.11b}$$

Separation of variables and application of the boundary conditions gives

$$\begin{aligned} q^e(Y,z) &= \sum_{n=0}^{\infty} a_n e^{-\beta_n(|Y|-l)} B_n(z),\ (|Y| > l) \\ q^o(Y,z) &= \sum_{n=0}^{\infty} b_n \mathrm{sgn}(Y) e^{-\beta_n(|Y|-l)} B_n(z),\ (|Y| > l) \\ p^e(Y,z) &= \sum_{n=0}^{\infty} c_n \frac{\cosh \alpha_n Y}{\cosh \alpha_n l} A_n(z),\ (|Y| \le l) \\ p^o(Y,z) &= \sum_{n=0}^{\infty} d_n \frac{\sinh \alpha_n Y}{\sinh \alpha_n l} A_n(z),\ (|Y| \le l) \end{aligned} \tag{5.4.12}$$

where $a_n, b_n, c_n, d_n$ are constants to be determined and $A_n(z), B_n(z), \alpha_n, \beta_n$ are as defined in (3.3.4).

Substituting these definitions in (5.4.10) and using orthogonality gives

$$\begin{aligned} \sum_n^{\infty} I_{mn} a_n (\alpha_m \tanh \alpha_m l + \beta_n) &= 0, \\ \sum_n^{\infty} I_{mn} b_n (\alpha_m + \beta_n \tanh \alpha_m l) &= 0, \end{aligned}$$

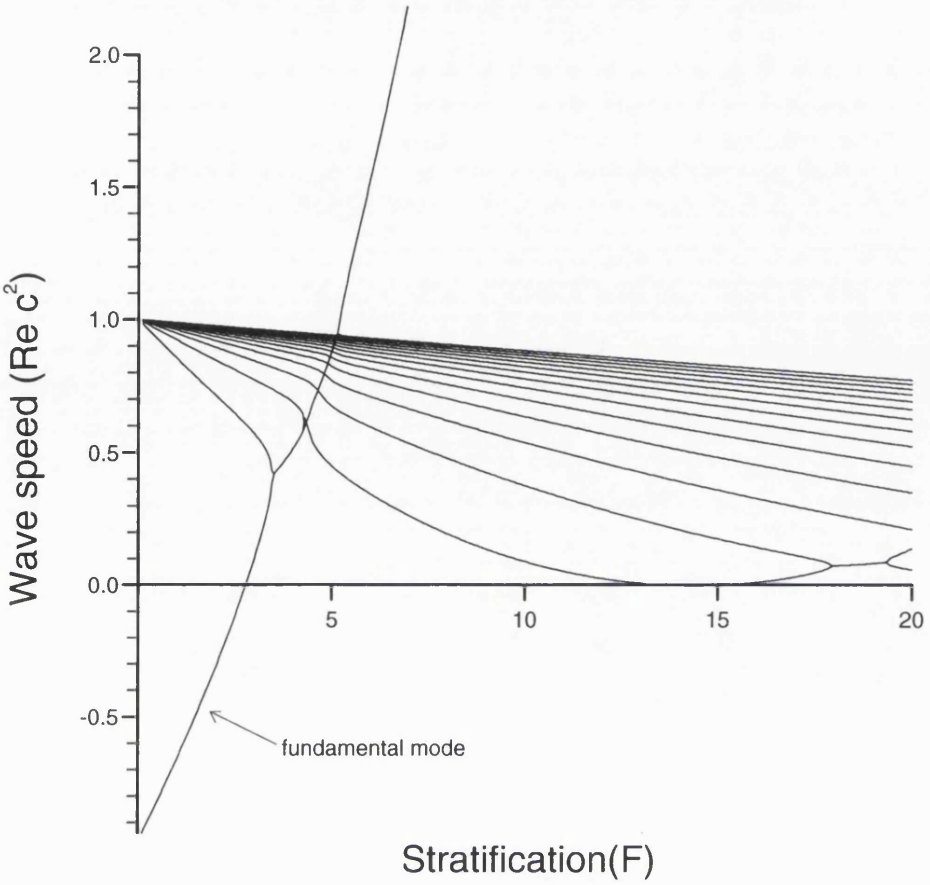


**Figure 5.3**: The variation with stratification of the real parts of $c$, the wave speed, in the long wave approximation. Here the Rossby radius $a = 10$, the rotation $\mu = 0.4$ and the height of the step $h = 0.5$. The external Kelvin wave mode matches the fundamental mode found in the barotropic case as $F \to 0$. All the other modes are advected with the shear flow in that limit. As the stratification increases the speeds of all the topographic Rossby waves increase and hence become unstable in turn.

$$K \sum_{n}^{\infty} J_{mn}\beta_n a_n = \sum_{n}^{\infty} J_{mn} b_n(\mu - l\beta_n),$$
$$K \sum_{n}^{\infty} J_{mn}\beta_n b_n = \sum_{n}^{\infty} J_{mn} a_n(\mu - l\beta_n), \qquad (5.4.13)$$

for each $m = 0, 1, 2 \ldots$ and where $I_{mn}$ and $J_{mn}$ are as defined in (3.3.6).

To solve these equations truncate the expansions and use the first two equations to eliminate half of the $a_n, b_n$. Substitute the rest into the remaining equations which can then be written as $A\mathbf{a} = KB\mathbf{b}$ and $C\mathbf{b} = KD\mathbf{a}$, and solved using standard eigenvalue techniques. Figure 5.3 shows the real part of the wave speed $c^2$, and fig. 5.4 the imaginary part for $h = 0.5$, $a = 10$ and $\mu = 0.4$.

As can be seen the stability of the flow is dominated by the external Kelvin wave mode which as $F \to 0$ matches the fundamental mode found in the baro-

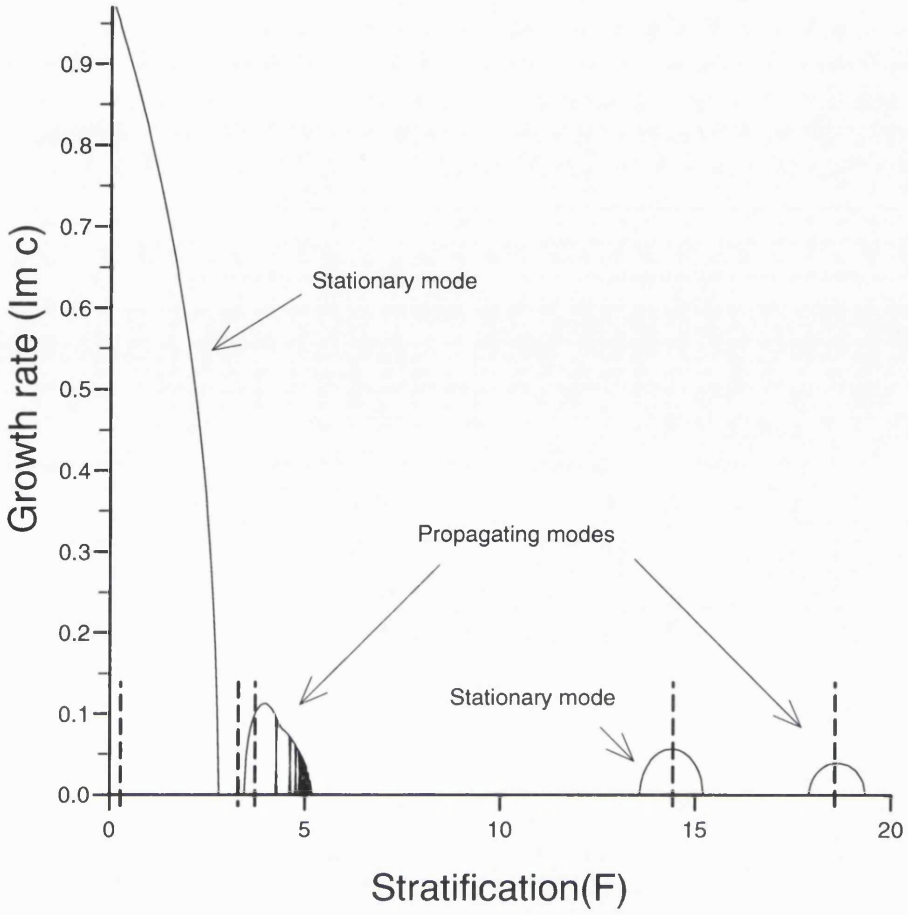


**Figure 5.4**: The variation with stratification of the imaginary parts of $c$, the wave speed, in the long wave approximation. Variables are as in fig. 5.3. The largest growth rate occurs for the fundamental mode in the barotropic limit. The dotted lines are where the instabilities are predicted to be assuming that two equivalent waves are brought relatively to rest.

tropic case. All other modes are advected with the shear flow in that limit. As for the barotropic case, the phase speeds of waves that would exist without the shear flow can be calculated using the work in §3.3. Write $B_{equiv} = \sqrt{(\mu(\mu+1))}F$ to compensate for the change in the background potential vorticity. As in fig. 3.6 only the EKW mode travels with a non-zero phase speed in the barotropic limit and as the stratification increases the phase speed of all these equivalent waves must increase.

In the example given here the two fundamental modes are simultaneously brought to rest by the shear flow at $F = 0.22$ and this is very close to the centre of the first stationary unstable mode. Similarly the mode 1 waves are brought to rest by the shear flow when $F = 14.4$, the centre of the second stationary instability. In fact, the speed of each pair of modes in turn will at some value of

$F$ match the speed of the shear flow at the discontinuities. Stationary unstable modes occur at each of these points.

If the stratification is increased further after such a stationary instability a series of propagating instabilities forms. At these points there is at least one pair of modes that are travelling faster than the shear flow and propagating in the opposite sense to all higher modes. As the stratification increases, the speed of these modes will match in turn the speeds of each higher mode on the opposite side of the ridge. The shear flow brings two opposing modes *relatively* to rest. By examining the equivalent waves this is predicted to happen at $F = 3.3$ between the fundamental mode and mode 1, at $F = 3.7$ between the fundamental mode and mode 2 and at $F = 18.6$ between mode 1 and mode 2. As can be seen in the figure these points provide very good estimates for the centres of the propagating instabilities.

The growth rates for the stationary unstable modes reduce sharply as the mode number increases and the growth rates for the propagating modes reduce as both the interacting mode numbers increase.

If the upper surface were taken to be rigid then the speed of the fundamental mode would be infinite and the important role this mode plays in any real situation would not be clear.

For more varied topography a Green's function integral formulation as used in §3.1 could be adapted to give an efficient numerical method.

**Multi-Step profile.** Consider a ridge with the stepped profile

$$h(y) = \begin{cases} 1, & |y| > 1, \\ h_n, & y_{n-1} < y < y_n, n = 1, 2, \ldots, N \end{cases} \tag{5.4.14}$$

where $h_n$ is the depth between $y_{n-1}$ and $y_n$ and $N$ is the total number of steps. As previously $h'$ is zero almost everywhere so that in the barotropic case at least the solution above each step can be immediately written down. For this discrete problem the exact (numerical) answer can be found and by increasing $N$ an approximate solution to any profile shape can be found.

*a. Barotropic limit*

This case can be solved simply in terms of the barotropic stream function.

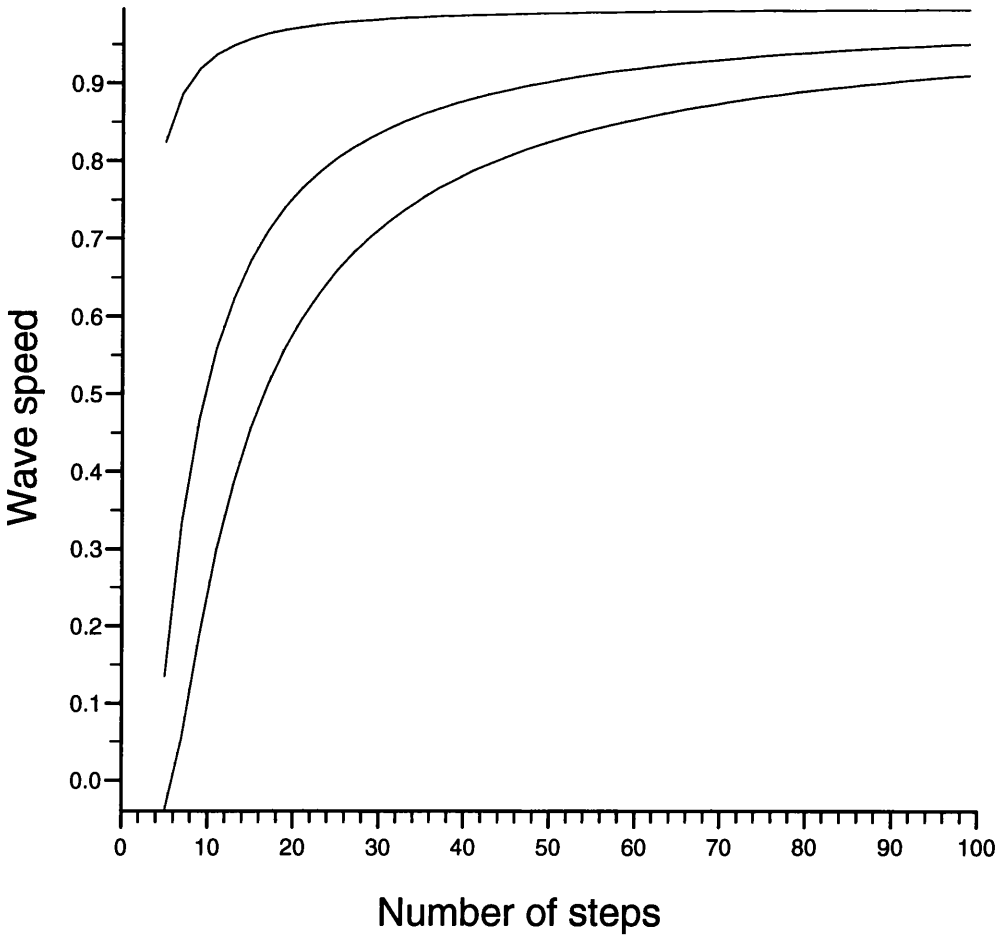


**Figure 5.5**: The convergence of the wave speed $c$, as the number of steps used to approximate a smooth sine profile, $h(y) = 1 - 0.5 \sin \pi(y+1)/2$, increases. The fundamental mode converges fastest and is reasonably accurate after only 20 or so steps.

The governing equation (5.2.4) reduces to

$$\psi'' - k^2\psi = 0, \tag{5.4.15}$$

which over each step has the solution $\psi_n = a_n \cosh ky + b_n \sinh ky$ or $a_0 \exp(-ky)$, $b_0 \exp(ky)$ for $y > 1$ and $y < -1$ respectively. It follows from (5.4.3) that across a discontinuity in $h(y)$, $\psi$ is continuous and

$$\left[\frac{1}{h}((c+y)\psi' - (1+\mu)\psi)\right]_-^+ = 0, \quad (y = y_n).\ n = 0, 1 \ldots, N \tag{5.4.16}$$

The conditions at $y = \pm 1$ can be used to eliminate $a_0$ and $b_0$ and the continuity of $\psi$ at $y = y_n$ can be used to progressively eliminate $b_n$, $n = 1, \ldots, N-1$. This leaves $N+1$ variables and $N+1$ equations which depend on $c$ linearly, a system which can be solved using standard techniques. There is no restriction on the

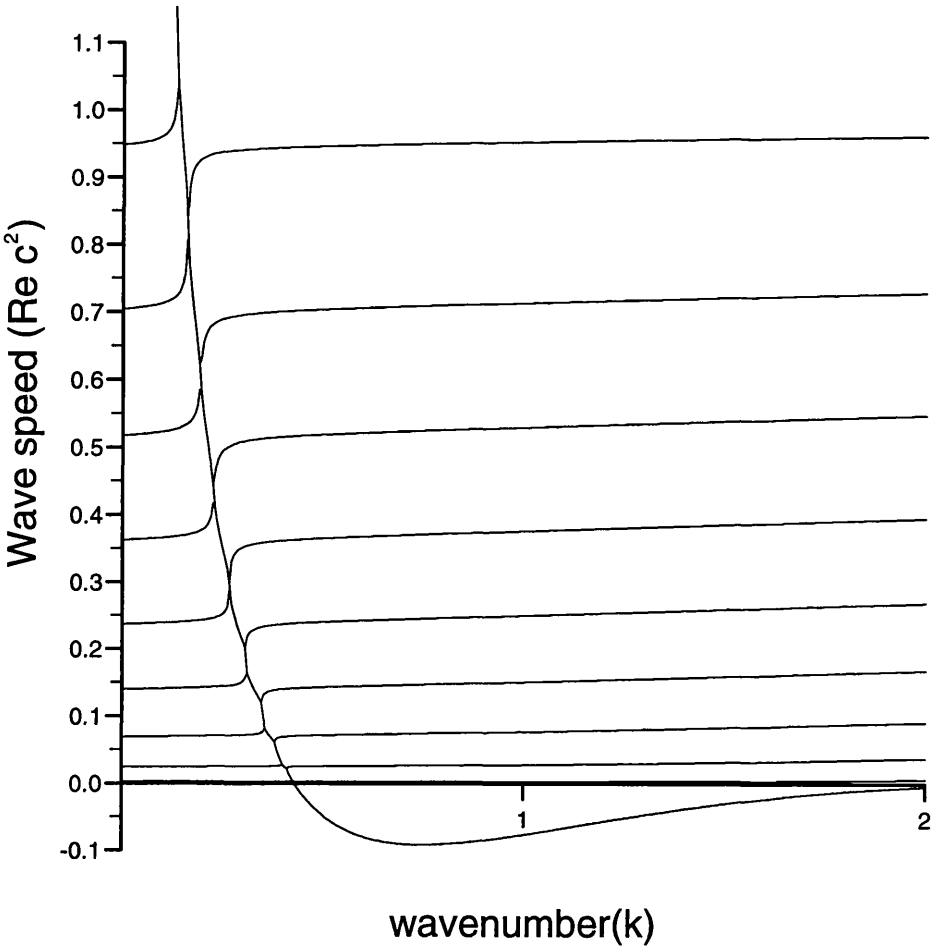


**Figure 5.6**: The real part of the wave speed squared plotted against wavenumber for the 20 step approximation to a sine shaped ridge profile in the barotropic limit with the height of the ridge $h = 0.55$ and the Rossby number $\mu = 1.6$. The fundamental mode is stable to long wave disturbances and dominates the stability diagram. Instability is apparent when $c^2$ is negative.

spacing of the $y_n$ so more points can be added wherever there is a need for greater definition. For simplicity here, the $y_n$ are evenly spaced across the ridge.

As an example consider the sine profile $h(y) = 1 - h\sin\pi(y+1)/2$ and approximate this using $N$ steps. Figure 5.5 shows the convergence of the first three wave speeds as $N$ increases for the situation where $\mu = 0.5$, $h = 0.5$ and the wavenumber $k = 1$. There is a rapid convergence especially for the fundamental mode and it suffices to take $N = 20$ for the following examples. In figs. 5.6, 5.7 and 5.8 the wave speeds are plotted for this profile as the wavenumber increases for two different parameter sets. In figs. 5.6 and 5.7 $\mu = 1.6$ and $h = 0.55$ and in fig. 5.8 $\mu = 0.0$ and $h = 0.5$. The real part of the wave speed squared is plotted as this gives greater clarity and for fig. 5.7 the imaginary part of the wave speed

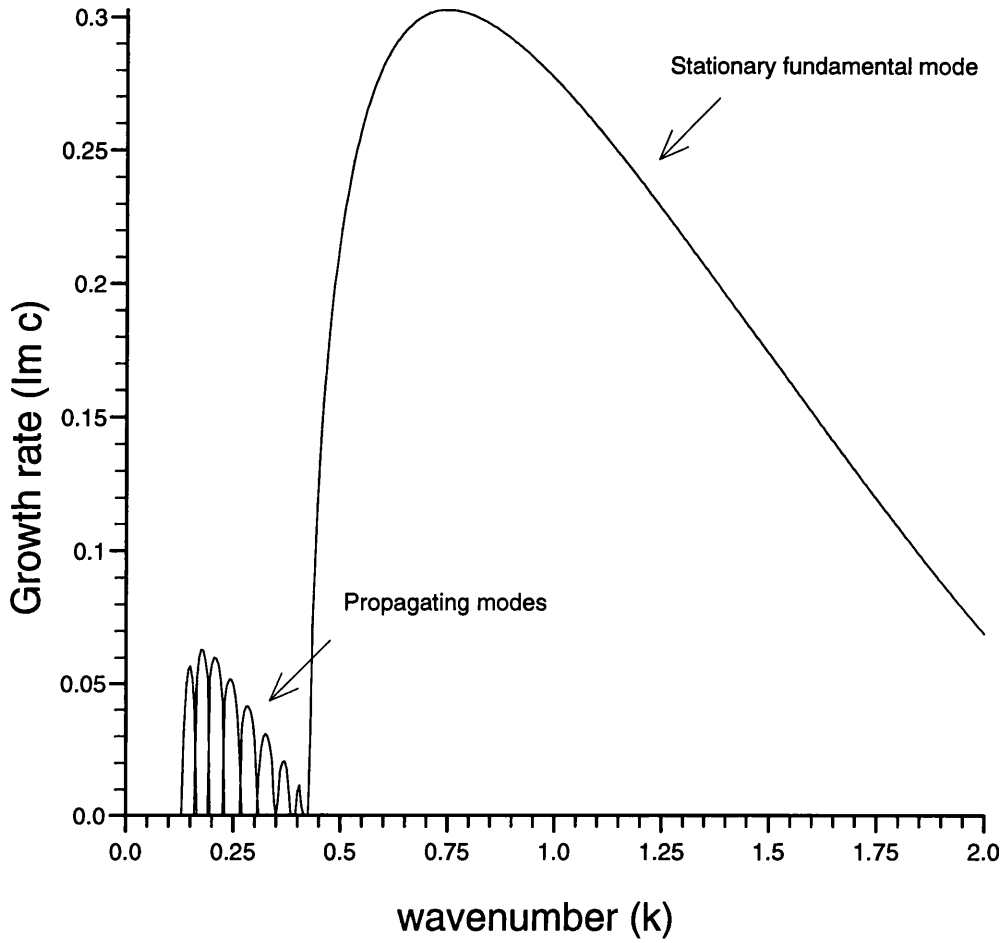


**Figure 5.7**: The imaginary part of the wave speed plotted against wavenumber for the same case as in fig. 5.6. The growth rate is greatest for the fundamental mode at a wavenumber $k = 0.7$.

(the growth rate of the unstable mode ) is plotted. These two cases typify the two main classes of behaviour observed. The basic difference is that in figs. 5.6–7 the fundamental mode is stable to long wave disturbances and in fig. 5.8 it is not. For very short waves the fundamental mode is very slow and stable for both diagrams and the more complicated behaviour in figs. 5.6–7 is solely due to the fundamental mode "crossing" the other modes.

It is not as straightforward to predict these results as in the previous two examples using a top-hat ridge. The equivalent waves can no longer be considered to be localised at a discontinuity of height and so it is difficult to assign a single speed measuring the effect on the wave of advection by the background flow.

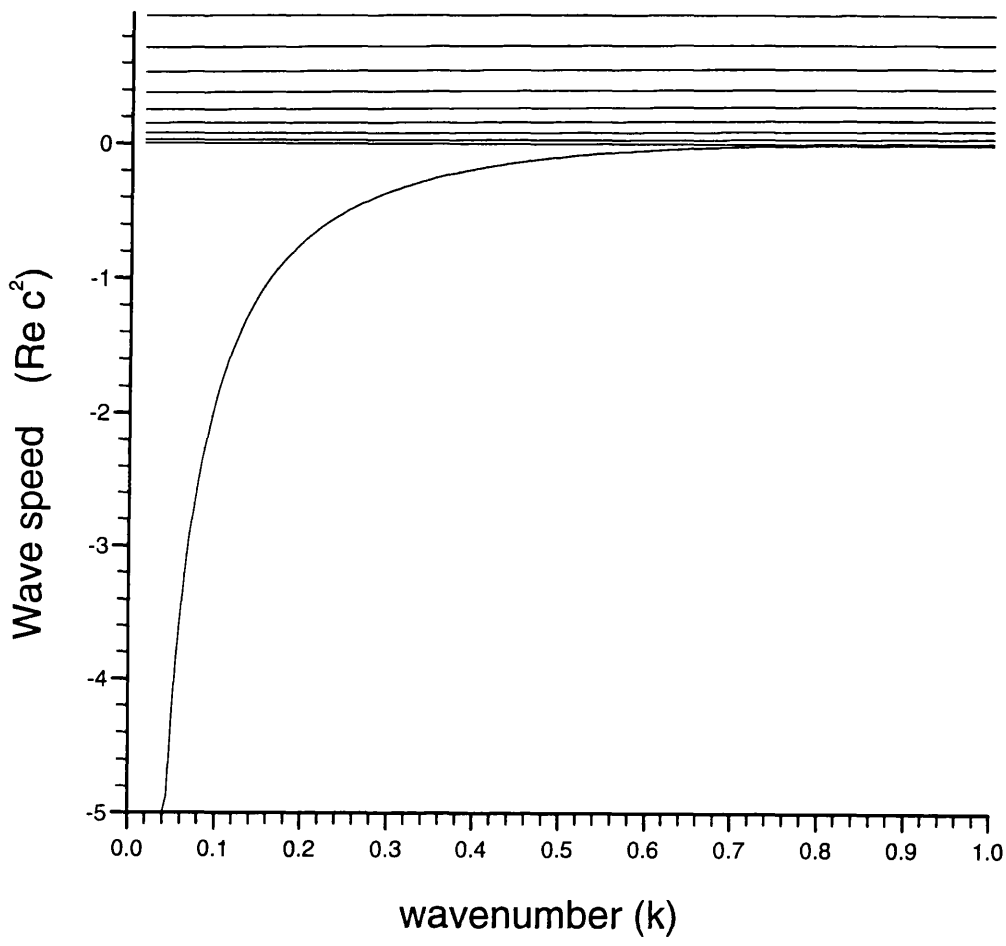


**Figure 5.8**: The wave speed squared plotted against wavenumber for the 20 step approximation to a sine shaped ridge profile in the barotropic limit with ridge height $h = 0.2$ and $\mu = 0.5$. In this case the fundamental mode is unstable to long wave disturbances and as in figs. 5.6–7 this mode dominates the stability. In fact no other mode ever becomes unstable and all short waves are stable for $k > 0.9$.

## §5.4 Results

There are a number of different parameters in this problem which each characterise a different aspect of the dynamics. The stratification $F$, the rotation $\mu$, the topography $h(y)$, the radius of deformation $a$ and the wavenumber $k$ all affect the stability of the flow. Unfortunately it is difficult to consider them all at once and still leave a tractable problem. To make any analytical progress at all it is necessary to isolate each feature and see what effect changing it has on its own and hence gain some understanding of how the problem depends on them all.

The cases covered here are; i) $F \to 0, a \gg 1$, top-hat profile, ii) $\omega, k \ll 1$, top-hat profile, and iii) $F \to 0, a \gg 1$ multi-step profile. All cases are for arbitrary $\mu$.

First consider the situation with no shear, then whatever the profile or stratification all modes are stable. The top-hat profile filters out all modes except the fundamental mode in the barotropic limit. As the stratification increases the speed of all the modes increase. In the long wave limit the existence of the fundamental mode depends on whether a rigid lid is imposed but as the wavenumber gets larger its speed decreases. Positive rotation also increases the wave speed. With a $N$-step profile there are $N+1$ (the number of height discontinuities ) modes which are present for all wavenumbers in the barotropic limit. The fundamental mode travels significantly faster than the other modes but the speed of all the modes decreases with increasing wavenumber.

Now consider the situation if a shear flow is imposed. This alters the background potential vorticity, which allow the wave modes to exist, and it advects the waves. If the velocity of the shear flow at a point of discontinuity of the profile is much greater than that of the wave mode there then it will be swept along with the shear. It is only when the velocities of the shear flow and of the mode are comparable and opposite that the possibility of unstable modes arises. A convincing model for the onset of instability concerns the speed of the waves in the absence of the shear flow but with an equivalent background potential vorticity. For instance in the barotropic limit, the background potential vorticity when the shear is imposed is $(U/L + f)/h$ so then the equivalent waves with no shear will have a new "rotation" parameter of $U/L + f$. In the stratified long-wave limit

the equivalent stratification parameter is given by $\sqrt{(}\mu(\mu+1))F$. Instability will occur if the shear flow brings two of these equivalent waves relatively to rest, hence in cases where the profile and shear are symmetric the speed of the shear flow has to either oppose exactly the speed of the equivalent wave mode at the relevant height discontinuity or bring two opposing equivalent wave modes to the same velocity.

Consider first the case of the barotropic limit with the top-hat profile. Figure 5.1 shows the variation of speed of the fundamental mode with the wavenumber and the height of the step. The dotted line shows the points at which the equivalent wave modes match exactly the shear at the edges of the step and it is clear that this lies at roughly the center of the unstable region (where $c_0^2 < 0$). The same is true for fig. 5.2. In this limit it is clear that for a ridge there are unstable modes for all $\Delta > 0$ and all $\mu > -1$. Analysis of (5.4.7) shows that long waves ($k \ll 1$) are unstable for $0 < \Delta < 1/(1 + 2\mu)$ and that these modes have the largest growth rate. For any fixed rotation and height there is a range of values of the wavenumber for which the modes are unstable and this range becomes narrower and the waves shorter as the height and rotation increase. The phase speed for the unstable modes is purely imaginary and therefore the disturbance is stationary.

The effect of the topography on the barotropic case can be examined using an $N$-step profile to approximate a smooth ridge. Instead of only one mode existing there will be $N + 1$ modes, one for each height discontinuity. However, as figs. 5.6–7 and fig. 5.8 show, the stability of the flow is completely dominated by the fundamental mode. Two main classes of results for fixed height and rotation can be determined and are distinguished by the behaviour of the fundamental mode for very small wavenumber $k$. If, as in figs. 5.6–7, this mode is stable the speed of the mode decreases as the wavenumber increases. This forces an interaction with the other modes present and destabilises them. The fundamental mode then becomes purely imaginary until for higher wavenumbers it returns to stability. On the other hand if, as in fig. 5.8, the fundamental mode is unstable to long wave disturbances there is no interaction with the other modes (which always remain stable). Note if a free surface is used the only qualitative difference would be the that the fundamental mode would remain finite in the long wave limit but this

would have little or no bearing on the structure of the problem for finite $k$.

Thus for barotropic flow the stability of the fundamental mode determines the behaviour of the system, regardless of the profile. Moreover, the basic properties of the fundamental mode can be obtained from a simple top-hat approximation of the topography.

The other main variable in this model is the stratification characterised by the parameter $F$. The example given here uses the simple top-hat profile but similar results would be expected even with more realistic topography. Semi-analytic results can be obtained in the long wave ($k \ll 1$) approximation.

In this limit the free surface plays an important role. The fundamental mode is seen to play a vital role in the stability of this flow in all the parameter regions studied and the same is true in this case. However, if a rigid lid is imposed the fundamental external Kelvin wave mode travels infinitely fast and the effect it has is obscured. It is therefore sensible to consider free surface effects in this limit. Figures 5.3–4 show the variation of the wave speeds for the Rossby radius $a = 10$, $\mu = 0.4$ and $h_0 = 0.5$. For weak stratification the external Kelvin wave mode matches the fundamental mode found in the barotropic limit. All the other modes are concentrated in a boundary layer of width $O(F)$ at the discontinuities and are advected with the shear flow.

As the stratification increases, the speeds of the equivalent waves all increase. Stationary instabilities occur when the phase speed of any equivalent wave is exactly equal and opposite to the speed of the shear flow at the discontinuities. Propagating instabilities occur when the shear flow causes two different equivalent wave modes to travel with the same velocity.

The growth rate for the stationary instabilities is greater than that for the propagating instabilities and the largest growth rate is for the fundamental mode.

## §5.6 Summary

The possibility of barotropic instability of homogeneous and continuously stratified flow along a ridge has been examined. Necessary conditions for the existence of instability have been derived in the barotropic and long wave limits.

The case of linear shear is examined in detail for top-hat and multi-step

profiles. Unstable modes exist in all cases.

The stability of the fundamental or external Kelvin wave mode is crucial in determining the behaviour of flow and the stability of other modes. It always has the highest growth rate of any unstable mode.

In the barotropic case and the long-wave stratified case the instabilities are found to centre on the points where the shear flow brings two opposing equivalent waves relatively to rest.

# Chapter 6

# Conclusion and discussion

This thesis has discussed the properties of topographic Rossby waves in various situations and parameter regimes. The variation in the phase speed and pressure field of free low-frequency waves has been examined as the stratification parameter $B$, the external Rossby radius $a$, the buoyancy frequency profile $N(z)$ and the topography have changed. The geometries studied include a monotonic coastal shelf, a submerged ridge and an isolated seamount.

There has been much previous work on the subject of low-frequency coastally trapped waves and on methods for deriving the possible wave modes. In Chapter 2 systematic extensions to asymptotic results at weak and strong stratification are given and are combined to give approximations good even for $B \sim O(1)$.

This procedure is only of real use for quite simple topographies. For more realistic situations a method is needed that works for any topography. The numerical method introduced in §2.4 uses a Green's function to convert the two-dimensional partial differential governing equation to a line integral on the shelf. The chief advantage of this is that the Green's function only has to satisfy the boundary conditions on the surface $z = 0$ and on the outer ocean floor $z = -1$. The variation of the shelf geometry is entirely confined to the line integral. The function has a particularly simple form in the rigid lid/uniform stratification case though free surface effects and an exponential buoyancy frequency profile can also be incorporated at little extra cost.

In the low-frequency case the integral equation can be reduced to a linear eigenvalue problem for the phase speed and the values of the pressure on the shelf. This has the advantage over previous methods of directness, one-dimensionality, higher resolution and the fact that all the modes are found simultaneously.

The asymptotic results are found to compare very well with the numerics. Stratification invariably increases the phase speed and in the limit of large stratification all modes are essentially Kelvin wave modes. The addition of a free surface does not significantly affect the structure of the lower modes for realistic values of the Rossby radius of deformation but it does allow the external Kelvin wave (mode 0) to travel at a finite speed.

Using this new method allows a closer examination of the interactions between

modes first noted by Allen (1975). "Kissing" modes are indeed found but are only apparent among higher modes or in rather special cases of shelf topography where a clear separation between internal Kelvin wave modes and barotropic shelf wave modes is possible. However in realistic situations higher modes or very special topography are not likely to be observed and hence it must be concluded that kissing modes are not of great importance.

An exponential profile for the buoyancy profile can also be introduced which models the stratification more realistically. Vertical velocities are confined to the e-folding scale layer at the surface and the structure of the mode at greater depth is essentially barotropic.

In Chapter 3 the theory of CTWs is extended to the ridge case, a geometry which has not received much attention in the literature. The extension is quite straightforward but a slight complication arises when the topography is approximated by a piecewise linear function. In the vicinity of a corner where the internal angle is greater than $\pi$ radians singularities can occur in the pressure gradients. If the flow near such a corner is confined sufficiently close to the apex not to feel the other boundaries the solution for the pressure behaves like $r^{\alpha}$ where $\alpha < 1$ and hence the gradients become infinite at that point.

This problem causes the numerical method to break down in case of medium to strong stratification if such a simple topography is used. However in cases where the topography is smooth ( a continuous normal vector) no such problem is found.

The semi-analytic method used in §3.3 works accurately to model the singularity when the topography is a simple top-hat ridge. In this case the equations are separable and Fourier expansions found over each segment and matched across the discontinuities in depth. The results from this section confirm the existence of very large pressure gradients (and hence velocities) at the corners.

It is important to note that this singularity is not a function of the numerics but of the governing equations and topography. Hence it would be expected to occur with other numerical codes which attempt to model topographic Rossby waves. An example of this is discussed in §3.4 with reference to the Cox code.

A right circular cylinder was used by Sherwin and Dale (1992) to model the topographic waves excited by a uniform flow passing over the Anton Dohrn

seamount. They found that the frequency of the fundamental mode depended heavily on the grid size used in their model. Using the same method as in §3.3 but in polar coordinates, the free modes for this configuration can be found. The results confirm the analysis and show that the same singularity can appear at the sharp edge of the cylinder.

Since most large numerical models use a finite difference scheme errors will be introduced into the calculation when very large sharp peaks arise in the pressure gradients or velocities. Extra resolution in regions where these singularities are expected to appear will reduce the error as will using smooth topography. Researchers hoping to use such models must be aware of the potential for error if simple step or piecewise linear topography is used.

The greatest advantage that the new numerical method has over previous work is its ease of use in applications. The theory of topographic Rossby waves has been profitably applied to the scattering of low-frequency energy by topography and the wind-forcing of low-frequency motions in coastal regions. Both applications rely on the fact that the wave modes are orthonormal and form a complete set on the topography and hence any pressure distribution there can be expressed as a linear combination of the free modes.

Since the only information needed about the modes is their phase speed and the pressure distribution on the topography, a method that restricts itself to finding these is inherently more efficient than a large two-dimensional finite difference method. Further, since all modes are found simultaneously the orthogonality of the modes is much higher than that found in the past.

In Chapter 4 the isobath tracing result of Johnson (1989a,1991) is used. This states that the pressure along an isobath is constant throughout a scattering region of order the shelf width. Hence the pressure on the shelf for the transmitted portion of the wave field can be found without having to consider the exact form of the solution in the intervening region. Up until now it has not been feasible to use this result in continuously stratified flow and general shelf profiles.

Calculations using this result are in terms of line integrals across the topography. If they are approximated using the same distribution of points and integration scheme as the numerical method uses, then the transmission coefficients are given by a simple sum.

The result is applied to the simplest case where two coastal shelves are connected by a scattering region. For most realistic cases energy from the incident mode scatters preferentially into the adjacent modes. The result in Johnson (1989a) that all scattering is suppressed at large stratification is confirmed. This is expected since all the modes are essentially internal Kelvin waves in this limit whatever the topography.

In the following sections the result was applied to two more interesting geometries. The scattering of a coastally trapped wave through a strait can be determined straightforwardly while the scattering of a wave as it is incident on a ridge abutting the shelf can be determined with a little linear algebra.

The results for both cases show similarities. The depth of the dividing isobath is the most important factor determining the amount of energy that is transmitted through the strait or over the ridge. The stratification and topography mainly affect the distribution of energy amongst the transmitted modes though an exponential buoyancy profile can significantly increase the total amount of energy that passes through the strait or over the ridge.

For an incident external Kelvin wave, the amount of energy that passes over the ridge or through the strait is roughly proportional to the depth of the dividing isobath. For higher incident modes, the energy divides less simply and depends much more on the structure of the incident modes.

In §4.4 the distribution of energy among the outwardly propagating modes on the ridge is determined by the zeros on the shelf of the incident pressure field. If there are no zeros in the pressure below the dividing isobath then only mode 0 will be present on the ridge. Similarly, if there are $n$ zeros below the dividing isobath only the first $n$ modes will be present. This rule of thumb is approximately correct for all the topographies and stratifications tested.

The problem of how much energy is passed through the Bass Strait by the scattering of coastally trapped waves from the Great Australian Bight has received much attention. The example in §4.3 shows that, as observed, the transmitted energy will be predominantly contained in the first and second modes. The shallow depth of the Strait though makes it unlikely that sufficient energy could be transmitted through to the East Australian coast to match the observed levels. Hence low frequency forcing within the Strait itself must play a part in

producing the CTW field seen.

This brings up the question of finding the wind-forced component of the low frequency field. Existing theory can determine this component in terms of an infinite sum of the free wave modes. However, only a finite sum of modes can be practically dealt with. The convergence of the sum then becomes of crucial importance. Previous methods of determining the free waves made it impractical to use more than a half dozen or so modes. This gives adequate results for the pressure but as the results in §4.5 show up to 40 modes may be needed to accurately model the alongshore velocities. Various further approximations have been made to get around this practical problem but with the new numerical method as many modes as desired can be used with no problem.

In Chapter 5 the stability of horizontal shear flow along topography is considered. Modified topographic Rossby waves can propagate in this flow and in some cases can be unstable. Necessary conditions for instability corresponding to the classical Rayleigh and Fjørtoft criteria are derived in the barotropic and long wave cases. These imply that for a coastal shelf linear shear is stable and that for a ridge instability is only possible when the shear flow is opposing the direction of the topographic Rossby waves.

In the barotropic case with linear shear flow along a top-hat ridge only one pair of modes can exist (one propagating in each direction). There is a simple algebraic form for the speed of these waves which can be imaginary. Hence for some parameter regions the shear flow is unstable to small disturbances.

Waves can however exist without the presence of the shear flow. The addition of the shear flow has two main effects. It advects the waves but it also changes the background potential vorticity upon which the waves depend. If the velocity of the shear flow at a point of discontinuity of the profile is much greater than that of the wave mode there then it will be swept along with the shear. It is only when the velocities of the shear flow and of the mode are comparable and opposite that the possibility of unstable modes arises.

In fact, the regions of instability are centred upon the points where the shear flow velocity exactly matches the phase speed of the topographic Rossby wave that would exist if the shear flow was not present but the background potential vorticity was the same. As in Taylor (1931) the mechanism for instability seems

to be that the shear flow is bringing two opposing waves relatively to rest.

The addition of either continuous stratification or a multi-step profile allows other modes to exist. However it is still the fundamental mode (or the external Kelvin wave mode in the stratified case) that dominates the stability. Higher modes have only small windows of instability with much lower growth rates.

As in the previous case the instabilities are found to centre upon points where the shear flow brings two opposing waves relatively to rest. If the two modes are both the same (i.e. the same mode number but travelling in opposite directions) then a stationary instability will result. However, if the two waves have different mode numbers the disturbance will propagate.

It is less clear how to apply this idea in the cases where a multi-step ridge is used since the wave modes can no longer be considered to be localised at a discontinuity of height. The qualitative interpretation remains valid. As the speed of the equivalent fundamental mode decreases with increasing wavenumber a similar pattern to the stratified case would be expected but in reverse. i.e. a series of propagating unstable modes coming before a more unstable stationary mode.

Further work remains to be done in the general case and in particular the long-wave stratified case with smooth topography to see whether Taylor's mechanism continues to be a valid description for the instabilities.

## References


Allen, J.S., 1975: Coastal trapped waves in a stratified ocean. *J. Phys. Oceanogr.*, **5**, 300–325

Allen, S.E. and R.E. Thomson, 1993: Bottom-trapped subinertial motions over mid-ocean ridges in a stratified rotating fluid. *J. Phys. Oceanogr.*, **23**, 566–581

Bjerknes, V., 1937: Application of line integral theorems to the hydrodynamics of terrestrial and cosmic vortices. *Astrophys. Norv.*, **2**, 263–339

Boussinesq, J., 1903: "Théorie analytique de la chaleur," Vol. 2. Gauthier-Villars, Paris.

Brink, K.H. and D.C. Chapman, 1985: Programs for computing properties of coastal trapped waves and wind driven motions over the continental shelf and slope. *Woods Hole Oceanographic Institute Tech. Rep.* WHOI –85– 17 99pp

Brink, K.H., 1989: The effect of stratification on seamount-trapped waves. *Deep Sea Res.*, **36**, 6, 825–844

Brink, K.H., 1991: Coastal-trapped waves and wind-driven currents over the continental shelf. *Annu. Rev. Fluid Mech.*, **23**, 389–412

Brunt, D., 1927: The period of simple vertical oscillations in the atmosphere. *Q. J. R. Meteorol. Soc.*, **53**, 30–32

Buchwald V.T., and B.J. Kachoyan, 1987: Shelf waves generated by a coastal flux. *Aust. J. Mar. Freshwater Res.*, **38**, 429–437

Charney, J.G., 1947: The dynamics of long waves in a baroclinic westerly current. *J. Meteorol.*, **4**, 135–163

Clarke, A.J., 1976: Coastal upwelling and coastally trapped long waves. Ph.D. thesis, Cambridge University, 178pp

Clarke A.J. and K.H. Brink, 1985: The response of stratified, frictional flow of shelf and slope waters to large-scale, low-frequency wind forcing.*J. Phys. Oceanogr.*, **15**, 439–453

Clarke A.J. and S. Van Gorder, 1986: A method for estimating wind-driven frictional, time-dependent, stratified shelf and slope water flow. *J. Phys. Oceanogr.*, **16**, 1013–1028

Collings, I.L. and R. Grimshaw, 1980a: The effect of current shear on topographic Rossby waves. *J. Phys. Oceanogr.*, **10**, 363–371

Collings, I.L. and R. Grimshaw, 1980b: The effect of topography on the stability of a barotropic coastal current. *Dyn. Atmos. Oceans*, **5**, 83–106

Collings, I.L., 1986: Barotropic instability of long continental shelf waves in a two-layer ocean. *J. Phys. Oceanogr.*, **16**, 298–308

Coriolis, G., 1835: Mémoire sur les équations du mouvement rélatifs des systèmes de corps. *J. Ec. Polytech. (Paris)*, **15**, 142

Cox, M.D., 1984: A primitive equation, three-dimensional model of the Ocean. *GFDL Ocean Group Technical Rep. No. 1*, GFD Lab., Princeton University, Princeton NJ.

Drazin, P.G., and W.H. Reid, 1981: "Hydrodynamic Stability." Cambridge University Press, Cambridge, England.

Eady, E.T., 1949: Long waves and cyclone waves. *Tellus*, **1**, 33–52

Ertel, H., 1942: Ein neuer hydrodynamischer Wirbelsatz. *Meteorol. Z.*, **59**, 271–281

Euler, L., 1755: Principes généraux du mouvement des fluides. *Mém. Acad. Berlin*, **11**, 274–315, 316–361

Freeland, H.J., F.M. Boland, J.A. Church, A.J. Clarke, A.M.G. Forbes, A. Huyer, R.L. Smith, R.O.R.Y. Thompson and N.J. White, 1986: The Australian Coastal Experiment: A search for coastal-trapped waves. *J. Phys. Oceanogr.*, **16**, 1230–1249

Gill, A.E., 1982: "Atmosphere-Ocean Dynamics." Academic Press.

Hadley, G., 1735: Concerning the cause of the general trade winds. *Philos. Trans. R. Soc. London* , **39**, 58–62

Halley, E., 1686: An Historical Account of the Trade Winds and Monsoons, observable in the Seas between and near the Tropicks, with an attempt to assign a Phisical cause of the said Winds. *Philos. Trans. R. Soc. London* , **16**, 153–168

Hamon, B.V., 1966: Continental shelf waves and the effects of atmospheric pressure and wind stress on sea level. *J. Geophys. Res.* , **71**, 2883–2893

Helmholtz, H. von, 1888: Über atmospharische Bewegungun I. *Sitzungsberichte Akad. Wissenschaften Berlin.*, **3**, 647–663

Hughes, C.W., 1992: A warning about topography in the Cox code. Unpublished manuscript. Robert Hooke Institute, 5pp

Huthnance, J., 1978: On coastal trapped waves: Analysis and numerical calculation by inverse iteration. *J. Phys. Oceanogr.*, **8**, 74–92

Johnson, E.R., 1977: The effects of bottom topography in rotating flows. Ph.D. thesis. Cambridge University.

Johnson, E.R., 1989a: Connection formulae and classification of scattering regions for low-frequency shelf waves. *J. Phys. Oceanogr.*, **19**, 1303–1312

Johnson, E.R., 1989b: The low-frequency scattering of Kelvin waves by stepped topography. *JFM*, **215**, 23–44

Johnson, E.R., 1991: The scattering at low frequencies of coastally trapped waves. *J. Phys. Oceanogr.*, **21**, 913–932

Johnson, E.R., 1993: Low frequency scattering of Kelvin waves by continuous topography. *JFM*, **248**, 173–201

Killworth, P.D., 1980: Barotropic and baroclinic instability in rotating stratified fluids. *Dyn. Atmos. Oceans*, **4**, 143–184

Killworth, P.D., 1989a: How much of a baroclinic coastal Kelvin wave gets over a ridge? *J. Phys. Oceanogr.*, **19**, 321–341

Killworth, P.D., 1989b: Transmission of a two-layer coastal Kelvin wave over a ridge. *J. Phys. Oceanogr.*, **19**, 1131–1148

Laplace, P.S., 1778,1779: Recherches sur plusiers points du système du monde. *Mém. Acad. R. Sci. Paris* , 1775; 75–182 (publ. 1778), 1776; 117–267, 525–552 (publ. 1779)

Longuet-Higgins, M.S., 1968: Double Kelvin waves with continuous depth profiles. *J. Fluid Mech.*, **34**, 49–80

Lopez, M., and A.J. Clarke, 1989: The wind-driven shelf and slope water flow in terms of a local and a remote response. *J. Phys. Oceanogr.*, **19**, 1091–1101

Lorenz, E.N., 1972: Barotropic instability of Rossby wave motion. *J. Atmos. Sci.*, **29**, 258–269

Middleton, J.F. and D.C. Wright, 1990: Coastally trapped waves in a stratified ocean. *J. Phys. Oceanogr.*, **20**, 1521–1527.

Middleton, J.F., 1991: Coastal-trapped wave scattering into and out of straits and bays.*J. Phys. Oceanogr.*, **21**, 681–694

Middleton, J.F. and F. Viera, 1991: The forcing of low frequency motions within Bass Strait. *J. Phys. Oceanogr.*, **21**, 695–708

Middleton, J.F., 1993: The scattering of long coastal-trapped waves in frictional seas. (preprint)

Morse, P.M., and H. Feshbach, 1953: Methods of theoretical physics. McGraw-Hill. New York.

Mysak, L.A., 1967: On the theory of continental shelf waves. *J. Mar. Res.*, **25**, 205–227

Mysak, L.A., 1980: Recent advances in shelf wave dynamics. *Rev. Geophys. Space. Phys.*, **18**, 1, 211–241

Pedlosky, J., 1979: "Geophysical Fluid Dynamics." Springer-Verlag, Berlin.

Rayleigh, Lord, 1880: On the stability, or instability of certain fluid motions. *Proc. London Math. Soc.*, **9**, 57–70

Rhines, P.B., 1969a: Slow oscillations in an ocean of varying depth. 1. Abrupt topography. *J. Fluid Mech.*, **37**, 161–189

Rhines, P.B., 1969b: Slow oscillations in an ocean of varying depth. 2. Islands and seamounts. *J. Fluid Mech.*, **37**, 191–205

Robinson, A.R., 1964: Continental shelf waves and the response of sea level to weather systems. *J. Geophys. Res.*, **69**, 367–368

Rossby, C.G., 1937: On the mutual adjustment of pressure and velocity distributions in certain simple current systems (I). *J. Mar. Res.*, **1**, 15–28

Rossby, C.G., 1938: On the mutual adjustment of pressure and velocity distributions in certain simple current systems (II). *J. Mar. Res.*, **2**, 239–263

Sherwin, T and A. Dale, 1992: Grid dependence of the resonant frequency of a submerged cylinder in a stratified ocean. *Ocean Modelling*, **95**, (Unpublished manuscript)

Taylor, G.I., 1917: Motion of solids in fluids when the flow is not irrotational. *Proc. R. Soc.*, **A93**, 99–113

Taylor, G.I., 1923: Experiments on the motion of solid bodies in rotating fluids. *Proc. R. Soc.*, **A104**, 213–218

Taylor, G.I., 1931: Effect of variation in density on the stability of superposed streams of fluid. *Proc. R. Soc.*, **A132**, 499–523

Thompson, W. (Lord Kelvin), 1879: On gravitational oscillations of rotating water. *Proc. Roy. Soc. Edin.*, **10**, 92–100

Väisälä, V., 1925: Über die Wirkung der Windschwankungen auf die Pilotbeobachtungen. *Soc. Sci. Fenn. Commentat. Phys.-Math.*, **2** (19), 19–37

Wang, D.P. and C.N.K. Mooers, 1976: Coastal trapped waves in a continuously stratified ocean. *J. Phys. Oceanogr.*, **6**, 853–863